**Peptide Design for Mesenchymal Stem Cell Specific Attachment on Apatite Surfaces for Bone Tissue Regeneration**

**by**

Sriharsha Ramaraju

A dissertation submitted in partial fulfillment
of the requirements for the degree of
Doctor of Philosophy
(Biomedical Engineering)
in The University of Michigan
2015

Doctoral Committee:

Professor David H. Kohn, Chair
Professor Renny T. Franceschi
Associate Professor Andrew J. Putnam
Professor Jan P. Stegemann

To my family

## ACKNOWLEDGMENTS

This work would not have been possible without the mentorship and support provided by my graduate advisor David Kohn. Thanks for providing me the freedom to develop my own scientific curiosity while facilitating access to necessary resources. Thank you as well for allowing me to seek out and pursue my professional interests. I would like to thank my dissertation committee, Dr. Franceschi, Dr. Stegemann, and Dr. Putnam, for their insightful feedback that improved the focus of my research questions.

I would like to thank my labmates whom I've had the pleasure of working with over the years. Thank you Janani Ramaswamy, Erin McNerny, and Joseph Gardinier for the long chats that helped me shape my scientific questions and the many ice-cream and coffee breaks. Thank you Genny Romanowicz for your various academic and confectionary contributions. I would like to thank Nianli Zhang, Nicholas Landgraf and Michelle Lynch for their assistance with various experimental procedures. Thank you Nadder Sahar, Linh Luong, and Michael Friedman for your constructive feedback during presentations. A special thanks to Sharon Miller for applying phage-display technology to bone tissue engineering, identifying the peptides that are the focus of this work, and for being a co-author on my publications.

I would like to thank Dr. Paul Krebsbach's lab. Specifically, I would like to thank Dr. Hongli Sun for assistance with animal surgeries, and Dr. Luis Villa-Diaz for generating iPS-MSCs and assistance with iPS-MSC characterization which allowed me to complete

my subsequent aims. I would also like to thank Dr. Sergei Kuznetsov for the generous contribution of primary MSCs derived from human bone marrow stroma. I would also like to thank Chris Strayhorn from the Dental Histology Core, Taocong Jin from the Dental Molecular biology core, Dr. Henriette Remmer at the Proteomics Core, and the staff at the microscopy and image analysis core for speeding up materials and data acquisition. I would also like to thank our past and present administrative staff Liz Rodriguiz, Kumud Danak, Deb Keedy, Joel Clandenin, and Maria Steele for making things run smoothly.

I would like to thank and acknowledge my undergraduate research advisor Dr. Alfred H. Merrill, Jr for introducing me to academic research and providing me the opportunity to continue my undergraduate research beyond graduation. I would like to thank Dr. Dennis Liotta, Dr. John Petros, Dr. Carrie Sun and Dr. Rebecca Arnold for providing me the guidance, environment, and confidence to broaden my research skills and experiences.

I would like to thank all of my friends and my sister for their various visits to Ann Arbor when I was unable to travel and for enduring Michigan winters. I would like to thank my wife Neelima for being a constant source of strength throughout my graduate school. Your patience, positivity, and support were integral to the completion of this work. Lastly, I would like to thank my parents for the struggles they've endured and the sacrifices they have made in order to provide me the opportunities to pursue my academic interests.

# TABLE OF CONTENTS

# LIST OF FIGURES

**CHAPTER FOUR FIGURES**

# LIST OF TABLES

# LIST OF APPENDICIES

# ABSTRACT

Over 2 million bone grafting procedures are performed annually worldwide for the treatment of bone defects. Cell transplantation therapies are promising alternatives to conventional auto-, allo-, and xenograft therapies. Successfully delivering stem and progenitor cells to the defect site requires biomaterials that support and guide reconstruction. Biomaterial functionalization with extracellular matrix derivatives to improve adhesion and guide tissue regeneration lacks specificity towards particular regenerative cell populations. In order to direct cell specific adhesion to specific biomaterial surface chemistries, we used a combinatorial phage display strategy to identify 2 sequences, 1 with high affinity towards apatite (VTK) and a second with high affinity to clonally derived mesenchymal stem cells (MSC) from human bone marrow stroma (DPI) and combined the two sequences into a dual-functioning peptide (DPI-VTK).

Dual-functioning peptide DPI-VTK exhibited greater apatite binding compared to single peptide controls ($p < 0.01$). Mesenchymal stem cells on DPI-VTK coated apatite substrates exhibited greater adhesion strength compared to pre-osteoblasts and fibroblasts ($p < 0.01$). DPI-VTK also increased MSC spreading ($p < 0.001$) and proliferation ($p < 0.001$) compared to apatite controls while supporting differentiation on apatite substrates. Competitive inhibition revealed RGD-binding integrin involvement in MSC attachment

to DPI-VTK. MSC driven bone formation, cellularity and vascularization in a subcutaneous mouse model were greater on DPI-VTK coated PLGA-mineral composite scaffolds compared to VTK ($p < 0.017$) and uncoated controls ($p < 0.001$) and acellular peptide-coated controls ($p < 0.002$). Taken together, DPI-VTK improves MSC specific attachment and subsequent adhesion on mineralized substrates driving greater proliferation and bone formation compared to acellular and non-peptide coated controls.

A vast array of biomaterials and multitude of regenerative cell sources are available for tissue regeneration applications. As tissue engineering shifts from developing technologies to meet general clinical challenges to addressing more focused clinical applications, there will be an increased need for delivering cell specific cues to material surfaces with defined surface chemistries. Combinatorial phage display is a powerful platform to enable focused cell based tissue regeneration through the discovery of cell specific and material specific peptide sequences.

# CHAPTER ONE

# INTRODUCTION

## CLINICAL SIGNIFICANCE

Current clinical solutions for tissue replacement and regeneration utilize auto-, allo- or xenografts which require multiple interventional procedures and could result in donor site morbidity and immunogenicity[1], [2]. *De novo* tissue regeneration utilizing cells extracted from the host offers a promising alternative to the current clinical standards. Most organ systems in the body contain a repository of stem and progenitor cells that replace dying and injured cells to preserve the integrity of tissues. For instance, cells of the bone marrow stroma contain a mesenchymal population that can give rise to osteogenic, chondrogenic, myogenic, and adipogenic lineages[1], [3], [4]. These cells secrete tropic factors to improve tissue repair, suppress immune responses and are a readily available and relatively non-invasive cell source to extract from the host. Moreover, stem and progenitors can be expanded in monolayer culture or 3D culture under perfusion to be delivered to a defect site on an appropriate transplant material[3], [5]–[8]. Stem and progenitor cell mediated bone regeneration *in vivo* is dependent on biomaterial properties that control cell seeding efficiency, and cell distribution, and can provide instructive cues to guide cell proliferation and differentiation[9]–[12].

## BIOMATERIAL DESIGN

The ideal 3D biomaterial provides an environment that allows cell adhesion and encourages cell growth and differentiation while allowing transport of nutrients and waste to facilitate new tissue formation[8], [13]. A conductive biomaterial supports cell adhesion, which is an important starting point for functional tissue regeneration. In addition to the number of cells seeded on a 3D biomaterial construct, the distribution of cells plays a critical role in bone formation as well. Constructs that improve cell seeding density and promote uniform distribution of cells in a 3D biomaterial while directing cell-cell communication and cell-matrix interactions are hypothesized to improve bone formation in vivo[9], [14], [15].

Both bulk and surface properties of a material contribute to cell adhesion. Metals, ceramics, polymers, and composites are used in conjunction with an array of surface and bulk modification techniques to yield material properties conducive to supporting cell based tissue regeneration [2], [8], [16]–[18]. In the context of bone, properties such as compliance, surface free energy, wettability, surface topography, and crystallinity influence cell mediated bone formation *in vivo*[19]–[21]. Many of these properties exhibit collinear relationships due to the underlying biological processes driving cell adhesion, proliferation, and differentiation.

Osteoinductive biomaterials stimulate and drive differentiation of primitive undifferentiated pluripotent or multipotent cells towards a terminal bone forming cell lineage[22]. Inductive biomaterials utilize growth factors, recombinant DNA, and

peptides to regulate cell growth and differentiation[22]–[24]. These biomolecules can be adsorbed, encapsulated within or immobilized to biomaterials in order to temporally and spatially control transplanted cell behavior. The conductive and inductive properties of a material that impact cell adhesion, proliferation, and differentiation result in an expansive number of design considerations for developing the ideal carrier for functional tissue regeneration. Biomimetic biomaterial design strategies specifically addresses osetoconduction and osteoinduction by recapitulating physical and chemical attributes of the native ECM to drive functional tissue regeneration[25]–[28].

## RECAPITULATING CELLULAR MICROENVIRONMENTS

Biomimetic design of biomaterials involves studying the physical and chemical properties of functional tissues and incorporating these properties into biomaterial design. The extracellular matrix (ECM) of bone is comprised of 50-70% inorganic mineral matrix, 20-40% organic matrix, 5-10% water and less than 3% lipids. The inorganic matrix is comprised of a non-stoichiometric, semi-crystalline, calcium and hydroxide deficient carbonate substituted hydroxyapatite mineral [Ca10(PO4)6(OH)2]. The organic matrix is predominantly comprised of Type I collagen. Non-collagenous proteins comprise the remaining 10-15% of the organic component and include proteoglycans, glycosylated proteins, and γ-carboxylated proteins. These non-collagenous proteins are involved in directing organic matrix assembly, maintaining structural integrity of the tissue, sequestering and interacting with growth factors, and regulating bone metabolism and mineralization. Both the organic and inorganic components of bone contribute to conductive and inductive properties. Therefore reproducing aspects of both organic and

inorganic components of bone tissue in biomaterial design is hypothesized to improve regeneration.

Surface coating via a biomimetic procedure can be used to form a biomimetic apatite coating on biocompatible and biodegradable polymer substrates. For instance, 3D porous poly-Lactide-co-Glycolide (PLGA) scaffold surfaces can be coated with a continuous bone like mineral (BLM) layer through immersion in a supersaturated simulated body fluid (SBF). This SBF contains similar ionic concentrations to that of blood plasma and results in the precipitation of a bone-like-mineral that is semicrystalline, nano-structured, and is carbonate substituted [29]–[31]. Biomimetically mineralized polymers exhibit a 5-fold increase in compressive modulus, support higher bone marrow stromal cell adhesion through well distributed fibrillar contacts, and higher bone volume fractions when used to transplant BMSCs in vivo compared to non-mineralized polymer scaffolds[18], [29], [32], [33].

The organic components of extracellular matrices are comprised of collagenous and non-collagenous proteins that provide mechanical support and cell instructive cues that facilitate tissue growth and preserve tissue integrity. These components impart cues that regulate an elegant sequence of spatially and temporally controlled events resulting in tissue repair and regeneration. Collagen, fibronectin, vitronectin, osteocalcin, osteopontin, bone morphogenetic protein-2 (BMP-2) and fibroblast growth factor-2 (FGF-2) have all been used to drive osteoblastic differentiation of and improve quantity of regenerated bone [34]–[36]. However, full length recombinant ECM proteins are challenged by degradation rate, conformational control, and high processing costs.

## PEPTIDE THERAPIES FOR TISSUE REGENERATION

Peptide epitopes offer a promising alternative to protein based therapies by allowing control of conformation, cell and material specificity, degradation rate, and reduced processing costs. Peptides derived from the active sites of ECM proteins have been used to impart instructive cues to stem and progenitor cell lines that form bone [34], [36]–[38]. The method of delivering these signals onto a biomaterial and the modification of these peptides play an important role in mediating cell responses. Peptide delivery methods involve adsorption, covalent immobilization or encapsulation into a biomaterial. Adsorption of peptides on a biomaterial surface involves weak molecular and electrostatic forces at the substrate-peptide interface. While adsorption allows conformational freedom of peptides, it is challenged by control of release rates and short half-lives of some unbound peptide. Peptide mediated control of cell viability, differentiation, and tissue formation, are variable across cell sources, materials, and mode of delivery. This variability can be linked to both the specificity of the peptide sequences to cell lineages and the proper presentation of these sequences suggesting the important interplay of these factors.

## PEPTIDE SPECIFICITY

The cell binding sites of ECM protein domains exhibit different binding affinities to different integrin receptors. For instance, DGEA and GFOGER peptides from collagen predominantly bind to α2β1 integrin receptors, whereas fibronectin and vitronectin fragments bind α5β1 receptors. Most ECM proteins also have multiple binding domains that interact and contribute to this specificity. As an example, the RGD sequence

prevalent in many proteins binds $\alpha_V\beta_3$ integrins whereas co-delivery with the fibronectin sequence PHSRN synergistically improves binding affinity to $\alpha_5\beta_1$[34], [38]–[40]. Targeting different integrins results in variable cell responses across cell lineages. For instance, the DGEA collagen fragment and RGD preferentially bind different integrin subunits and increase FAK signaling pathways, but only the DGEA peptide improves MAPK mediated signal transduction [41]. Differences in specificity for these integrin receptors could also be responsible for variability of tissue regeneration in vivo. For example, collagen derived peptides improve MSC cell differentiation in vitro and bone formation in vivo, whereas RGD exhibits inverse effects [41], [42].

In addition to using components of known ECM peptides, novel cryptic peptides from collagen have also been derived to improve conductive properties [43], [44]. Strategies using components of known ECM proteins targeting specific integrins lack specificity to a particular cell type. The ability to adhere and recruit specific stem or progenitor cell populations to a biomaterial surface and impart instructive cues can improve tissue repair and regeneration[38]. In addition to delivering cell specific sequences, proper presentation of these signals can also improve specificity, cell adhesion, proliferation and differentiation.

## PEPTIDE PRESENTATION

In addition to different delivery methods, peptide structure and conformation can be altered to improve loading efficiency on biomaterials and binding affinity to cell surface receptors. For example, recapitulating the circular conformation of RGD that is commonly found in ECM proteins by altering the structure of RGD not only improves

solution stability and adsorption to biominerals, but also increases bone formation when immobilized on alginate hydrogels[45], [46].

Many ECM proteins have multifunctional domains that work in conjunction with one another to present the cell instructive domains to the cell surface receptors. Combining the cell adhesive sequence with a material binding sequence can improve presentation of the cell instructive peptide to the cell and enhance cellular response[47], [48]. For example, peptide fragment 17-25 of the bone ECM protein osteocalcin contains 3 glutamic acid residues at positions 17, 21, and 24. These residues strongly bind hydroxyapatite and have been used to improve RGD, BMP, and VEGF derived peptide adsorption to biomineral surfaces[37], [47]–[49]. Improving the binding affinity of the cell adhesive peptides by attaching them to material binding sequences improves cell proliferation, differentiation and mineralization *in vitro*.

The combination of sequence specificity, peptide modification methods, and peptide loading methods with respect to the carrier material contribute to the presentation of the cell instructive cues to the cell surface. Therefore, the ability to systematically design specific peptides and appropriately present them to the cell surface receptor can improve tissue regeneration.

## DISPLAY TECHNOLOGIES FOR PEPTIDE-BASED TISSUE REGENERATION THERAPIES

Bacteriophage display, bacterial display and cell surface display technologies are commonly used in oncology and immunology to humanize targeted monoclonal antibody(MAb) based therapies[50], [51]. The application of phage display for tissue

regeneration is gaining traction through the development of biomaterial specific or cell specific peptides. Material specific peptides are used to increase physiochemical deposition of biomineral on biomaterials or deliver growth factors to the surface of mineralized biomaterials[52]–[55]. Cell binding phage-derived peptides have been tethered to polymer biomaterials or self-assembled into 3D structures to improve conductivity and inductivity [56]–[58] . Phage-derived mimetic peptides of the enamel protein amelogenin improve cell conductivity and tissue formation *in vivo*[59].

## PHAGE DISPLAY PEPTIDES THAT FORM THE BASIS FOR THIS DISSERTATION

The primary aim of this dissertation is to evaluate the bone forming potential of MSCs specifically tethered to an apatite surface using a phage display derived apatite specific peptide combined with a cell specific peptide. A commercially available M13 bacteriophage display kit containing $10^9$ sequences of 12-mers was used to identify biomineral and cell specific sequences to improve the specificity of human bone marrow stromal cell binding to apatite surfaces[60], [61].

After 3 rounds of phage panning on HA disks and BLM coated PLGA films, 243 sequences were identified. Amongst these 243 sequences, 68 sequences were identified as high information clones through RELIC analysis. From the 68 sequences, 19 were ordered in terms of their binding affinity to different crystal faces of HA [001, 200], and 10 sequences were selected for ELISA on PLGA, BLM-PLGA films, HA disks, and tissue cultured polystyrene(TCPS). The top 5 sequences exhibiting positive ELISA signals, compared to high information clones from RELIC, and high binding affinity sequences form computational modeling resulted in 3 consensus sequences. Adsorption

assays measuring efficiency of peptide binding to apatite, resulted in the identification of 1 peptide sequence, VTKHLNQISQSY (VTK), with superior binding affinity to BLM[50], [60], [61].

After 3 rounds of phage panning on BMSCs, 50 recurring sequences were identified, amongst which 27 were high information clones and 10 high information and 10 low information peptides were tested using immunohistochemistry (IHC). From the 50 sequences identified, the MOTIF1 program identified continuous motif sequences 3 and 4 amino acids long as NHT, and (S/T)(I/V)LS. Although no consensus sequences were found from MOTIF1 and RELIC analysis, two sequences were identified as having high scores from both RELIC and IHC. A cell adhesion assay with BMSCs attached to peptide laden BLM coated PLGA films and peptide coated TCPS resulted in the identification of 1 sequence, DPIYALSWSGMA (DPI), that improves cell seeding efficiency on BLM in vitro[60]. The cell specific and mineral specific peptides were combined using glycine residues to yield GGDPIYALSWSGMAGGGSVTKHLNQISQSY (DPI-VTK).

In addition to combining these peptides, post-translational modification of the mineral binding sequence improves apatite binding affinity in vitro. Many naturally occurring ECM proteins contain phosphorylated serine residues which improve apatite binding affinity. Phosphorylation of the C-terminal serine residues of VTK improves binding affinity to apatite but reduces cell adhesion to apatite surfaces [60].

## SUMMARY OF SIGNIFICANCE

The ability to provide specific cues to stem and progenitor cells is an increasing area of focus for biomaterial design. Combining these cues with material specific cues can have

broad implications for tissue regeneration. Dual functioning peptides could impart spatial control over cell adhesion and differentiation, which can translate to increased quantity and quality of tissue regenerated in vivo. Moreover, dual functioning peptides containing material and cell specific domains could also be translated to enhance mineralized implant integration *in vivo.*

## AIMS AND HYPOTHESIS

The primary aims of this dissertation were to: 1) design and verify peptide functionality towards specifically recruiting MSCs to mineral substrates. 2) assess osteoconduction and osteoinduction of MSCs on dual peptide coated biomimetic apatite surfaces *in vitro,* and 3) examine the relationship between initial cell attachment and peptide distribution on dual peptide coated 3D mineralized PLGA scaffolds in-vitro and the quantity, quality and distribution of regenerated bone *in vivo*.

***Global hypothesis:*** Combining material and cell specific peptides into a dual-functioning peptide can improve initial cell attachment, cell-specific adhesion, proliferation and differentiation *in vitro* and improve quality, quantity and distribution of bone formation *in vivo* compared to non-specific peptides or specific peptides with only a single functionality.

The overall aim of this thesis is to demonstrate the utility of phage display technologies towards improving cell-specific attachment to biomaterials contributing to increased proliferation, differentiation and tissue regeneration. With the growing abundance of regenerative cell sources, it will become increasingly important to control cell specific delivery and recruitment to biomaterial surfaces (Figure 1.1).

**Aim 1:** Quantify material binding affinity and MSC binding affinity of dual functioning peptide

**Hypothesis:** Combining a mineral specific peptide sequence with a clonally-derived HBMSC specific peptide sequence will improve the binding affinity of cell specific peptides to mineralized substrates and subsequently improve cell specific adhesion to mineralized substrates

**Aim 1.1:** Quantify the influence of mineral binding sequence on dual functioning peptide binding affinity to mineralized biomaterials with Langmuir isotherms

**Hypothesis:** Attaching phage display derived mineral specific sequences to human bone marrow stromal cell specific sequences will improve the binding affinity of the dual sequence to mineral surfaces in vitro

**Aim 1.2:** Quantify dual functioning peptide specificity to human bone marrow stromal cells with a cell detachment assay

**Hypothesis:** Addition of a mineral binding sequence to a cell specific sequence to yield a dual functioning peptide can improve initial HBMSC attachment to 2D mineralized surfaces in vitro

**Chapter 2,** which relates to **Aim 1,** demonstrates the ability of our combinatorial phage display process to select material-specific and cell-specific sequences with dual functionality. The dual peptide DPI-VTK exhibits strong affinity towards hydroxyapatite and biomimetic apatite while concomitantly promoting MSC specific adhesion on apatite surfaces.

**Aim 2:** Determine effects of dual functioning peptides on HBMSC specific adhesion, proliferation, and differentiation on 2D mineral films *in vitro*

**Hypothesis:** Dual functioning peptides improve cell spreading and influence proliferation and differentiation on 2D mineral films *in vitro*

**Chapter 3,** which relates to **Aim 2,** demonstrates the ability of the dual peptide DPI-VTK to improve cell adhesion and promotes cell proliferation by binding an RGD-integrin specific receptor. There was only a marginal improvement of MSC differentiation on DPI-VTK compared to uncoated apatite films; however, MSC specificity towards DPI-VTK, improved adhesion compared to untreated mineral and cooperative interactions with serum proteins translate to improved cell delivery for tissue regeneration *in vivo*.

**Aim 3:** Demonstrate that dual functioning peptides improve HBMSC seeding efficiency and distribution on biomimetically mineralized PLGA scaffolds and consequently improve quantity, distribution and quality of bone formation *in vivo*

**Hypothesis:** Dual functioning peptides improve cell seeding efficiency and distribution of HBMSCs on biomimetically mineralized PLGA scaffolds, which correlates with improved quantity, distribution, and quality of bone formation *in vivo.*

**Chapter 4,** which relates to **Aim 3,** demonstrates the ability of dual peptide DPI-VTK to improve the quantity, cellularity and vascularization of bone formation in vivo compared to uncoated controls. Although bone quantity, cellularity and vascularization of reconstructed ossicles were greater on DPI-VTK coated constructs, ossicles still exhibited a shell of bone formation with less bone volume in the interior. Regardless, the quantity

of regenerated bone was significantly improved by coating DPI-VTK on mineralized scaffolds for cell-based tissue regeneration.

Overall, this work demonstrates the specificity and bioactivity of DPI-VTK *in vitro* and its osteogenic potential *in vivo* while demonstrating the significance of display technology towards tissue regeneration applications.

## CHAPTER ONE FIGURES

### FIGURE 1.1 OVERVIEW OF AIMS

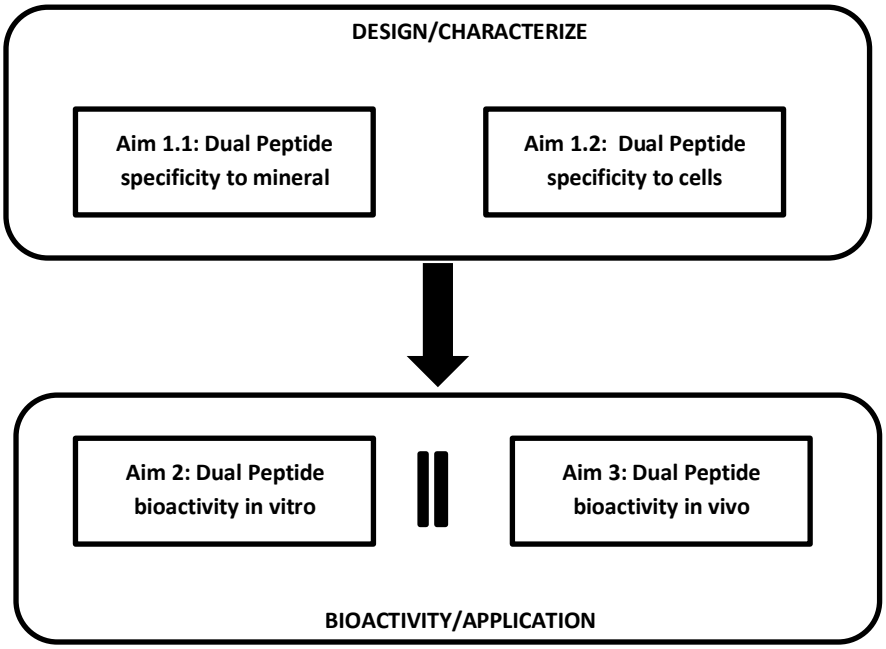

## REFERENCES


[1] P. H. Krebsbach, S. a. Kuznetsov, P. Bianco, and P. Gehron Robey, “Bone Marrow Stromal Cells: Characterization and Clinical Application,” *Crit. Rev. Oral Biol. Med.*, vol. 10, no. 2, pp. 165–181, Jan. 1999.

[2] E. Alsberg, E. E. Hill, and D. J. Mooney, “Craniofacial tissue engineering.,” *Crit. Rev. Oral Biol. Med.*, vol. 12, no. 1, pp. 64–75, Jan. 2001.

[3] P. G. Robey, S. A. Kuznetsov, M. Riminucci, and P. Bianco, “Skeletal (‘mesenchymal’) stem cells for tissue engineering.,” *Methods Mol. Med.*, vol. 140, pp. 83–99, Jan. 2007.

[4] P. G. Robey and P. Bianco, “The use of adult stem cells in rebuilding the human face.,” *J. Am. Dent. Assoc.*, vol. 137, no. 7, pp. 961–72, Jul. 2006.

[5] D. Benayahu, U. D. Akavia, and I. Shur, “Differentiation of bone marrow stroma-derived mesenchymal cells.,” *Curr. Med. Chem.*, vol. 14, no. 2, pp. 173–9, Jan. 2007.

[6] A. I. Caplan, “Review: mesenchymal stem cells: cell-based reconstructive therapy in orthopedics ,” *Tissue Eng.*, vol. 11, no. 7–8, pp. 1198–1211, 2005.

[7] J. R. Mauney, C. Jaquiéry, V. Volloch, M. Heberer, I. Martin, and D. L. Kaplan, “In vitro and in vivo evaluation of differentially demineralized cancellous bone scaffolds combined with human bone marrow stromal cells for tissue engineering,” *Biomaterials*, vol. 26, no. 16, pp. 3173–3185, 2005.

[8] A. G. Mikos, S. W. Herring, P. Ochareon, J. Elisseeff, H. H. Lu, R. Kandel, F. J. Schoen, M. Toner, D. Mooney, A. Atala, M. E. Van Dyke, D. Kaplan, and G. Vunjak-Novakovic, “Engineering complex tissues.,” *Tissue Eng.*, vol. 12, no. 12, pp. 3307–39, Dec. 2006.

[9] K. Kim, D. Dean, A. G. Mikos, and J. P. Fisher, “Effect of initial cell seeding density on early osteogenic signal expression of rat bone marrow stromal cells cultured on cross-linked poly(propylene fumarate) disks.,” *Biomacromolecules*, vol. 10, no. 7, pp. 1810–7, Jul. 2009.

[10] C. E. Wilson, W. J. A. Dhert, C. A. Van Blitterswijk, A. J. Verbout, and J. D. De Bruijn, “Evaluating 3D bone tissue engineered constructs with different seeding densities using the alamarBlue assay and the effect on in vivo bone formation.,” *J. Mater. Sci. Mater. Med.*, vol. 13, no. 12, pp. 1265–9, Dec. 2002.

[11] M. H. Mankani, S. A. Kuznetsov, B. Fowler, A. Kingman, and P. G. Robey, “In vivo bone formation by human bone marrow stromal cells: effect of carrier particle size and shape.,” *Biotechnol. Bioeng.*, vol. 72, no. 1, pp. 96–107, Jan. 2001.

[12] P. H. Krebsbach, S. A. Kuznetsov, K. Satomura, R. V Emmons, D. W. Rowe, and P. G. Robey, “Bone formation in vivo: comparison of osteogenesis by transplanted mouse and

human marrow stromal fibroblasts.," *Transplantation*, vol. 63, no. 8, pp. 1059–69, Apr. 1997.

[13] V. Mouriño and A. R. Boccaccini, "Bone tissue engineering therapeutics: controlled drug delivery in three-dimensional scaffolds.," *J. R. Soc. Interface*, vol. 7, no. 43, pp. 209–27, Feb. 2010.

[14] R. A. Rossello and D. H. Kohn, "Gap junction intercellular communication: a review of a potential platform to modulate craniofacial tissue engineering ," *J. Biomed. Mater. Res. B, Appl. Biomater.*, vol. 88, no. 2, pp. 509–518, Feb. 2009.

[15] J. Eyckmans, T. Boudou, X. Yu, and C. S. Chen, "A hitchhiker's guide to mechanobiology.," *Dev. Cell*, vol. 21, no. 1, pp. 35–47, Jul. 2011.

[16] J. D. Kretlow and A. G. Mikos, "Review: mineralization of synthetic polymer scaffolds for bone tissue engineering.," *Tissue Eng.*, vol. 13, no. 5, pp. 927–38, May 2007.

[17] G. J. Meijer, J. D. de Bruijn, R. Koole, and C. A. van Blitterswijk, "Cell-Based Bone Tissue Engineering ," *PLoS Med.*, vol. 4, no. 2, p. e9, Feb. 2007.

[18] W. L. Murphy, S. Hsiong, T. P. Richardson, C. a Simmons, and D. J. Mooney, "Effects of a bone-like mineral film on phenotype of adult human mesenchymal stem cells in vitro.," *Biomaterials*, vol. 26, no. 3, pp. 303–10, Jan. 2005.

[19] Ramaswamy, J., Ramaraju, S., and Kohn D. H., "Bone-Like Mineral and Organically Modified Bone-Like Mineral Coatings," in *Biological and Biomedical Coatings Handbook, Processing and Characterization*, S. Zhang, Ed. Boca Raton, FL: CRC Press, 2011, pp. 1–36.

[20] P. Habibovic, H. Yuan, C. M. van der Valk, G. Meijer, C. A. van Blitterswijk, and K. de Groot, "3D microenvironment as essential element for osteoinduction by biomaterials ," *Biomaterials*, vol. 26, no. 17, pp. 3565–3575, Jun. 2005.

[21] J. S. Temenoff and A. G. Mikos, *Biomaterials: The Intersection of Biology and Materials Science*. Prentice Hall, 2008.

[22] T. Albrektsson and C. Johansson, "Osteoinduction, osteoconduction and osseointegration.," *Eur. Spine J.*, vol. 10 Suppl 2, pp. S96–101, Oct. 2001.

[23] K. Y. Lee, M. C. Peters, K. W. Anderson, and D. J. Mooney, "Controlled growth factor release from synthetic extracellular matrices.," *Nature*, vol. 408, no. 6815, pp. 998–1000, 2000.

[24] J. A. Hubbell, "Bioactive biomaterials," *Curr. Opin. Biotechnol.*, vol. 10, no. 2, pp. 123–129, Jan. 1999.

[25] H. Shin, S. Jo, and A. G. Mikos, “Biomimetic materials for tissue engineering ,” *Biomaterials*, vol. 24, no. 24, pp. 4353–4364, Nov. 2003.

[26] J. Yuan, Y. Cao, and W. Liu, “Biomimetic scaffolds: implications for craniofacial regeneration.,” *J. Craniofac. Surg.*, vol. 23, no. 1, pp. 294–7, Jan. 2012.

[27] J. a Burdick and G. Vunjak-Novakovic, “Engineered microenvironments for controlled stem cell differentiation.,” *Tissue Eng. Part A*, vol. 15, no. 2, pp. 205–19, Feb. 2009.

[28] L. E. Freed, G. Vunjak-Novakovic, R. J. Biron, D. B. Eagles, D. C. Lesnoy, S. K. Barlow, and R. Langer, “Biodegradable Polymer Scaffolds for Tissue Engineering”, *Bio/Technology*, vol. 12, no. 7, p. 689 <last_page> 693, 1994.

[29] W. L. Murphy, D. H. Kohn, and D. J. Mooney, “Growth of continuous bonelike mineral within porous poly(lactide-co-glycolide) scaffolds in vitro.,” *J. Biomed. Mater. Res.*, vol. 50, no. 1, pp. 50–8, Apr. 2000.

[30] H. M. Kim Miyaji, F., Kokubo,T., Nakamura T., “Bonding strength of bonelike apatite layer to Ti metal substrate,” *J. Biomed. Mater. Res. Part B Appl. Biomater.*, vol. 38, no. 2, pp. 121–127, 1998.

[31] T. Kokubo, “Bioactive glass ceramics: properties and applications ,” *Biomaterials*, vol. 12, no. 2, pp. 155–163, Mar. 1991.

[32] E. V Leonova, K. E. Pennington, P. H. Krebsbach, and D. H. Kohn, “Substrate mineralization stimulates focal adhesion contact redistribution and cell motility of bone marrow stromal cells.,” *J. Biomed. Mater. Res. A*, vol. 79, no. 2, pp. 263–70, Nov. 2006.

[33] G. A. Hudalla and W. L. Murphy, “Using ‘click’ chemistry to prepare SAM substrates to study stem cell adhesion ,” *Langmuir*, vol. 25, no. 10, pp. 5737–5746, May 2009.

[34] A. Shekaran and A. J. García, “Extracellular matrix-mimetic adhesive biomaterials for bone repair.,” *J. Biomed. Mater. Res. A*, vol. 96, no. 1, pp. 261–72, Jan. 2011.

[35] A. Bhat, S. a Boyadjiev, C. W. Senders, and J. K. Leach, “Differential growth factor adsorption to calvarial osteoblast-secreted extracellular matrices instructs osteoblastic behavior.,” *PLoS One*, vol. 6, no. 10, p. e25990, Jan. 2011.

[36] M. P. Lutolf, F. E. Weber, H. G. Schmoekel, J. C. Schense, T. Kohler, R. Muller, and J. A. Hubbell, “Repair of bone defects using synthetic mimetics of collagenous extracellular matrices ,” *Nat. Biotechnol.*, vol. 21, no. 5, pp. 513–518, May 2003.

[37] D. Itoh, S. Yoneda, S. Kuroda, H. Kondo, A. Umezawa, K. Ohya, T. Ohyama, and S. Kasugai, “Enhancement of osteogenesis on hydroxyapatite surface coated with synthetic peptide (EEEEEEEPRGDT) in vitro.,” *J. Biomed. Mater. Res.*, vol. 62, no. 2, pp. 292–8, Nov. 2002.

[38] R. G. LeBaron and K. A. Athanasiou, “Extracellular matrix cell adhesion peptides: functional applications in orthopedic materials ,” *Tissue Eng.*, vol. 6, no. 2, pp. 85–103, Apr. 2000.

[39] D. L. Hern and J. a Hubbell, “Incorporation of adhesion peptides into nonadhesive hydrogels useful for tissue resurfacing.,” *J. Biomed. Mater. Res.*, vol. 39, no. 2, pp. 266–76, Feb. 1998.

[40] J. Benesch, J. F. Mano, and R. L. Reis, “Proteins and their peptide motifs in acellular apatite mineralization of scaffolds for tissue engineering.,” *Tissue Eng. Part B. Rev.*, vol. 14, no. 4, pp. 433–45, Dec. 2008.

[41] M. Gilbert, W. J. Shaw, J. R. Long, K. Nelson, G. P. Drobny, C. M. Giachelli, and P. S. Stayton, “Chimeric peptides of statherin and osteopontin that bind hydroxyapatite and mediate cell adhesion.,” *J. Biol. Chem.*, vol. 275, no. 21, pp. 16213–8, May 2000.

[42] K. M. Hennessy, B. E. Pollot, W. C. Clem, M. C. Phipps, A. A. Sawyer, B. K. Culpepper, and S. L. Bellis, “The effect of collagen I mimetic peptides on mesenchymal stem cell adhesion and differentiation, and on bone formation at hydroxyapatite surfaces.,” *Biomaterials*, vol. 30, no. 10, pp. 1898–909, Apr. 2009.

[43] V. Agrawal, J. Kelly, S. Tottey, K. A. Daly, S. A. Johnson, B. F. Siu, J. Reing, and S. F. Badylak, “An isolated cryptic peptide influences osteogenesis and bone remodeling in an adult mammalian model of digit amputation.,” *Tissue Eng. Part A*, vol. 17, no. 23–24, pp. 3033–44, Dec. 2011.

[44] V. Agrawal, S. Tottey, S. A. Johnson, J. M. Freund, B. F. Siu, and S. F. Badylak, “Recruitment of progenitor cells by an extracellular matrix cryptic peptide in a mouse model of digit amputation.,” *Tissue Eng. Part A*, vol. 17, no. 19–20, pp. 2435–43, Oct. 2011.

[45] S. X. Hsiong, T. Boontheekul, N. Huebsch, and D. J. Mooney, “Cyclic arginine-glycine-aspartate peptides enhance three-dimensional stem cell osteogenic differentiation ,” *Tissue Eng. A*, vol. 15, no. 2, pp. 263–272, Feb. 2009.

[46] M. Kantlehner, P. Schaffner, D. Finsinger, J. Meyer, A. Jonczyk, B. Diefenbach, B. Nies, G. Holzemann, S. L. Goodman, and H. Kessler, “Surface coating with cyclic RGD peptides stimulates osteoblast adhesion and proliferation as well as bone formation ,” *Chembiochem*, vol. 1, no. 2, pp. 107–114, Aug. 2000.

[47] J. S. Lee, J. S. Lee, A. Wagoner-Johnson, and W. L. Murphy, “Modular peptide growth factors for substrate-mediated stem cell differentiation.,” *Angew. Chem. Int. Ed. Engl.*, vol. 48, no. 34, pp. 6266–9, Jan. 2009.

[48] J. S. Lee, A. J. Wagoner Johnson, and W. L. Murphy, “A modular, hydroxyapatite-binding version of vascular endothelial growth factor.,” *Adv. Mater.*, vol. 22, no. 48, pp. 5494–8, Dec. 2010.

[49] R. Fujisawa, M. Mizuno, Y. Nodasaka, and Y. Kuboki, “Attachment of osteoblastic cells to hydroxyapatite crystals by a synthetic peptide (Glu7-Pro-Arg-Gly-Asp-Thr) containing two functional sequences of bone sialoprotein.,” *Matrix Biol.*, vol. 16, no. 1, pp. 21–8, Apr. 1997.

[50] S. Segvich and D. H. Kohn, “Phage Display as a Strategy for Designing Organic/Inorganic Biomaterials,” in *Biological Interactions on Material Surfaces*, D. A. Puleo and R. Bizios, Eds. Springer US, 2009, pp. 115–132.

[51] A. Sergeeva, M. G. Kolonin, J. J. Molldrem, R. Pasqualini, and W. Arap, “Display technologies: application for the discovery of drug and gene delivery agents.,” *Adv. Drug Deliv. Rev.*, vol. 58, no. 15, pp. 1622–54, Dec. 2006.

[52] H.-E. Jin, W.-J. Chung, and S.-W. Lee, “Phage display for the discovery of hydroxyapatite-associated peptides.,” *Methods Enzymol.*, vol. 532, pp. 305–23, Jan. 2013.

[53] D. Khatayevich, M. Gungormus, H. Yazici, C. So, S. Cetinel, H. Ma, A. Jen, C. Tamerler, and M. Sarikaya, “Biofunctionalization of materials for implants using engineered peptides.,” *Acta Biomater.*, vol. 6, no. 12, pp. 4634–41, Dec. 2010.

[54] U. O. S. Seker, B. Wilson, J. L. Kulp, J. S. Evans, C. Tamerler, and M. Sarikaya, “Thermodynamics of engineered gold binding peptides: establishing the structure-activity relationships.,” *Biomacromolecules*, vol. 15, no. 7, pp. 2369–77, Jul. 2014.

[55] L. M. Alvarez, J. J. Rivera, L. Stockdale, S. Saini, R. T. Lee, and L. G. Griffith, “Tethering of Epidermal Growth Factor (EGF) to Beta Tricalcium Phosphate (βTCP) via Fusion to a High Affinity, Multimeric βTCP-Binding Peptide: Effects on Human Multipotent Stromal Cells/Connective Tissue Progenitors.,” *PLoS One*, vol. 10, no. 6, p. e0129600, Jan. 2015.

[56] R. N. Shah, N. a Shah, M. M. Del Rosario Lim, C. Hsieh, G. Nuber, and S. I. Stupp, “Supramolecular design of self-assembling nanofibers for cartilage regeneration.,” *Proc. Natl. Acad. Sci. U. S. A.*, vol. 107, no. 8, pp. 3293–8, Feb. 2010.

[57] J. Wang, M. Yang, Y. Zhu, L. Wang, A. P. Tomsia, and C. Mao, “Phage nanofibers induce vascularized osteogenesis in 3D printed bone scaffolds.,” *Adv. Mater.*, vol. 26, no. 29, pp. 4961–6, Aug. 2014.

[58] J.-Y. Lee, J.-E. Choo, Y.-S. Choi, J.-S. Suh, S.-J. Lee, C.-P. Chung, and Y.-J. Park, “Osteoblastic differentiation of human bone marrow stromal cells in self-assembled BMP-2 receptor-binding peptide-amphiphiles.,” *Biomaterials*, vol. 30, no. 21, pp. 3532–41, Jul. 2009.

[59] M. Gungormus, E. E. Oren, J. A. Horst, H. Fong, M. Hnilova, M. J. Somerman, M. L. Snead, R. Samudrala, C. Tamerler, and M. Sarikaya, “Cementomimetics-constructing a cementum-like biomineralized microlayer via amelogenin-derived peptides.,” *Int. J. Oral Sci.*, vol. 4, no. 2, pp. 69–77, Jun. 2012.

[60] S. J. Segvich, “Design of Peptides with Targeted Apatite and Human Bone Marrow Stromal Cell Adhesion for Bone Tissue Engineering.,” University of Michigan, 2008.

[61] S. Segvich, S. Biswas, U. Becker, and D. H. Kohn, “Identification of peptides with targeted adhesion to bone-like mineral via phage display and computational modeling.,” *Cells. Tissues. Organs*, vol. 189, no. 1–4, pp. 245–51, Jan. 2009.

[62] Y. Liu, K. de Groot, and E. B. Hunziker, “BMP-2 liberated from biomimetic implant coatings induces and sustains direct ossification in an ectopic rat model ,” *Bone*, vol. 36, no. 5, pp. 745–757, May 2005.

# CHAPTER TWO

# DUAL-FUNCTIONING PEPTIDES DISCOVERED BY PHAGE DISPLAY IMPROVE BMSC SPECIFIC ATTACHMENT TO MINERALIZED BIOMATERIALS

## INTRODUCTION

Cell based tissue regeneration is a promising alternative to auto-, allo- or xenografts [1], [2]. Regeneration of large defects *in vivo* using transplanted stem and progenitor cells is dependent on having a biomaterial carrier with surface properties that maximize cell attachment and promote cell growth, differentiation and formation of functional extracellular matrix (ECM) [3]–[6]. Additionally, designing a biomaterial that can promote adhesion of specific cell populations can improve the efficiency of cell based therapies [7].

In the context of bone tissue engineering, inorganic biomaterials and mineralized synthetic or natural polymers, as well as polymer-mineral composites are often used to deliver physical and chemical cues to drive osteogenesis [8]–[10]. Biomaterials with a mineral component provide a favorable environment for osteogenic differentiation of stem and osteogenic progenitor cells. Providing cell-specific and cell-instructive cues on the mineral component can further improve osteogenic differentiation and bone formation. For example, functionalizing mineralized

biomaterials with ECM proteins increases cell attachment, proliferation and differentiation, leading to increased bone healing [11]–[13].

Peptides derived from the functional domains of ECM proteins have been used to direct stem and progenitor cells toward a bone lineage [7], [11], [14], [15]. Peptide delivery methods involve adsorption, covalent immobilization or encapsulation into a biomaterial. The method of delivery along with post-synthesis modification involving cyclization, post-translational modification, and combining with other peptides play an important role in mediating cell responses (17). Adsorption is the primary mode of peptide delivery to mineral surfaces since covalent immobilization is not possible. Therefore the accessibility of cell binding domains once the peptide is delivered to a mineral substrate is an important design consideration.

Variability of peptide mediated cell attachment, proliferation, differentiation and tissue regeneration can be linked to both the lack of proper presentation of these sequences to cells and a lack of peptide specificity to certain sequences [16], [17]. For example, recapitulating the cyclized conformation of the RGD motif prevalent in native ECM proteins increases adsorption to biominerals, and also increases cell adhesion and subsequent bone formation when immobilized on alginate hydrogels [12], [18]. Furthermore, a competitive interaction between peptide coatings and serum proteins can have an inhibitory effect on tissue regeneration. For instance, RGD peptide coatings on HA reduce serum protein adsorption through charge-charge repulsions[19]. In addition to changing the structure of a peptide, a dual functioning peptide having a material adsorption component can independently control the presentation of the cell binding sequence to cell surface receptors [13], [20].

Many ECM proteins have multifunctional domains that work in conjunction with one another to present cell instructive domains to cell surface receptors. In addition to a cell binding sequence, incorporating a second sequence that tethers the peptide to a biomaterial can recapitulate these

ECM multifunctional domains. For example, peptide fragment 17-25 of the bone ECM protein osteocalcin contains 3 glutamic acid residues at positions 17, 21, and 24. These residues strongly bind hydroxyapatite and improve RGD, BMP, and VEGF derived peptide adsorption to biomineral surfaces [13], [15], [20], [21]. Increased control of cell binding peptide presentation to cell surface by combining them to appropriate material binding peptides can improve cell proliferation, differentiation and mineralization *in vitro* [21], [22].

Peptide sequence, post-translational modification, peptide conformation, and peptide loading method influence presentation of the cell instructive cues to the cell surface. By combining cell adhesive peptides with specific material binding domains, we can systematically control factors that influence cell recognition. This ability to systematically design specific peptides and appropriately present them to the cell surface can improve cell-material interactions, leading to greater quantity and quality of regenerated tissue *in vivo*.

We have identified peptides specific for human bone marrow stromal cells (hBMSC) (DPIYALSWSGMA, DPI) and apatite surfaces (VTKHLNQISQSY,VTK) using phage display**.** The primary aims of this study were to combine cell specific DPI sequence with VTK and measure apatite binding affinity, hBMSC adhesion strength, and specificity to hBMSCs when the apatite and cell-specific peptides are combined into a dual functioning peptide.

## MATERIALS AND METHODS

### BIOMATERIAL PREPARATION

Hydroxyapatite disks (HA) for the phage display experiments (10 mm diameter x 4 mm thick) were pressed from powder (Plasma Biotal Ltd. P220) at 1 metric ton for 1 minute and sintered at 1350°C for 5 hours (heating rate of 10°C/minute). Biomimetic apatite films were used to model a heterogeneous apatite surface similar to the inorganic bone microenvironment to characterize cell attachment. Apatite films were prepared by immersing PLGA thin films in simulated body fluid

to precipitate carbonate substitute apatite with plate like nanofeatures. A 5 w/v% 85:15 polylactic-co-glycolic acid (PLGA, Alkermes)-chloroform solution was cast on 15mm diameter glass slides. The PLGA films were etched in 0.5M NaOH and immersed in modified simulated body fluid (mSBF) for 5 days at 37°C with fluid changes every 24 hrs. The mSBF was made by dissolving the following reagents in Millipore water at 25°C and titrating to pH 6.8 using NaOH: 141 mM NaCl, 4.0 mM KCl, 0.5 mM MgSO4, 1.0 mM MgCl2, 4.2 mM NaHCO3, 5.0 mM CaCl2•2H2O, and 2.0 mM KH2PO4.

**CELL SOURCES AND CULTURE**

Clonally derived human bone marrow stromal cells (hBMSC), were a generous gift from the NIH[23], [24]. Murine bone marrow stromal cells(mBMSCs) were harvested from femora and tibiae of 5-6 week old C57/BL 6 mice (Jackson Laboratories). All BMSCs were maintained in alpha minimum essential media (α-MEM) (Gibco, #12561) with glutamine containing 20% fetal bovine serum (FBS) and antibiotics (100 U/mL penicillin, 0.1 mg/mL streptomycin (P/S)) (Gibco, #15140) at 37°C in a 5% CO2 incubator. Induced Pluripotent Stem Cell derived MSCs (IPS-MSC) were a generous gift from Dr. Paul Krebsbach. IPS-MSCs were maintained in (**α**-MEM), 20% FBS, antibiotics, 200mM L-glutamine, and 10mM non-essential amino acids. MC3T3-E1 and mouse dermal fibroblasts (MDFs) were a gift from Dr. Renny Franceschi. MC3T3-E1 cells and mouse dermal fibroblasts were cultured in alpha minimum essential media (**α**-MEM), 10% FBS, and antibiotics. All cells were passaged when they reached 80-90% confluence. Media was replaced every 2-3 days.

**PEPTIDE SYNTHESIS**

Single and dual function experimental and control peptides were synthesized using solid phase synthesis and protective chemistry (Table 2.1). High performance liquid chromatography was used to verify > 95% purity. Peptides were stored at -20$^{o}$C until use in each experiment.

**LANGMUIR ISOTHERMS**

Peptides were solubilized in water and diluted in Trizma buffer (pH 7.5). Photometric readings for peptide standard curves and samples were taken at 25$^{o}$C using a multi-well plate reader measuring UV absorbance from 205-240nm at 5nm increments. The absorbance wavelength that produced the best linear curve fit for standards was used to calculate sample concentrations before and after the adsorption assay. This wavelength varied between 205-215nm for single peptides and 230-235nm for dual peptides. Isotherm studies were conducted using HA powder with an average particle size of 18-30 μm and a surface area of 50m$^2$/g suspended in Trizma buffer pH 7.5 for 2-3 hrs at 37$^{o}$C prior to experiments. A powder presents a relatively high surface to volume ratio allowing less peptide usage in a smaller volume. Adsorption assays were conducted by incubating an HA suspension and peptide solution in a 96-well Millipore filter plate for 3hr at 37$^{o}$C under agitation. Solution was filtered into a fresh 96-well plate and the amount of unbound peptide was determined using UV absorbance and standards. Bulk peptide concentrations tested ranged from 0-2000μg/mL. Material specific peptides demonstrated no affinity towards tissue culture polystyrene surfaces, negating the possibility of non-specific binding. To assess peptide affinity to apatite, Langmuir isotherms of bulk versus bound peptide were constructed to determine binding affinity (1/$K_D$) and maximal adsorption concentration ($V_{max}$) using the following equation: [25], [26]

$$\frac{Cb}{Cs} = \frac{Kd + Cb}{Vmax}$$

Where Cb is the bulk concentration of peptide and Cs is the concentration of peptide bound to substrate, and $K_D$ is the dissociation constant. Two experiments were done, each with 3 replicates(n=6). The Gibbs free energy of adsorption $\Delta G^0_{ads}$ was calculated as previously described[27] using the following equation:

$$\Delta G^0_{ads} = -RT \ln(\frac{C_{solv}}{K_D})$$

Where the gas constant (R) = 8.314 J $mol^{-1}$ $K^{-1}$, ambient temperature (T) = 310 K, and the molar concentration of solvent water is $C_{solv}$ = 55.5 mol $L^{-1}$.

**CELL ATTACHMENT ASSAYS**

Biomimetic apatite films were incubated in dd$H_2O$ overnight to remove excess salts, and then incubated in Trizma buffer prior to use. Mineralized films were attached to the bottom of 24 well plates with sticky tabs. Films were subsequently incubated in 100 μg/mL of peptide solution for 3 hrs, washed and blocked with 1% denatured BSA to reduce non-specific cell attachment. The amount of peptide on apatite coated films was quantified using UV absorbance and a BCA assay. Loading efficiency on biomimetic apatite was not significantly different across peptide groups. Cell centrifugation assays using hBMSCs, IPS-MSCs, mBMSCs, MC3T3s and MDFs were conducted using a seeding density of 35,000 cells/$cm^2$. Peptide coated films, no peptide controls, and films used for standard curves were incubated with cells for 3hrs at 37°C and 5% $CO_2$ in serum-free media. Peptide coated films and no-peptide controls were subsequently washed, wells were filled with PBS, inverted, sealed and centrifuged with forces of $10^{-8}$ $10^{-7}$ dynes using an Eppendorf 5810r centrifuge[28], [29]. At forces above $10^{-6}$ dynes, mineral and FITC-BSA were washed away. Detached cells were removed, and cell numbers on peptide coated films, no peptide controls and standard curves were determined using the WST-1 assay (Clontech Laboratories, Inc.). Adherent cell fractions on peptide coated apatite groups were normalized to no-peptide biomimetic apatite film controls at each centrifugation speed. Half-cell detachment forces ($\tau_{50}$) were calculated by fitting the remaining adherent cell fraction(%) to sigmoidal curves using the Boltzmann equation.

$$y = \frac{L_1 + (L_1 - L_2)}{\left(1 + e^{\left(\frac{x - x_0}{dx}\right)}\right)}$$

Where L1 = lower asymptote, L2 = upper asymptote, $x_0$ is the inflection point, and $dx$ is the slope at the inflection point. A least squares regression with the current data allows for determination of these parameters. The $\tau_{50}$ values, detachment force where 50% cells are detached, are determined using these parameters. Using excel solver, a least squares regression was done with bounded constraints on x0.

**CELL MORPHOLOGY AND IMMUNOHISTOCHEMISTRY**

A range of hBMSC seeding densities spanning 1,000-50,000 cells/cm$^2$ was used to demonstrate the interplay between initial cell seeding density and seeding efficiency on dual-peptide coated apatite surfaces. Mineralized peptide coated and uncoated controls containing adherent cells from detachment forces assays and seeding density experiments were washed twice in PBS, fixed in 10% formalin buffer, permeabilized in Triton X, and stained with Rhodhamine-Pholloidin(ThermoFisher Scientific) for F-Actin and mounted in Vectashield containing DAPI (Vectorlabs) on glass coverslips. Images were acquired with a NIKON Ti-Eclipse Confocal Microscope using a 20x objective. Images from 4 samples per group and 10 fields per sample(n=40) were analyzed using Image J software (NIH). Each field was analyzed for cell number using the dapi stain, total cell spread area marked by F-actin stain, and total cell spread area per cell was calculated from the initial two measurements.

**STATISTICAL METHODS**

Single factor ANOVA was used to determine differences in binding affinity, half-cell detachment forces and quantitative histomorphometry amongst the different peptides using Sigmastat. Two-way ANOVA on ranks with Tukey test pairwise comparisons and interactions was used to determine differences and interaction between peptide groups across seeding densities.

# RESULTS

## PEPTIDE BINDING ISOTHERMS ON HA

Mineral binding and dual peptides reached an adsorption equilibrium between 0-1000µg/mL indicating apatite saturation (Fig 2.1a,b). The phosphorylated mineral specific sequence $VTK_{phos}$ demonstrated a greater binding affinity to apatite than VTK (Table 2.2). The concentration required to reach the equilibrium condition is lower for $VTK_{phos}$ than for VTK. The dual-functioning phage derived peptides DPI-VTK ($p<0.001$), DPI-$VTK_{phos}$, ($p <0.01$) and dual functioning peptide with cell binding control RGD-VTK ($p < 0.01$) demonstrated higher binding affinities than the single peptides. DPI-VTK had a lower $K_D$ than DPI-$VTK_{phos}$ ($p < 0.01$). Although the acidic residues in E7 bind strongly with the cationic components of HA, the binding affinity of RGD-E7 was lower than predominantly charge neutral RGD-VTK and DPI-VTK ($p<0.01$).

Values for $V_{max}$ were within the range of reported monolayer adsorption concentrations for proteins and peptides [25], [26]. Moreover, calculated $V_{max}$ values based on cross-sectional area of each peptide in a linear and cyclic conformation fall within the range of experimentally observed values(Table 2.2). $V_{max}$ for single peptides was higher than dual peptides ($p < 0.01$) with the exception of RGD-E7.

## CELL ADHESION STRENGTH ON DUAL-PEPTIDE COATED MINERAL

Dual peptides RGD-VTK and RGD-E7 yielded the highest cell attachment when no force was applied compared to remaining peptide coated and control groups (Fig. 2.2a, $p < 0.01$). However, as forces were applied, larger cell fractions were adherent to DPI-VTK compared to other peptide coated and control groups. Consequently, $\tau 50$ for the DPI-VTK sequence was higher than for the rest of the peptides (Fig. 2.2b, $p<0.01$).

HBMSCs exhibited a more spread morphology on RGD-VTK, DPI-VTK and RGD-E7 compared to other peptides (Fig. 2.2c). The total surface area covered by cells was greater on RGD-VTK and RGD-E7 coated surfaces, however, spread area/cell was greater on DPI-VTK compared to RGD-VTK and RGD-E7 (Fig. 2.2d,e $p<0.01$).

**HBMSC SPECIFICITY TO DUAL-PEPTIDE COATED MINERAL**

HBMSCs, mBMSCs and IPS-MSCs bound more strongly to DPI-VTK than murine pre-osteoblasts and fibroblasts (Fig. 2.3a, $p<0.01$). RGD-VTK bound weakly to hBMSCs, however it promoted stronger adhesion to MC3T3s and MDFs than DPI-VTK ($p < 0.01$). Although IPS-MSC adhesion to DPI-VTK was greater than to RGD-VTK ($p < 0.01$), IPS-MSCs demonstrated similar adhesion strength on RGD-VTK compared to pre-osteoblasts and fibroblasts.

HBMSC morphology on DPI-VTK and RGD-VTK (Fig. 2.2c) was rounder and less spread compared to mBMSC and IPS-MSC morphology on these peptides (Fig. 2.3b). MC3T3s and MDFs spread more on RGD-VTK compared to DPI-VTK. Conversely, MSCs spread more on DPI-VTK compared to RGD-VTK. Total cell spread area was greater on RGD-VTK compared to DPI-VTK across all cell types ($p < 0.01$), with the exception of mBMSCs. However, spread area normalized to number of MSCs was greater on DPI-VTK compared to RGD-VTK and the converse relationship was observed with MC3T3 and MDFs (Fig. 2.3c).

HBMSCs on RGD-VTK had higher total cell spread area than MC3T3 and MDF. This indicates that more hBMSCs bound RGD-VTK, but MC3T3s and MDFs bound and spread more favorably on these surfaces. This could arise from interplay between cell spreading and cell density after initial cell attachment.

**MSC ADHESION DEPENDENCE ON CELL SEEDING DENSITY**

Adherent cell numbers are dependent on peptide groups and initial cell seeding density ($p<0.001$). The total cell coverage area is correlated with initial cell seeding density ($p < 0.05$)

which is stronger than the correlation between spread area per cell and initial seeding density. The interaction between initial seeding density, initial cell attachment and spread area per cell can be observed at the higher seeding densities 50, 40, and 30 k cells/$cm^2$(Fig. 2.4a). DPI-VTK improves initial cell attachment on apatite compared to VTK. However at 50k cells/$cm^2$, although the total spread area is higher on DPI-VTK, there is equivalent spread area/cell to that of VTK (Fig. 2.4 b,c). This indicates a surface saturation of hBMSCs on VTK. HBMSCs exhibit more spreading on DPI-VTK at 40k cells/$cm^2$ compared to 50k cells/$cm^2$ but spread area/cell on DPI-VTK and VTK at 50k cells/$cm^2$ is not significantly different. Moreover, there is no significant difference between spread area/cell between HBMSCs on DPI-VTK at 30k cells/$cm^2$ and HBMSCs on VTK at 50k cells/$cm^2$. Trends in spread area per cell between both peptides across various densities are aligned with data attained at a seeding density of 37.5 k cells/$cm^2$ for cell centrifugation assays.

## DISCUSSION

HBMSC specific peptide sequences were identified using a combinatorial phage display. Apatite-specific peptide sequences were similarly identified using a combinatorial phage display [30] and in this study were combined with cell-specific sequences to create dual functioning peptides with one domain having preferential affinity for a specific material chemistry and a second domain having preferential affinity for a specific cell population.

Both cell and mineral binding domains contributed to the binding of dual functioning peptides to apatite (Table 2.2). Phosphorylation is a common post translational modification in natural ECM peptides and proteins that interact with mineral [16], [31]. Molecular dynamics simulations of dentin phosphoproteins(DPP) reveal un-phosphorylated DPP peptide derivatives are more mobile, flexible, and can fold over HA surfaces however phosphorylated peptides drive mineral association [32]. Although phosphorylation drives apatite binding affinity of DPP and osteopontin derived ASARM peptides, it is the glutamic and aspartic acid residues that are

involved in binding the apatite surface [32], [33]. These data indicate the interplay between sequence, conformation, charge distribution and apatite affinity of phosphorylation which could all be contributing to the differences between DPI-VTK and DPI-$VTK_{phos}$ compared to $VTK_{phos}$ and VTK. Moreover, RGD-E7, which has an acidic mineral binding motif, had the lowest binding affinity amongst the dual functioning peptides. The $K_D$ values for RGD-E7 (Table 2.2) are consistent with studies using similar materials and assay conditions [21]. Conformational and charge distributions of bound peptide could also be contributing to the differences in $V_{max}$. Single peptides can pack more efficiently because of smaller size, however the increased saturation concentration of RGD-E7 could be a result of non-Langmuir kinetics and potential aggregation in the solution state. Taken together, peptide sequence and conformation also contribute to packing efficiency.

The half-cell detachment force is the force at which 50% of the initially bound cell population becomes detached. Detachment forces are a surrogate for how strongly cells attach to the substrate. The strength of attachment is related to the formation of specific peptide and cell surface receptor interactions. Since the adhesion timeframe in serum-free media allows for initial attachment only, the detachment force correlates with the average number of peptide-cell ligand interactions over a population of cells [29]. The dual-functioning phage derived peptide DPI-VTK had the highest hBMSC adhesion strength (Fig. 2.3b). Although VTK and $VTK_{phos}$ exhibited similar initial attachment to DPI-VTK, they did not exhibit the same level of adhesion strength as DPI-VTK. This indicates that adhesion strength of cells to DPI-VTK is largely driven by the interaction with the DPI domain of the peptide.

Moreover, the weaker attachment of hBMSCs to DPI-$VTK_{phos}$ compared to DPI-VTK (Fig. 2.3b) indicates that phosphorylating the mineral sequence compromises the presentation of the DPI sequence to the cell. Favorable binding to apatite and improved adhesion strength to hBMSCs of DPI-VTK, compared to DPI-$VTK_{phos,}$ indicates an involvement indirect effect of the

cell specific sequence on mineral association and an indirect effect of mineral sequence in directing cell association. For instance, adding DPI to the VTK sequence could lead to conformational changes to either the mineral or cell binding sequences that enhance mineral binding affinity. Once bound, association with the biomimetic apatite could cause another structural change in either DPI or VTK, resulting in a change in affinity to cell binding targets. Structural changes occur in both solution and apatite-bound states and can drive adsorption of peptides [34]–[36].

More hBMSCs were initially bound to RGD-VTK, RGD-E7, DPI-VTK, and DPI-VTKphos compared to VTK and VTKphos (Fig. 2.3a). The increase in cell attachment to these peptides also indicates that hBMSC cell surface receptors bind to both DPI and RGD peptides, as expected. Although there was less initial cell attachment on DPI-VTK compared to RGD-VTK, DPI-VTK was more favorable for cell spreading (Fig. 2.3d), a finding that also supports the adhesion data as force is applied (Fig. 2.3a). The prevalence of more spread cells indicates more cell-matrix interactions that result in stronger attachment forces.

The adhesion strength of MSCs to DPI-VTK was greater than to MC3T3-E1 cells and MDFs (Fig. 2.4a). This data indicates that the phage derived peptide has interactions that are specific to cell-surface receptors on MSCs, and verifies that phage display is capable of yielding cell-specific peptide sequences. Although hBMSCs demonstrated higher initial attachment to RGD-VTK and RGD-E7 (Fig. 2.3a), the weaker adhesion strength is indicative of weak association between hBMSC binding targets and RGD when presented with either E7 or VTK material binding sequences. Another driver of DPI-VTK specificity to MSCs could arise from differential integrin expression profiles of MC3T3c and MDFs compared to MSCs.

Initial cell seeding density plays a critical role in the degree of cell spreading. This supports the contributions of both cell-cell and cell-substrate interactions to cell adhesion. The

differences in hBMSC spreading on DPI-VTK and VTK at 50k, 40k, and 30k cells/$cm^2$ (Fig. 2.4) indicate an interaction between cell density and peptide function. HBMSCs are able to attach specifically to DPI-VTK and have sufficient room to spread below the seeding density of 30k - 40k cells/$cm^2$. However, as seeding density increased to 50k cells/$cm^2$, initial cell attachment was so prevalent that the cells were unable to spread past a critical threshold. Initial cell attachment, subsequent adhesion and spreading, and density of seeded cells all contribute to tissue regeneration.

Phage display identifies sequences that bind strongly to markers expressed on the cell surface. The absence of highly acidic residues in either set of sequences is an interesting outcome of the phage selection process. Phage display has been used to identify peptides that target biomaterials [37], [38], as well as stem, progenitor, carcinogenic and bacterial cells (22,23,34), and there is a bias for hydrophobic peptide selection [39]. The prevalence of hydrophobic sequences could be an artifact of the selection process and needs to be further explored. Although this hydrophobic bias seems counterintuitive for apatite binding, it could be a promising tool for biomolecule delivery. Peptides with acidic residues that react with the defined periodicity of $Ca^{2+}$ ions in the HA crystal lattice also interfere with the adsorption of serum proteins [19], [40]. For instance, RGD improves cell attachment, proliferation and differentiation in vitro, but has varied results in vivo. This could be both a function of how cells attach and spread on RGD covered surfaces and how the presence of RGD interferes with adsorption of serum proteins. Moreover, RGD is not specific to any particular cell type and can react with various integrin subunits. Therefore, using a hydrophobic mineral binding sequence like VTK to deliver a human bone marrow stromal cell specific sequence like DPI will not only anchor cell-specific sequences to HA surfaces, but could also allow adsorption of serum proteins and facilitate specific cell mediated tissue regeneration. The results collectively indicate that phage display can be used to

identify cell specific hBMSCs and material specific peptides that improve cell attachment and spreading on biomaterial surfaces, potentially leading to improved regeneration.

DPIYALSWSGMA was identified as a high MSC binding sequence. This peptide was combined with previously identified mineral binding sequence VTKHLNQISQSY to specifically recruit MSCs to biomimetic apatite substrates. The dual peptide DPI-VTK increased binding affinity to apatite compared to cell, mineral, and dual peptide controls. Moreover, DPI-VTK improved MSC attachment and specificity, and promoted cell promote spreading on apatite. These data demonstrate the utility of phage display to recruit specific cell populations to specific biomaterial substrates.

## ACKNOWLEDGEMENTS

We would like to thank Dr. Sergei Kuznetsov for the generous contribution of primary human bone marrow stromal cells and Dr. Paul Krebsbach for the induced pluripotent mesenchymal cells. Funded by NIH DE015411 and NIH DE13380.

## CHAPTER TWO TABLES

### TABLE 2.1 AIM 1 PEPTIDE PROPERTIES

| Peptide | Sequence | Description | MW (g/mol) | Net Charge | Acidic residues |
|---|---|---|---|---|---|
| VTK | VTKHLNQISQSY | Phage derived mineral binding sequence | 1417.59 | 1 | 2 |
| $VTK_{phos}$ | VTKHLNQIS**p**QS**p**Y | Phosphorylated phage derived mineral binding sequence (control) | 1577.55 | -3 | 2 |
| RGD | GRGDS | Cell binding control | 346.34 | 0 | 1 |
| DPI | DPIYALSWSGMA | Phage derived cell binding sequence | 1310.49 | -1 | 3 |
| DPI-VTK | GGDPIYALSWSGMAGG GSVTKHLNQISQSY | **Dual functioning phage derived peptide** | 3025.35 | 0 | 5 |
| DPI-$VTK_{phos}$ | GGDPIYALSWSGMAGG GSVTKHLNQIS**p**QS**p**Y | Dual functioning mineral binding control sequence | 3185.31 | -5 | 5 |
| RGD-VTK | GGRGDGGGSVTKHLNQ ISQSY | Dual functioning cell binding control | 2061.20 | 1 | 3 |
| RGD-E7 | EEEEEEEPRGDT | Dual functioning peptide control | 1448.00 | -7 | 8 |

**TABLE 2.2: BINDING ISOTHERM RESULTS**

| | $K_{d.}$ ($\mu M$) | $V_{max}$ ($\mu mol/cm^2$) | $\Delta G_{ads}$ (kJ)/mol | $r^2$ |
|---|---|---|---|---|
| VTK | 74.57±3.59 | 30.67±5.44 | -34.8 | 0.94 |
| VTKphos * | 32.67±1.69 | 21.49±4.35 | -37.0 | 0.93 |
| RGD-E7 | 74.13±3.47 | 328.86±54.39 | -34.9 | 0.95 |
| RGD-VTK** | 7.36±0.35 | 4.92±2.56 | -40.8 | 0.90 |
| DPI-VTKphos** | 5.04±0.55 | 30.05±6.41 | -41.8 | 0.97 |
| DPI-VTK*** | 2.68±0.57 | 17.94±3.22 | -43.4 | 0.93 |

* significantly different from RGD-E7 and VTK($p < 0.01$)

**significantly different from dual peptides * and ***($p<0.01$)

$\Delta G = -RT \ln(C_{solv}/Kd)$ $R = 8.314$ J mol$^{-1}$ K$^{-1}$ $T = 310$ K $C_{solv} = 55.5$ mol/L

## CHAPTER TWO FIGURES

### FIGURE 2.1 (A,B). LANGMUIR ISOTHERMS

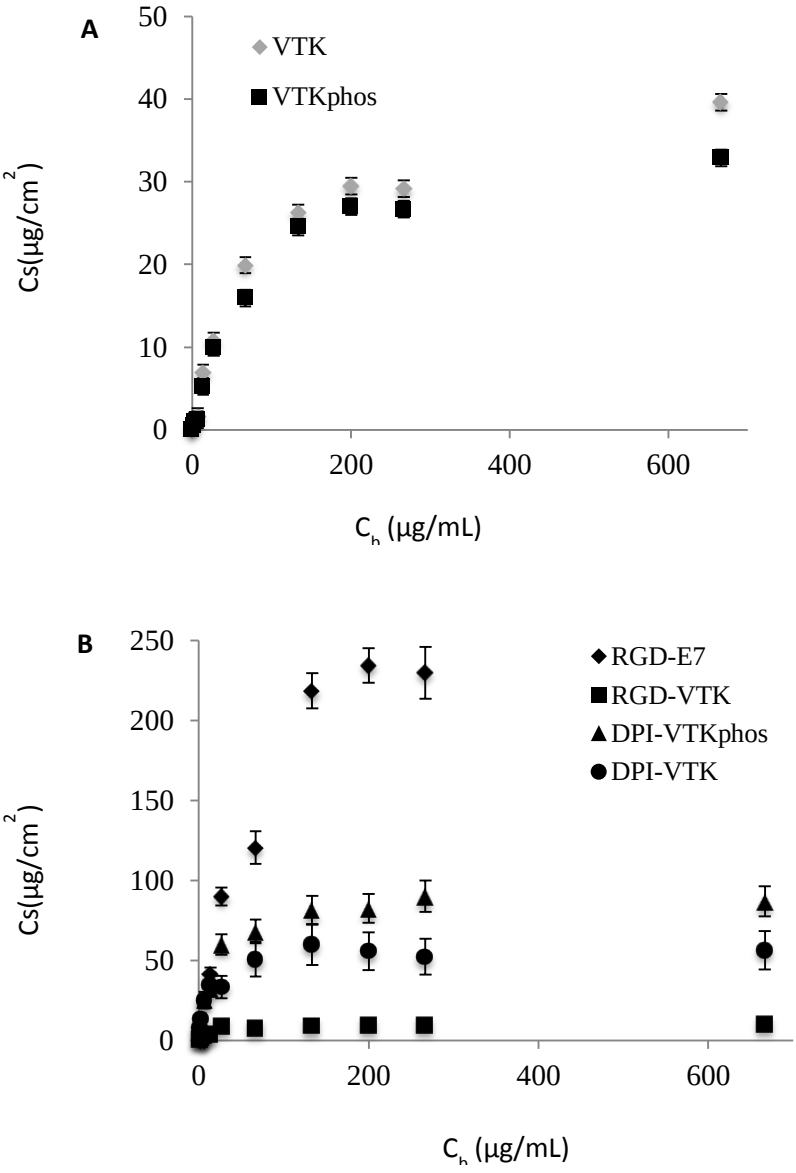


**Figure 2.1.** Langmuir isotherms of A)mineral binding and B)dual functioning peptides on HA powder. $C_b$ is the bulk concentration of peptide in solution and Cs is the bound concentration of peptide on hydroxyapatite particles. Data points represent triplicates from 2 separate adsorption studies (n=6).

**FIGURE 2.2(A-E). HBMSC ATTACHMENT, ADHESION STRENGTH AND SPREADING ON SINGLE AND DUAL-FUNCTIONING PEPTIDE COATED APATITE FILMS**

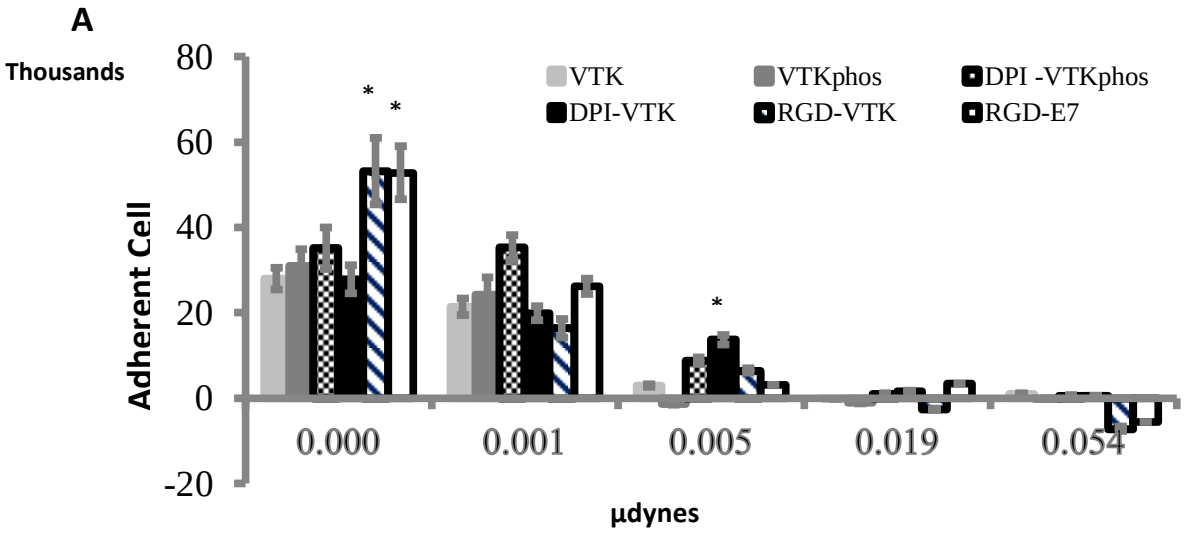


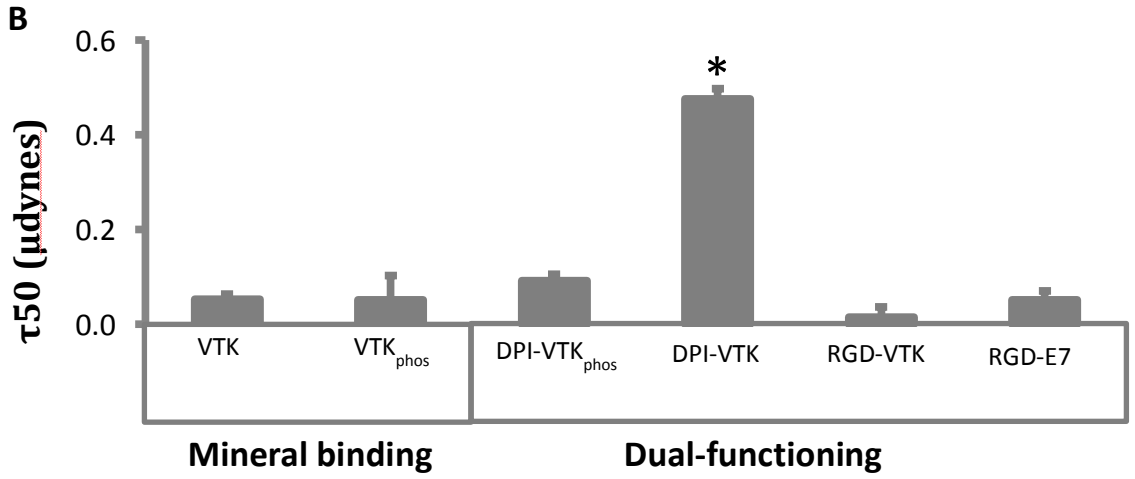

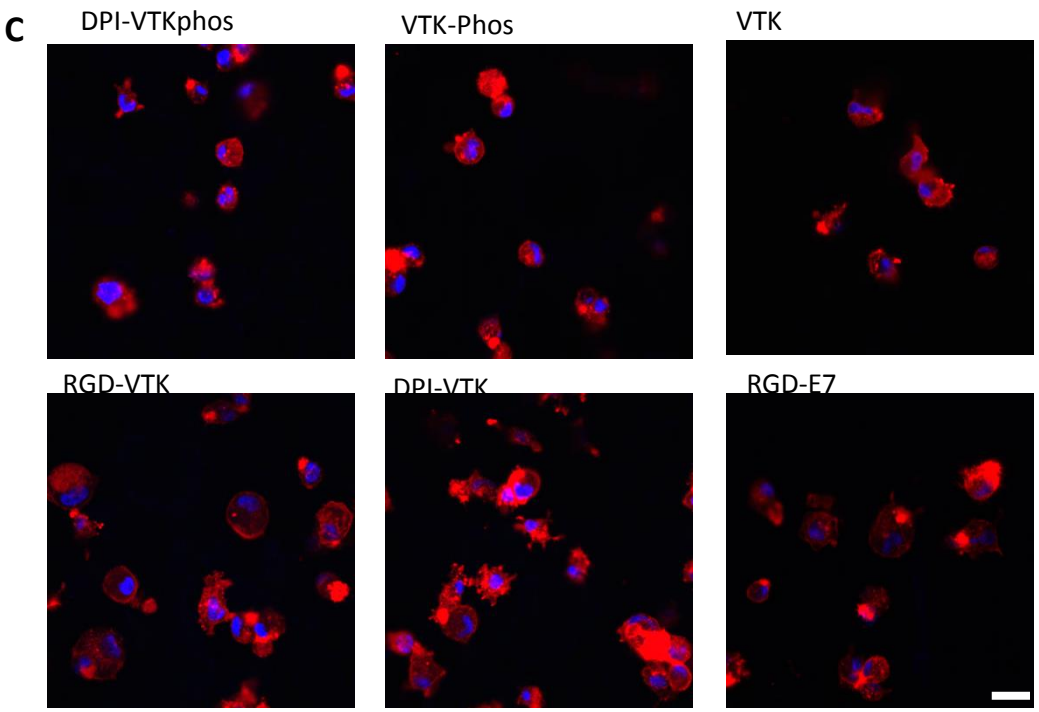
C
DPI-VTKphos
VTK-Phos
VTK
RGD-VTK
DPI-VTK
RGD-E7

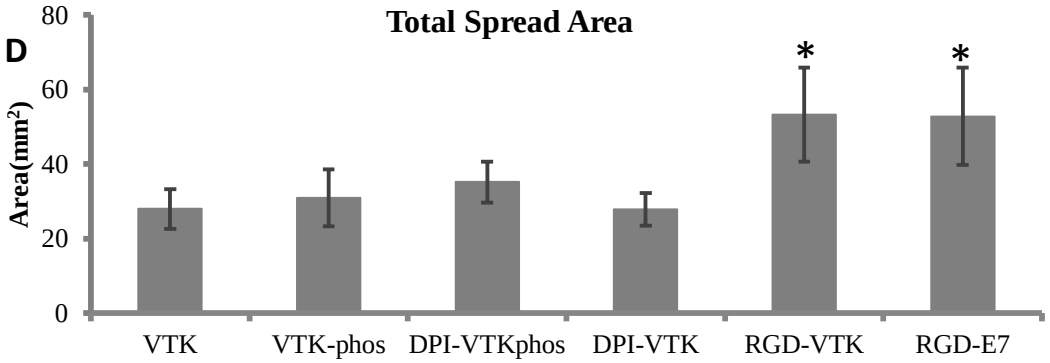
D
Total Spread Area
Area(mm²)
80
60
40
20
0
*
*
VTK
VTK-phos
DPI-VTKphos
DPI-VTK
RGD-VTK
RGD-E7

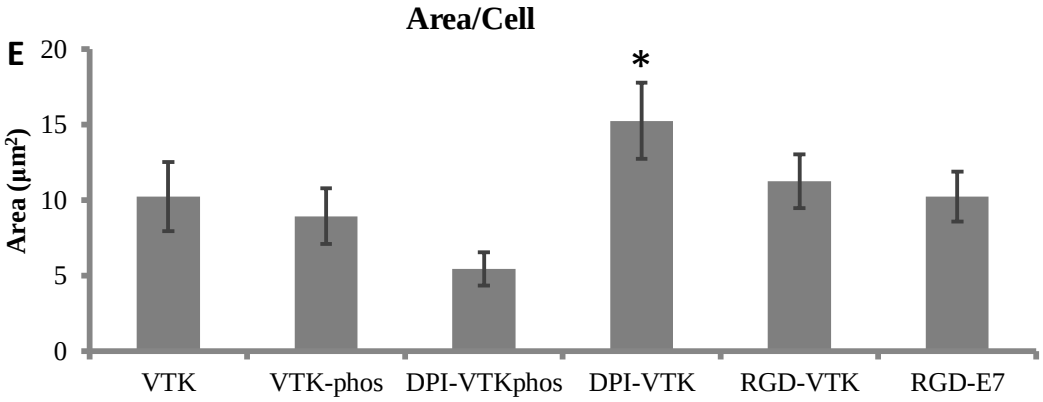
E
Area/Cell
Area (μm²)
20
15
10
5
0
*
VTK
VTK-phos
DPI-VTKphos
DPI-VTK
RGD-VTK
RGD-E7

**Figure 2.2.** HBMSC attachment, adhesion strength and spreading on single and dual-functioning peptide coated apatite films. A) Cell attachment across different peptide groups exposed to a range of detachment forces(n=6). *denotes significance from unmarked peptide groups within detachment forces ($p < 0.01$). B) Half-cell detachment forces calculated from sigmoidal curve-fitting of cell attachment data indicating force at which 50% of the initially adherent cell populations become detached (n=6). * denotes difference form remaining peptide groups ($p<0.01$). C) Representative confocal microscopy images at 40x depicting cell spreading on peptide coated apatite films. F-actin labeled with Rhodhamine-Pholloidin and nuclei labeled with DAPI. Scale bars 10μm. D) Total cell spread area calculated from Image J analysis of Pholloidin-stained area (n=4 per group x 10 FOV per sample). * denotes different from unmarked groups($p<0.01$) E) Area /cell calculated from Image J(NIH) analysis of Pholloidin-stained area (n=4 per group x 10 FOV per sample). * denotes different from unmarked groups($p<0.01$)

**FIGURE 2.3(A-D). MSC SPECIFIC ADHESION STRENGTH AND SPREADING ON DPI-VTK AND RGD-VTK COATED APATITE FILMS.**

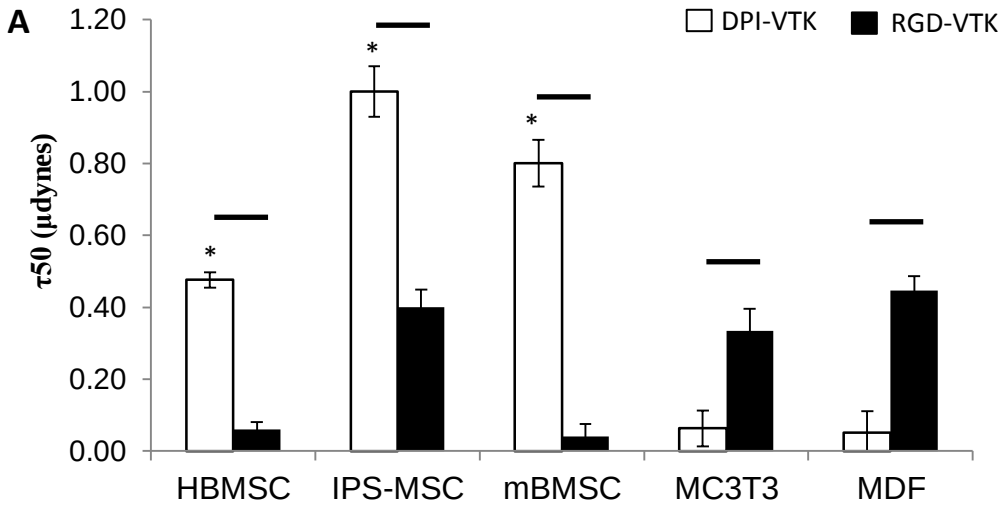


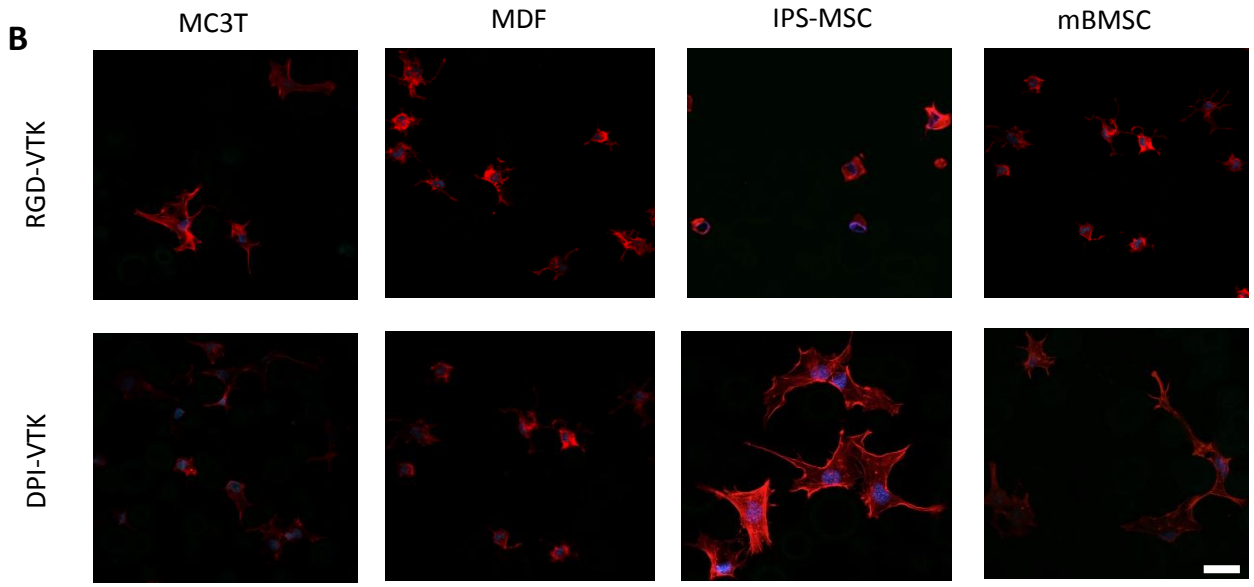

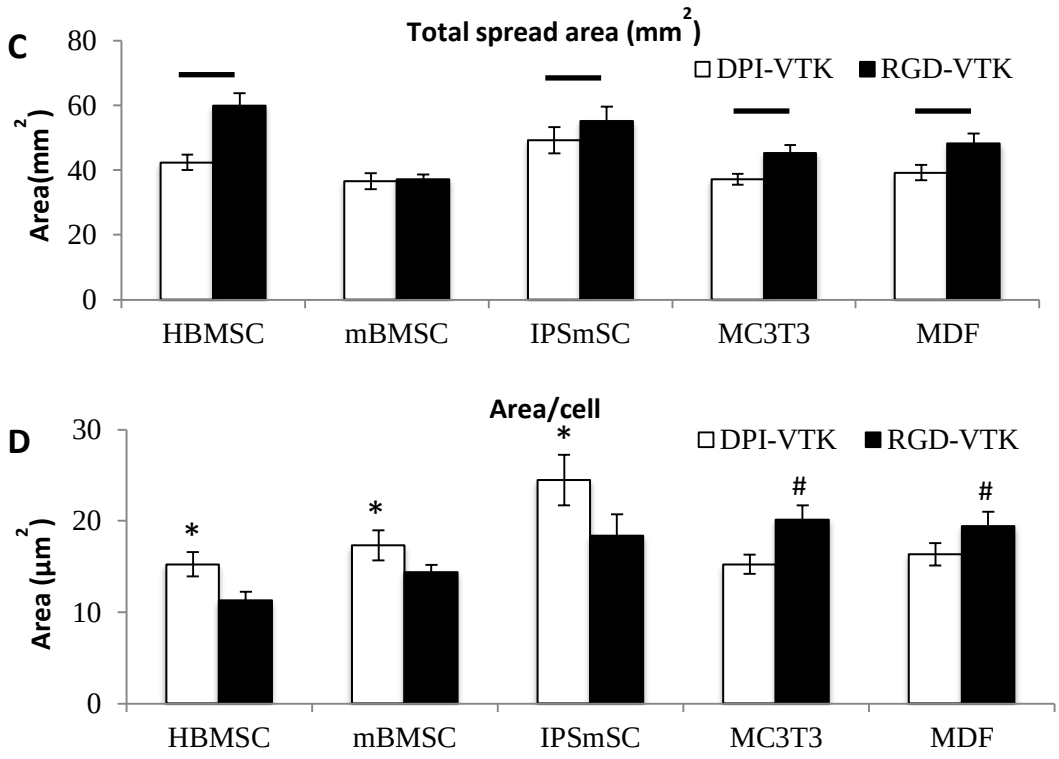


**Figure 2.3**. MSC specific adhesion strength and spreading on DPI-VTK and RGD-VTK coated apatite films. A) Half-cell detachment forces calculated from sigmoidal curve-fitting of cell attachment data indicating force at which 50% of the initially adherent cell populations become detached (n=6). Bars denote differences between peptide groups ($p < 0.01$). * denotes difference form MC3T3 and MDFs in peptide coated groups. B) Representative confocal microscopy images at 40x depicting spreading on peptide coated apatite films. F-actin labeled with Rho-Pholloidin and nuclei labeled with DAPI. Scale bars 10µm. C) Total cell spread area calculated from Image J analysis of Pholloidin-stained area (n=4 per group x 10 FOV per sample Bars denote difference within cell type ($p<0.01$). D) Area /cell calculated from Image J(NIH) analysis of Pholloidin-stained area (n=4 per group x 10 FOV per sample). * denotes greater than RGD-VTK($p<0.01$). # denotes greater than DPI-VTK ($p<0.01$).

**FIGURE 2.4(A-C). CELL SEEDING DENSITY EFFECTS ON CELL SPREADING ON VTK AND DPI-VTK COATED APATITE FILMS.**

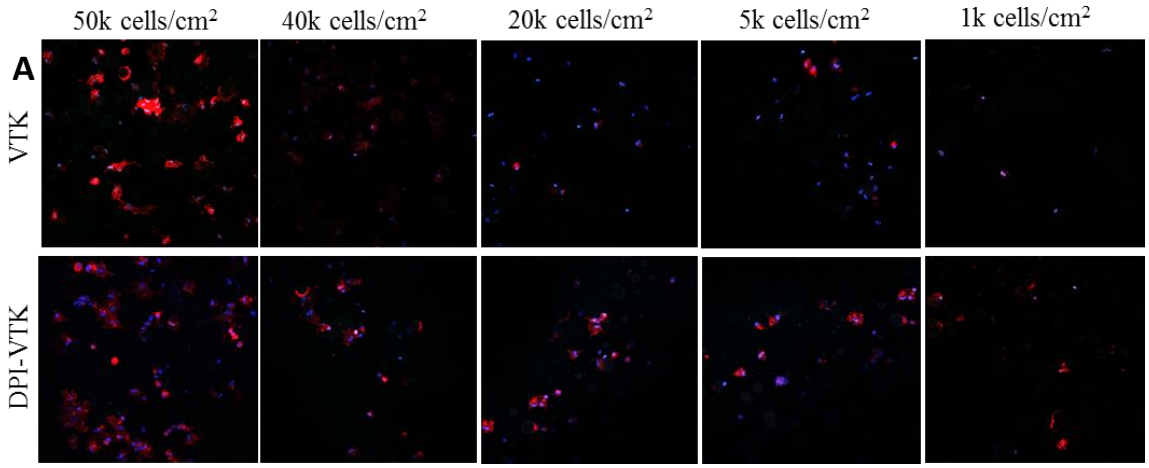


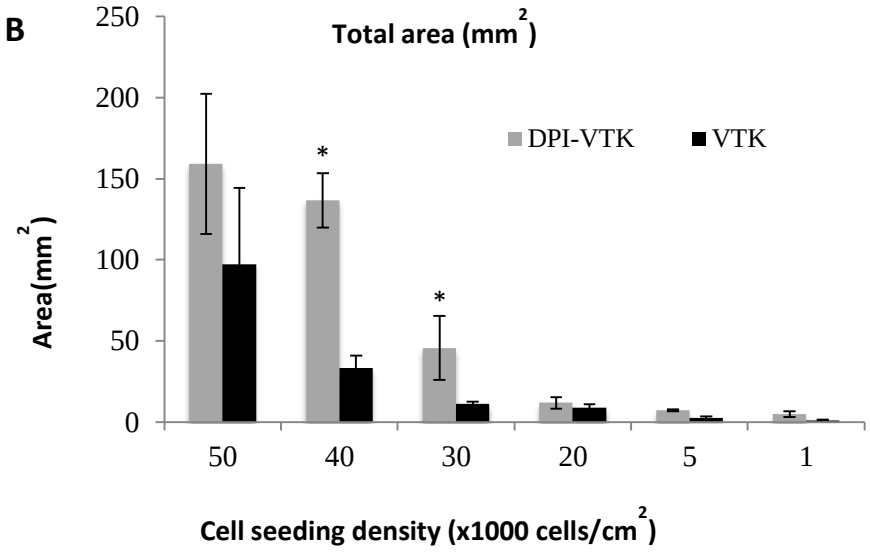

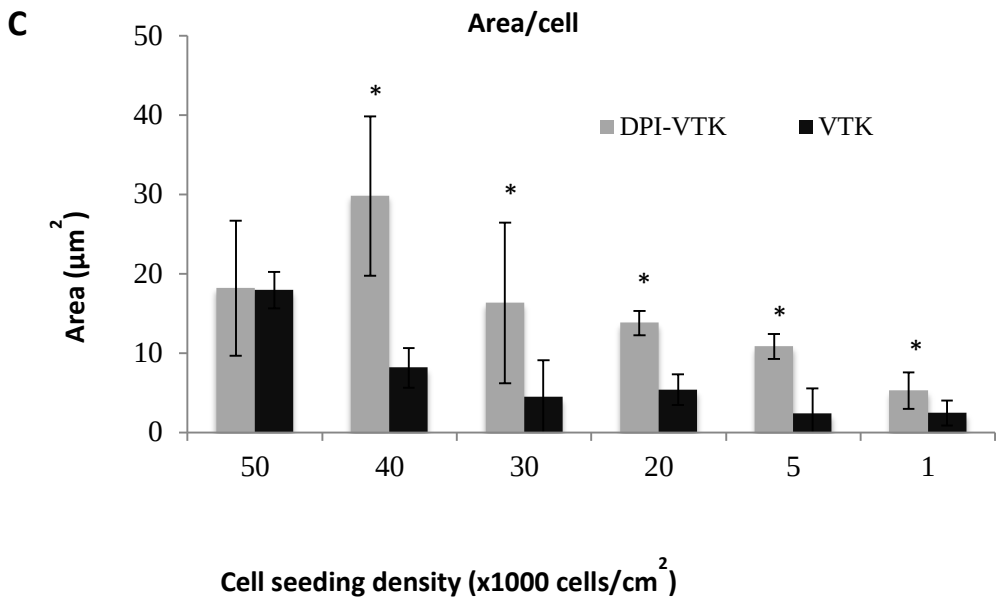


**Figure 2.4.** Cell seeding density effects on cell spreading on VTK and DPI-VTK coated apatite films. A) Representative confocal microscopy images at 20x depicting cell spreading on peptide coated apatite films. F-actin labeled with Rho-Pholloidin and nuclei labeled with DAPI. Scale bars 20µm. B) Total cell spread area calculated from Image J analysis of Pholloidin-stained area (n=4 per group x 10 FOV per sample Bars denote difference within cell type ($p<0.01$).* denotes difference from VTK ($p < 0.01$) C) Area/cell calculated from Image J(NIH) analysis of Pholloidin-stained area (n=4 per group x 10 FOV per sample). * denotes difference from VTK ($p < 0.01$)

# REFERENCES


[1] P. H. Krebsbach, S. a. Kuznetsov, P. Bianco, and P. Gehron Robey, “Bone Marrow Stromal Cells: Characterization and Clinical Application,” *Crit. Rev. Oral Biol. Med.*, vol. 10, no. 2, pp. 165–181, Jan. 1999.

[2] E. Alsberg, E. E. Hill, and D. J. Mooney, “Craniofacial tissue engineering.,” *Crit. Rev. Oral Biol. Med.*, vol. 12, no. 1, pp. 64–75, Jan. 2001.

[3] K. Kim, D. Dean, A. G. Mikos, and J. P. Fisher, “Effect of initial cell seeding density on early osteogenic signal expression of rat bone marrow stromal cells cultured on cross-linked poly(propylene fumarate) disks.,” *Biomacromolecules*, vol. 10, no. 7, pp. 1810–7, Jul. 2009.

[4] C. E. Wilson, W. J. A. Dhert, C. A. Van Blitterswijk, A. J. Verbout, and J. D. De Bruijn, “Evaluating 3D bone tissue engineered constructs with different seeding densities using the alamarBlue assay and the effect on in vivo bone formation.,” *J. Mater. Sci. Mater. Med.*, vol. 13, no. 12, pp. 1265–9, Dec. 2002.

[5] M. H. Mankani, S. A. Kuznetsov, B. Fowler, A. Kingman, and P. G. Robey, “In vivo bone formation by human bone marrow stromal cells: effect of carrier particle size and shape.,” *Biotechnol. Bioeng.*, vol. 72, no. 1, pp. 96–107, Jan. 2001.

[6] P. H. Krebsbach, S. A. Kuznetsov, K. Satomura, R. V Emmons, D. W. Rowe, and P. G. Robey, “Bone formation in vivo: comparison of osteogenesis by transplanted mouse and human marrow stromal fibroblasts.,” *Transplantation*, vol. 63, no. 8, pp. 1059–69, Apr. 1997.

[7] R. G. LeBaron and K. A. Athanasiou, “Extracellular matrix cell adhesion peptides: functional applications in orthopedic materials ,” *Tissue Eng.*, vol. 6, no. 2, pp. 85–103, Apr. 2000.

[8] S. J. Segvich and D. H. Kohn, *Biological Interactions on Materials Surfaces*. New York, NY: Springer US, 2009.

[9] Ramaswamy, J., Ramaraju, S., and Kohn D. H., “Bone-Like Mineral and Organically Modified Bone-Like Mineral Coatings,” in *Biological and Biomedical Coatings Handbook, Processing and Characterization*, S. Zhang, Ed. Boca Raton, FL: CRC Press, 2011, pp. 1–36.

[10] W. L. Murphy, D. H. Kohn, and D. J. Mooney, “Growth of continuous bonelike mineral within porous poly(lactide-co-glycolide) scaffolds in vitro.,” *J. Biomed. Mater. Res.*, vol. 50, no. 1, pp. 50–8, Apr. 2000.

[11] A. Shekaran and A. J. García, “Extracellular matrix-mimetic adhesive biomaterials for bone repair.,” *J. Biomed. Mater. Res. A*, vol. 96, no. 1, pp. 261–72, Jan. 2011.

[12] S. X. Hsiong, T. Boontheekul, N. Huebsch, and D. J. Mooney, “Cyclic arginine-glycine-aspartate peptides enhance three-dimensional stem cell osteogenic differentiation ,” *Tissue Eng. A*, vol. 15, no. 2, pp. 263–272, Feb. 2009.

[13] J. S. Lee, J. S. Lee, A. Wagoner-Johnson, and W. L. Murphy, “Modular peptide growth factors for substrate-mediated stem cell differentiation.,” *Angew. Chem. Int. Ed. Engl.*, vol. 48, no. 34, pp. 6266–9, Jan. 2009.

[14] M. P. Lutolf, F. E. Weber, H. G. Schmoekel, J. C. Schense, T. Kohler, R. Muller, and J. A. Hubbell, “Repair of bone defects using synthetic mimetics of collagenous extracellular matrices ,” *Nat. Biotechnol.*, vol. 21, no. 5, pp. 513–518, May 2003.

[15] D. Itoh, S. Yoneda, S. Kuroda, H. Kondo, A. Umezawa, K. Ohya, T. Ohyama, and S. Kasugai, “Enhancement of osteogenesis on hydroxyapatite surface coated with synthetic peptide (EEEEEEEPRGDT) in vitro.,” *J. Biomed. Mater. Res.*, vol. 62, no. 2, pp. 292–8, Nov. 2002.

[16] M. Gilbert, W. J. Shaw, J. R. Long, K. Nelson, G. P. Drobny, C. M. Giachelli, and P. S. Stayton, “Chimeric peptides of statherin and osteopontin that bind hydroxyapatite and mediate cell adhesion.,” *J. Biol. Chem.*, vol. 275, no. 21, pp. 16213–8, May 2000.

[17] P. S. Stayton, G. P. Drobny, W. J. Shaw, J. R. Long, and M. Gilbert, “Molecular Recognition At the Protein-Hydroxyapatite Interface,” *Crit. Rev. Oral Biol. Med.*, vol. 14, no. 5, pp. 370–376, Sep. 2003.

[18] M. Kantlehner, P. Schaffner, D. Finsinger, J. Meyer, A. Jonczyk, B. Diefenbach, B. Nies, G. Holzemann, S. L. Goodman, and H. Kessler, “Surface coating with cyclic RGD peptides stimulates osteoblast adhesion and proliferation as well as bone formation ,” *Chembiochem*, vol. 1, no. 2, pp. 107–114, Aug. 2000.

[19] K. M. Hennessy, W. C. Clem, M. C. Phipps, A. A. Sawyer, F. M. Shaikh, and S. L. Bellis, “The effect of RGD peptides on osseointegration of hydroxyapatite biomaterials.,” *Biomaterials*, vol. 29, no. 21, pp. 3075–83, Jul. 2008.

[20] J. S. Lee, A. J. Wagoner Johnson, and W. L. Murphy, “A modular, hydroxyapatite-binding version of vascular endothelial growth factor.,” *Adv. Mater.*, vol. 22, no. 48, pp. 5494–8, Dec. 2010.

[21] R. Fujisawa, M. Mizuno, Y. Nodasaka, and Y. Kuboki, “Attachment of osteoblastic cells to hydroxyapatite crystals by a synthetic peptide (Glu7-Pro-Arg-Gly-Asp-Thr) containing two functional sequences of bone sialoprotein.,” *Matrix Biol.*, vol. 16, no. 1, pp. 21–8, Apr. 1997.

[22] R. Fujisawa, Y. Wada, Y. Nodasaka, and Y. Kuboki, “Acidic amino acid-rich sequences as binding sites of osteonectin to hydroxyapatite crystals.,” *Biochim. Biophys. Acta*, vol. 1292, no. 1, pp. 53–60, Jan. 1996.

[23] S. A. Kuznetsov, M. H. Mankani, and P. G. Robey, “In vivo formation of bone and haematopoietic territories by transplanted human bone marrow stromal cells generated in medium with and without osteogenic supplements.,” *J. Tissue Eng. Regen. Med.*, vol. 7, no. 3, pp. 226–35, Mar. 2013.

[24] S. a Kuznetsov, P. H. Krebsbach, K. Satomura, J. Kerr, M. Riminucci, D. Benayahu, and P. G. Robey, “Single-colony derived strains of human marrow stromal fibroblasts form bone after transplantation in vivo.,” *J. Bone Miner. Res.*, vol. 12, no. 9, pp. 1335–47, Sep. 1997.

[25] B. . Young, W. . Pitt, and S. . Cooper, “Protein adsorption on polymeric biomaterials I. Adsorption isotherms,” *J. Colloid Interface Sci.*, vol. 124, no. 1, pp. 28–43, Jul. 1988.

[26] T. Tsai, R. C. Mehta, and P. P. Deluca, “Adsorption of peptides to poly(D,L-lactide-co-glycolide): 1. Effect of physical factors on the adsorption,” *Int. J. Pharm.*, vol. 127, no. 1, pp. 31–42, Jan. 1996.

[27] F. Meder, H. Hintz, Y. Koehler, M. M. Schmidt, L. Treccani, R. Dringen, and K. Rezwan, “Adsorption and Orientation of the Physiological Extracellular Peptide Glutathione Disul fi de on Surface Functionalized Colloidal Alumina Particles,” 2013.

[28] N. D. Gallant, “Stick and Grip,” *Cell Biochem. Biophys.*, vol. 39, no. 9, 2003.

[29] D. R. McClay and P. L. Hertzler, “Quantitative measurement of cell adhesion using centrifugal force.,” *Curr. Protoc. Cell Biol.*, vol. Chapter 9, p. Unit 9.2, May 2001.

[30] S. J. Segvich, H. C. Smith, and D. H. Kohn, “The adsorption of preferential binding peptides to apatite-based materials.,” *Biomaterials*, vol. 30, pp. 1287–1298, 2009.

[31] W. N. Addison, S. J. Miller, J. Ramaswamy, A. Mansouri, D. H. Kohn, and M. D. McKee, “Phosphorylation-dependent mineral-type specificity for apatite-binding peptide sequences.,” *Biomaterials*, vol. 31, no. 36, pp. 9422–30, Dec. 2010.

[32] E. Villarreal-Ramirez, R. Garduño-Juarez, A. Gericke, and A. Boskey, “The role of phosphorylation in dentin phosphoprotein peptide absorption to hydroxyapatite surfaces: a molecular dynamics study.,” *Connect. Tissue Res.*, vol. 55 Suppl 1, pp. 134–7, Aug. 2014.

[33] W. N. Addison, D. L. Masica, J. J. Gray, and M. D. McKee, “Phosphorylation-dependent inhibition of mineralization by osteopontin ASARM peptides is regulated by PHEX cleavage.,” *J. Bone Miner. Res.*, vol. 25, no. 4, pp. 695–705, Apr. 2010.

[34] D. L. Masica, J. J. Gray, and W. J. Shaw, “Partial High-resolution structure of phosphorylated and non-phosphorylated leucine-rich amelogenin protein adsorbed to hydroxyapatite,” *J. Phys. Chem. C*, vol. 115, pp. 13775–13785, 2011.

[35] W. N. Addison, D. L. Masica, J. J. Gray, and M. D. McKee, “Phosphorylation-dependent inhibition of mineralization by osteopontin ASARM peptides is regulated by PHEX cleavage.,” *J. Bone Miner. Res.*, vol. 25, pp. 695–705, 2010.

[36] D. L. Masica and J. J. Gray, “Solution- and adsorbed-state structural ensembles predicted for the statherin-hydroxyapatite system.,” *Biophys. J.*, vol. 96, no. 8, pp. 3082–91, Apr. 2009.

[37] M. C. Weiger, J. J. Park, M. D. Roy, C. M. Stafford, A. Karim, and M. L. Becker, “Quantification of the binding affinity of a specific hydroxyapatite binding peptide.,” *Biomaterials*, vol. 31, no. 11, pp. 2955–63, Apr. 2010.

[38] M. Gungormus, E. E. Oren, J. A. Horst, H. Fong, M. Hnilova, M. J. Somerman, M. L. Snead, R. Samudrala, C. Tamerler, and M. Sarikaya, “Cementomimetics-constructing a cementum-like biomineralized microlayer via amelogenin-derived peptides.,” *Int. J. Oral Sci.*, vol. 4, no. 2, pp. 69–77, Jun. 2012.

[39] K. Luck and G. Travé, “Phage display can select over-hydrophobic sequences that may impair prediction of natural domain-peptide interactions.,” *Bioinformatics*, vol. 27, no. 7, pp. 899–902, Apr. 2011.

[40] K. M. Hennessy, B. E. Pollot, W. C. Clem, M. C. Phipps, A. A. Sawyer, B. K. Culpepper, and S. L. Bellis, “The effect of collagen I mimetic peptides on mesenchymal stem cell adhesion and differentiation, and on bone formation at hydroxyapatite surfaces.,” *Biomaterials*, vol. 30, no. 10, pp. 1898–909, Apr. 2009.

# CHAPTER THREE

# PHAGE DISPLAY DERIVED BI-FUNCTIONAL PEPTIDE IMPROVES MSC ADHESION, PROLIFERATION AND DIFFERENTIATION ON APATITE

## INTRODUCTION

Cell based tissue regeneration strategies often require a biomaterial carrier with defined surface chemistries. With the proliferation of biomaterials and regenerative cell sources, it is important to recruit specific regenerative cell populations to specific biomaterial chemistries to meet clinical challenges[1]. In addition to attachment of specific cell populations, filling critical sized defects with adequate transplanted cell numbers becomes non-trivial. Improving the seeding efficiency of transplanted cell populations on biomaterial carriers can have a significant impact on reducing material requirements, healing time and healthcare costs[2].

Mesenchymal stem cells (MSCs) are a promising source for cell-based tissue regeneration [3], [4]. MSCs can form various tissues, including bone, cartilage, hematopoiesis-supporting stroma, and fat. In addition to multi-potent tissue formation, MSCs are immunomodulatory and can induce angiogenesis . Since their initial discovery in the bone marrow stromal niche, MSCs have been identified in various adult and neonatal tissues including but not limited to adipose tissue, peripheral blood, amniotic fluid, and umbilical cord[5]. MSCs can also be derived from embryonic and induced

pluripotent stem cell (iPS) lineages[6]–[8]. Furthermore, induced pluripotent stem cell derived MSCs (iPS-MSCs) provide a more continuous supply compared to other sources of MSCs since they can be programmed from more readily available somatic sources. MSCs are characterized by their ability to adhere to plastic, proliferate readily in vitro and form multi-lineage tissue *in vivo.* A profile of cell surface markers, STRO-1, CD146, CD105, CD49a, positive for human bone marrow stroma and, $CD34^{-}$, $CD45^{-}$, $CD14^{-}$, negative for hematopoietic and endothelial lineages are also used to verify MSC sub-populations[9]. However, there are no markers or set of markers that can separate multipotent MSCs from non-multipotent MSCs[10], [11].

Improving specific attachment of multipotent MSCs to biomaterials towards cell-based therapies can improve *in vivo* tissue regeneration outcomes. In the context of bone tissue regeneration, materials containing a mineral component are used to mechanically and chemically support transplanted cell populations. Precipitation of a heterogeneous layer of biomimetic apatite on biomaterial surfaces by immersion in simulated body fluid (SBF) under physiological conditions improves osteoconductivity and mechanical properties of the underlying substrate[12], [13]. Adsorption of extracellular matrix cell binding proteins, functional peptide domains, and peptide motifs onto biomaterial surfaces can further enhance cell attachment[14], [15]. Mineral binding peptide domains and peptide motifs are also adsorbed to mineral surfaces to improve delivery of cell signals[16], [17]. Furthermore, peptide-based strategies to target $\alpha 2\beta 1$ integrin domains that are highly expressed in MSCs have been used to improve cell-specific attachment to mineral[18], [19]. In addition to being osteoconductive, these peptides exhibit

osteoinductivity by mechanotransductively regulating osteogenic signal transduction cascades within adherent MSCs[19]–[21].

However ECM peptide domains targeting integrins do not exhibit cell specificity; rather, they target cell surface receptors prevalent across many cell types. Using a combinatorial phage display we have identified peptides specific towards multipotent-MSCs clonally derived from human bone marrow stromal cells (hBMSC) (DPIYALSWSGMA, DPI) and apatite surfaces (VTKHLNQISQSY,VTK) and demonstrated conserved mineral and cell specificity when the peptides are combined into a single dual-functioning peptide (DPI-VTK)[22], [23] . In addition to mediating cell-specific attachment to apatite surfaces, in vitro spreading, proliferation, and differentiation are important indicators of biological performance. This study characterizes multi-potent MSC spreading and cytoskeletal contact distribution in the presence and absence of serum proteins, identifies biological targets for DPI mediated MSC attachment, assesses MSC proliferation and differentiation on DPI-VTK coated biomimetic apatite surfaces, and examines selectivity towards multi-potent MSC subpopulations.

## MATERIALS AND METHODS

### MINERALIZED FILM FABRICATION

Biomimetic apatite films were used to characterize cell adhesion, proliferation and differentiation *in vitro*. Apatite films were prepared by immersing PLGA thin films in simulated body fluid to precipitate carbonated apatite with plate like nanofeatures. A 5 w/v% 85:15 polylactic-co-glycolic acid (PLGA, Lakeshore Biomaterials)-chloroform solution was cast on 15mm diameter glass slides. The PLGA films were etched in 0.5M

NaOH and immersed in modified simulated body fluid (mSBF) for 5 days at 37°C with fluid changes every 24 hrs. The mSBF was made by dissolving the following reagents in Millipore water at 25°C and titrating to pH 6.8 using NaOH: 141 mM NaCl, 4.0 mM KCl, 0.5 mM $MgSO_4$, 1.0 mM $MgCl_2$, 4.2 mM $NaHCO_3$, 5.0 mM $CaCl_2 \cdot 2H_2O$, and 2.0 mM $KH2PO_4$.

**PEPTIDE SYNTHESIS AND ADSORPTION TO BONE-LIKE MINERAL**

Single, dual-function, and fluorescently labeled peptides were synthesized using solid phase synthesis and protective chemistry (Table 3.1). HPLC was used to verify > 95% purity. Peptides were stored at -20$^{o}$C until use. HBMSC specific peptide sequences were combined with previously identified mineral binding sequences VTK and VTKphos(Chapter 2). Films were subsequently incubated in 100 μg/mL of peptide solution for 3 hrs, washed and blocked with 1% denatured BSA to reduce non-specific cell attachment. The amount of peptide on apatite coated films was quantified using UV absorbance and a Pierce™ BCA assays (ThermoFisher Scientific ). Loading efficiency on biomimetic apatite was not significantly different across peptide groups 12.35±3nmol.

**CELL CULTURE**

Clonally derived human bone marrow stromal cells (hBMSC), were a generous gift from the NIH[24], [25]. Cells were maintained in alpha minimum essential media (α-MEM) (Gibco, #12561) with glutamine containing 20% fetal bovine serum (FBS) and antibiotics (100 U/mL penicillin, 0.1 mg/mL streptomycin (P/S)) (Gibco, #15140) at 37°C in a 5% CO2 incubator. Induced Pluripotent Stem Cell derived MSCs (iPS-MSC) verified for multi-potency were a generous gift from Dr. Paul Krebsbach[7]. iPS-MSCs were maintained in (**α**-MEM), 20% FBS, antibiotics, 200mM L-glutamine, and 10mM NEAA.

Cells were cultured in alpha minimum essential media (**α**-MEM), 10% FBS, and antibiotics. Cells were passaged when they reached 80-90% confluence was replaced every 2-3 days. Human bone marrow stromal cells were plated at 3000 cells/$cm^2$ for spreading (n=6/group) and proliferation assays (n=6/group). Mineralized films were held in place with Teflon O-rings for proliferation assays to prevent films from floating.

**COMPETITIVE ADHESION OF MSC**

iPS-MSCs were incubated in the presence of competing antibodies (Cell Signaling Technology, 10ug/mL) or soluble RGD (1, 0.1, 0.01mM) for 10 min at 37$^o$C under slight agitation (n=6/group) [26]–[28]. Mineralized films were attached to the bottom of 24 well plates with sticky tabs. Cells were subsequently added to peptide-coated apatite films in serum-free media for 3 hours. Adherent cells were measured using a WST-1 assay and a standard curve from 100-10,000 cells. Cells were subsequently fixed, F-actin was stained with Rhodhamine-Pholloidin, and nuclei were stained with DAPI. Cell number was evaluated using Image J and compared to the WST-1 assay standard curve. Cell spreading was qualitatively evaluated.

**CELL SPREADING AND HISTOMORPHOMETRY**

Mineralized films were attached to the bottom of 24-well plates using sticky tabs. Films were subsequently incubated in 100 μg/mL of peptide solution for 3 hrs. Human bone marrow stromal cells were plated at 3000 cells/$cm^2$ (n=6/group) with and without serum for 12 hrs. at 37$^o$C and 5% $CO_2$. Cells were fixed in 10% phosphate buffered formalin, permeabilized in Triton X and stained with Rhodhamine-pholloidin(Life technologies) for F-actin and anti-vinculin-Alexa 488 for focal adhesions. Nuclei were counterstained and cells were mounted in DAPI containing Vectashield(Vector Labs). Images were

acquired using a Nikon Ti Eclipse confocal microscope was used to image fluorescent sections. Cell counts and spreading were evaluated using Image J (NIH). A total of 4 samples per group with 10 fields of view per sample at 20x were imaged to attain histomorphometric data. Cell diameter was measured using pholloidin and vinculin as cell boundary measures. Vinculin labeling was used to measure focal contact distribution. A modified concentric circle algorithm combined with particle measurements was used to evaluate total focal contacts from the outermost region from the cell center to the innermost region[29].

**MSC DIFFERENTIATION ON PEPTIDE COATED APATITE**

Mineralized films were held in place with Teflon O-rings for proliferation and differentiation assays to prevent films from floating. Films were subsequently incubated in 100 μg/mL of peptide solution for 3 hrs. iPS-MSCs were plated at 15,000 cells/$cm^2$ and grown to confluence until differentiated in complete media containing osteogenic factors ($10^{-8}$M Dexamethasone, 2-5mM β-glycerophosphate, $10^{-4}$ M ascorbic acid). Cells were differentiated for 0, 3, 7, 10, 14, 21, 28 days and collected (n=3/group, 6 biological replicates pooled pairwise) in TRIZOL® (ThermoFisher Scientific). The manufacturer's protocol for mRNA extraction was followed for isolation of mRNA. Briefly, cells were homogenized in TRIZOL®, phase-separated in chloroform, and RNA was precipitated in 500uL isopropanol. RNA was subsequently washed in 80% ethanol, dried and dissolved in RNA grade double distilled water (Millipore) at 70$^{o}$C. The amount of RNA was measured using a spectrophotometer and 1μg was used for reverse transcription using SuperScript II reagents (ThermoFisher Scientific). TaqMan® Universal PCR Master Mix and TaqMan® primer probes were used for all qRT-PCR reactions. Cycle threshold ($C_T$)

values were normalized to GAPDH expression and day zero values were used to attain $\Delta\Delta C_T$ values. Gene expression was expressed as a fold change $2^{-\Delta\Delta C_T}$. Cells cultured on TCPS were stained using the Von Kossa method and images were acquired using a Leica dissection microscope.

**PEPTIDE CELL INTERNALIZATION**

Cells were plated at 15,000 cells/cm$^2$ on tissue culture treated glass coverslips in 24 well plates overnight in alpha-mem +10% FBS + 0.1% P/S at 37$^o$C and 5% CO2. Peptides were dissolved in ddH2O and diluted to 300μM in OPTIMEM (Invitrogen Carlsbad, CA). Media was removed from adherent cells, which were incubated in 300μM of FITC-VTK and OPTIMEM control media for 1hr. Cells were subsequently washed in PBS, fixed in 10% formalin, and mounted on glass slides in Vectashield containing the nuclear stain DAPI (Vector Labs Burlingame, CA). Nikon Ti-Eclipse confocal microscope was used to gather (n=10) images per group across 4 samples. Each fluorescent channel, DAPI and FITC, was imaged individually and images were merged using Image J.

**MSC RECRUITMENT ON PEPTIDE COATED APATITE**

To address the ability of DPI-VTK to specifically recruit multi-potent MSCs from primary bone marrow, murine bone marrow stromal cells were harvested from femora and tibiae of 5-6 week old C57/BL 6 mice (Jackson Laboratories). Cells were added to peptide coated apatite films and untreated controls in complete and serum-free media. Non-adherent cells were removed and complete media was replaced after 3 days of attachment. Adherent cells were collected after 5 days, counted using a hemocytometer, expanded, and proliferation (n=6/group) and differentiation (n=3/group, 6 biological replicates pooled pairwise) of adherent cell populations were examined on TCPS. Cell

proliferation was measured using CellTracker assay at 0, 3, 7, 10, and 14 days. Cell differentiation was assessed visually by observing mineral formation and staining using the Von Kossa method on day 14, 17, 21, and 28.

### STATISTICAL METHODS

All statistical analysis was done using SigmaPlot 13.0 (Systat Software Inc). One-way ANOVA with Tukey tests for pairwise comparisons was used to assess initial cell recruitment across peptide groups. Two-way ANOVA with Tukey tests for pairwise comparison was used to assess cell spreading(peptide, serum condition), competitive inhibition (peptide, inhibitor), cell proliferation(peptide, time) and differentiation(peptide, time). Three-way ANOVA with Tukey test for pairwise comparisons was used to evaluate focal adhesion contact distribution (peptide, serum condition, section from cell center).

## RESULTS

### MSC SPREADING AND CONTACT DISTRIBUTION ON PEPTIDE COATED APATITE

In serum-free media, cells interacting with DPI-VTK had a significantly greater cell diameter (Fig 3.1a,c) than cells on BLM ($p < 0.001$). In serum, cells attaching to DPI-VTK had a significantly greater cell diameter than cells attached to RGD-VTK ($p < 0.02$). However, cells interacting with RGD-VTK formed significantly more contacts than cells on either BLM or DPI-VTK in the serum free condition (Fig 3.1b,c; $p < 0.001$). Cells cultured with both RGD-VTK ($p < 0.004$) and DPI-VTK ($p < 0.014$) were able to form significantly more contacts than cells on BLM in serum. Cells on DPI-VTK formed significantly more contacts in serum compared to serum-free media ($p < 0.002$).

There were a significantly greater number of contacts at the periphery of the cells (sections 1-2) than at the center (sections 5,6) ($p < 0.01$), except on BLM in the serum-free condition (Fig 3.1d). Cells cultured on DPI-VTK and RGD-VTK demonstrated a significantly greater number of cell contacts towards the periphery (sections 1-3) compared to BLM ($p < 0.001$) in both culture conditions.

**COMPETITIVE MSC BINDING ASSAYS**

Cell attachment was significantly greater in the absence of soluble RGD compared to all concentrations and across both peptide groups ($p <0.001$). Cell attachment was significantly greater in the presence of 0.01mM soluble RGD compared to 0.1 or 1mM RGD (Fig. 3.2a; $p < 0.02$). There was significantly greater cell spreading in the absence of soluble RGD on both DPI-VTK and RGD-VTK (Fig 3.2b). There were significantly less adherent cell fractions in the presence of RGD binding integrin subunits versus the collagen binding integrin ($p < 0.001$) on both DPI-VTK and RGD-VTK coated apatite films (Fig 3.2c). The adherent cell fraction on DPI-VTK in the presence of $\alpha_V$, $\alpha_5$, and $\beta_3$ was significantly greater compared to RGD-VTK, indicating a weaker interaction between these domains and DPI peptide compared to RGD.

**MSC PROLIFERATION ON PEPTIDE COATED APATITE**

Cells cultured on BLM with RGD-VTK had significantly higher cell numbers at 18 hr compared to cells cultured on BLM (Fig. 3.3; $p < 0.016$). However, by day 7, there was a significant increase in cell number between DPI-VTK and BLM ($p < 0.001$). Cell numbers on DPI-VTK were also significantly higher than on VTK and RGD-VTK on day 10 ($p < 0.05$). By day 10 cells reached a saturation density beyond which proliferation slowed down and cell number exceeded detectable limits of the assay.

**MSC DIFFERENTIATION ON PEPTIDE COATED APATITE**

iPS-MSCs were cultured on TCPS to verify osteogenic differentiation potential and relative gene expression levels were expressed as fold changes $2^{-\Delta\Delta CT}$ (Fig 3.4). The osteogenic transcription factor Runx2 is elevated by day 10 followed by an increase in Osterix, indicative of early stage induction of osteogenic differentiation (Fig 3.4a,b). Markers of osteogenic differentiation alkaline phosphatase (ALP), osteocalcin (OCN), osteopontin (OPN), and bone sialoprotein (BSP) were all elevated by day 20 (Fig 3.4c-f), which coincided with mineralization (Fig 3.4g). The osteogenic genes Runx2 at day 10, OSX at day 15, ALP starting at day 10, OCN starting at Day 10, OPN starting at day 28 and BSP starting at day 20 were greater on TCPS compared to biomimetic apatite(Fig 3.4a-c, Fig 5 a-c; $p < 0.001$). Therefore, mineralized films were used as a baseline for comparing iPS-MSC differentiation on peptide coated apatite films (Fig 3.5). Although fold changes are depicted, $\Delta\Delta C_T$ values were used for all statistical analyses. iPS-MSCs cultured on VTK ($p < 0.001$) and DPI-VTK ($p < 0.023$) had significantly greater Runx2 expression(Fig 3.5a) compared to apatite films, whereas RGD exhibited no difference. All peptide groups had significantly increased Runx2 expression on day 7 compared to day 0, whereas Runx2 increased by day 10 on apatite controls ($p < 0.05$). RGD-VTK ($p < 0.001$) and VTK ($p < 0.01$) had greater OSX expression(Fig 3.5b) compared to apatite. Across all groups, OSX peaked at day 10 ($p < 0.001$). Similarly across all groups, ALP expression(Fig 3.5c) was greater on days 14, 21, and 28 compared to days 3 and 7 ($p < 0.001$). Both DPI-VTK at day 14 and VTK starting at day 20 exhibited higher OCN(Fig 3.5d) expression compared to BLM ($p < 0.001$). OPN(Fig 3.5e) and BSP(Fig 3.5f) expression on VTK coated apatite substrates was significantly higher than the other peptide and control groups ($p < 0.001$).

### PEPTIDE INTERNALIZATION

Fluorescently tagged peptides associate with cells and internalize within 1hr of incubation (Fig. 3.6). The fibrillar pattern of FITC fluorescence is indicative of cytoskeletal association. Moreover, punctate vesicular association indicates intracellular processing of the peptides.

### MULTIPOTENT-MSC RECRUITMENT FROM MURINE BONE MARROW

Improving the recruitment of multi-potent MSCs from bone marrow can have a significant impact on cell-based therapies. After 5 days of attachment, a greater number of cells adhered to VTK coated BLM (Fig 3.7a) compared to TCPS ($p < 0.017$), BLM ($p < 0.05$), and DPI-VTK without serum ($p < 0.001$). More cells adhered to DPI-VTK than TCPS ($p < 0 .05$) and DPI-VTK ($p < 0.008$) without serum. There were more cells from the VTK-adherent population by day 10 (Fig 3.7b) compared to DPI-VTK adherent population in the no serum condition ($p < 0.004$).

## DISCUSSION

DPI-VTK improves cell spreading and proliferation on apatite substrates compared to control and non-peptide coated surfaces, however differentiation and cell recruitment data suggest a biological effect is induced by VTK alone. Cells interact with material surfaces through adsorbed serum proteins such as fibronectin (Fn) and vitronectin (Vn). Interaction with serum components is also responsible for proliferation and differentiation of mesenchymal stem cells. Cell spreading and focal contacts on DPI-VTK are greater in the presence of serum compared to no serum, indicating a cooperative interaction between serum components and DPI-VTK(Fig 3.1). Conversely, RGD-VTK did not increase cell spreading, indicating a non-cooperative interaction with serum

proteins. This is consistent with the attributed negative interaction between RGD peptides and serum proteins [19], [30].

The greater percentage of cell contacts on DPI-VTK and RGD-VTK at the periphery of cells is indicative of greater adhesion strength(Fig 3.1 d,e). Focal adhesions result from an aggregation of integrin clustering and maturation of focal complexes[31], [32]. These transmembrane complexes are further reinforced by tethering the extracellular matrix to stabilizing actin-myosin cytoskeletal structures. As cells spread, focal adhesion reorganization and tension within the cytoskeleton can impart biological effects through phosphorylation of tyrosine kinases in signal transduction cascades regulating osteogenic differentiation[33], [34]. Decoupling the contributions of spatial distribution of adhesive complexes and cell spreading indicate the importance of focal adhesion distribution in regulating adhesion strength independent of the size and spread area of focal adhesions[35]. In addition to cell-peptide interactions, focal adhesion formation and distribution can also be regulated by underlying substrate stiffness [36]. Matrix elasticity, independent of soluble factors, is capable of driving differentiation. Surface roughness and surface chemistry of apatite films also play an important role on focal contact distribution in the presence of serum[12], [29]. The predominant effect of the underlying substrate properties is reflected in the similarities of spreading and contact distribution of cells in the presence of serum.

The increase in adhesion strength (Chapter 2) of MSCs on DPI-VTK coated apatite compared to RGD-VTK and VTK spurned further investigation of the mechanisms mediating cell-peptide interaction. Competition with soluble RGD indicated the role of RGD binding integrins in mediating cell-DPI interactions(Fig 3.2a). Furthermore,

inhibition of cell spreading on DPI-VTK in the presence of soluble RGD demonstrated the requirement of RGD binding integrins in mediating cell spreading on DPI-VTK. Competition with RGD-binding integrin antibodies $\alpha_5$, $\beta_1$, $\alpha_V$, $\beta_3$, $\beta_5$ further confirmed the role of DPI-VTK mediated cell attachment towards RGD-binding integrins(Fig 3.2c). However, the differences in adherent cell fractions between DPI-VTK and RGD-VTK in the presence of integrin antibodies can be attributed to either different affinities or conformational flexibility in binding different integrin domains. The reduced cell attachment on DPI-VTK in the presence of the collagen binding integrin $\alpha_2\beta_1$ also reveals some binding to this receptor with weaker affinity than to the RGD binding integrin subunits. This weak association may arise from the conformational flexibility in binding the β1 subunit.

The promiscuity of DPI-VTK adhesion to various RGD binding integrins can be attributed to phage display selection of cell surface targets that are highly expressed. MSCs express a distinct profile of integrins at distinct differentiation times [18], [37], [38]. The phage display derived cell binding sequence, DPI, could be selective towards a profile of integrins. Although an explicit DPI-VTK cell binding domain was not identified, the competitive inhibition findings suggest a role of RGD binding integrin mediated cell attachment towards DPI-VTK, while maintaining specificity towards MSCs.

Initially adherent cell fractions were greater on RGD-VTK compared to DPI-VTK consistent with previous studies[22]. Although initial adherent cells are greater on RGD-VTK, there were more adherent cells on DPI-VTK compared to apatite and VTK by day 7(Fig 3.3). Greater proliferation on DPI-VTK compared to VTK can result from co-

operative serum interactions coupled with integrin mediated attachment. MSCs reached a surface saturation density by day 10. Early expression of Runx2 and OSX followed by increased ALP expression indicate osteogenic differentiation of MSCs on DPI-VTK(Fig 3.5). Interestingly MSCs cultured on VTK exhibit elevated gene expression for differentiation markers OCN, SPPI, and BSP compared to apatite films. The osteoinductive properties of VTK can arise from an indirect physiochemical interaction with the cell secreted mineral or through a direct cellular interaction. Addition of soluble VTK indicates cell association, internalization, and intracellular compartmentalization suggests a role in direct osteogenic induction(Fig 3.6).

Interestingly, murine bone marrow stromal cell derived MSCs that were bound to VTK coated apatite substrates exhibited a much greater proliferation rate (Fig 3.7b). Moreover there were a greater number of adherent cells to VTK compared to DPI-VTK and DPI-VTK without serum (Fig 3.7a). Increased proliferation of VTK extracted cells indicates a more rapidly self-renewing population, often a characteristic of multipotent MSCs, or the ability of VTK to promote proliferation of initially adherent fractions. Inability of VTK to promote multipotent hBMSC proliferation (Fig 3.3) indicates a greater likelihood of a rapidly self-renewing population initially adherent to VTK coated apatite. However, none of the initially adherent cells across peptide and control groups differentiated *in vitro* to form mineralized cultures (data not shown). Future studies sorting fluorescent VTK and DPI labeled cells using conventional markers and testing multipotency can more thoroughly identify the specificity of DPI towards multi-potent MSC sub populations. Efficiently identifying multipotent-MSCs can reduce *ex vivo* expansion times, improve consistent expansion profiles, and reduce time and costs for cell-based

therapies. Furthermore, selectively recruiting multipotent-MSCs towards a biomaterial can improve tissue regeneration outcomes *in vivo*.

Taken together, phage display derived DPI-VTK peptide is an integrin associated MSC specific sequence that improves cell adhesion strength and promotes cell proliferation. Although there was a marginal improvement of MSC differentiation on DPI-VTK compared to apatite films, MSC specificity towards DPI-VTK, cooperative interactions with serum proteins, improved proliferation and improved adhesion strength (Chapter 2) compared to untreated mineral and can translate to improved cell delivery and tissue regeneration outcomes in vivo.

## ACKNOWLEDGEMENTS

I would like to thank Dr. Paul Krebsbach and Luis Villa for iPS-MSCs used in these studies. This work is supported by NIH R01 DE 013380, DE 015411 (DHK).

## CHAPTER THREE TABLES

### TABLE 3.1 PEPTIDE PROPERTIES

| Peptide | Sequence | Description | MW (g/mol) | Net Charge | Acidic residues |
|---|---|---|---|---|---|
| VTK | VTKHLNQISQSY | Phage derived mineral binding sequence | 1417.59 | 1 | 2 |
| DPI-VTK | GGDPIYALSWSGMAGGGSVTKHLNQISQSY | **Dual functioning peptide containing phage derived cell and mineral binding sequences** | 3025.35 | 0 | 5 |
| RGD-VTK | GGRGDGGGSVTKHLNQISQSY | Dual functioning peptide containing cell binding control sequence | 2061.20 | 1 | 3 |

## CHAPTER THREE FIGURES

### FIGURE 3.1(A-E) CELL SPREADING AND CONTACT DISTRIBUTION ON PEPTIDE COATED APATITE SURFACES

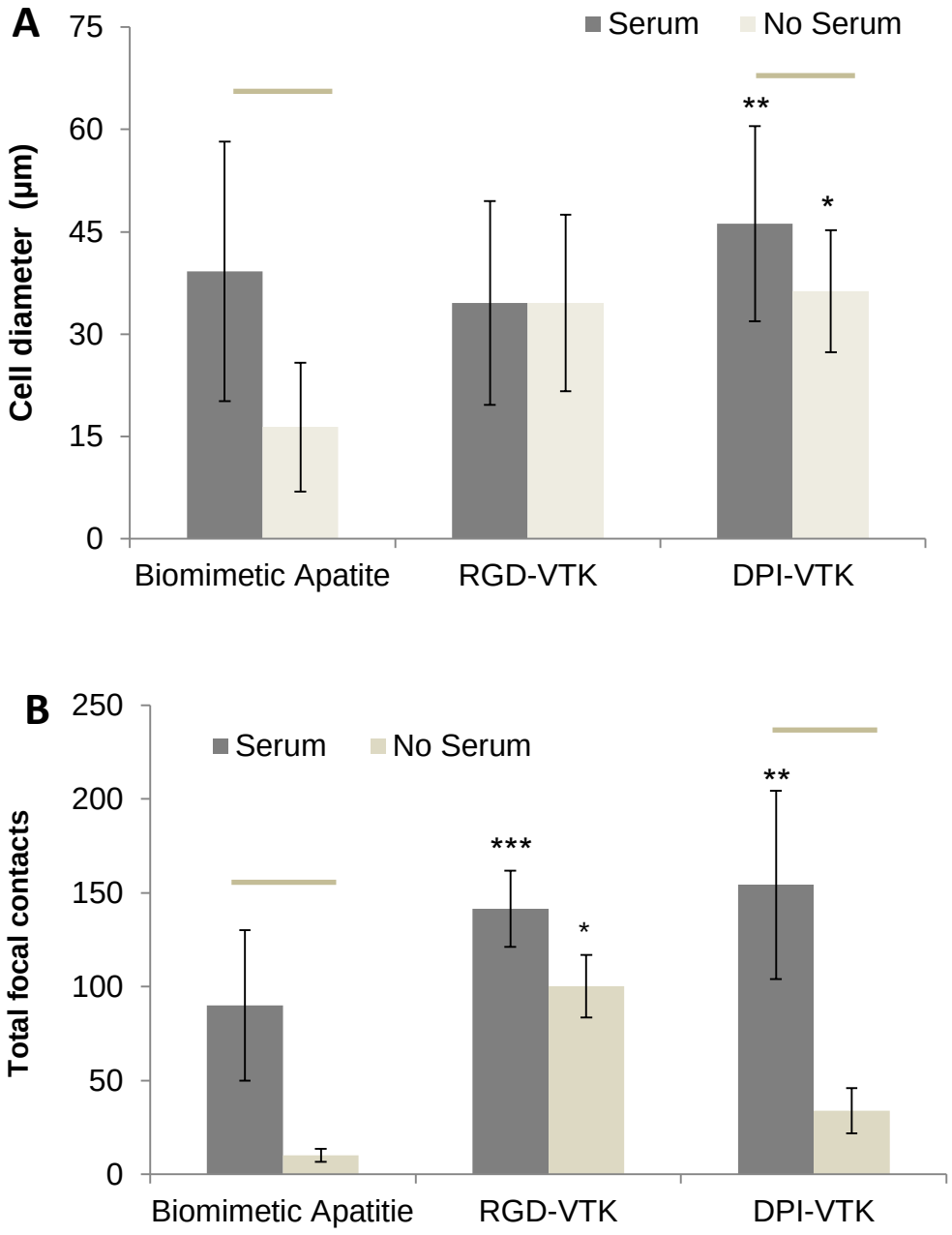

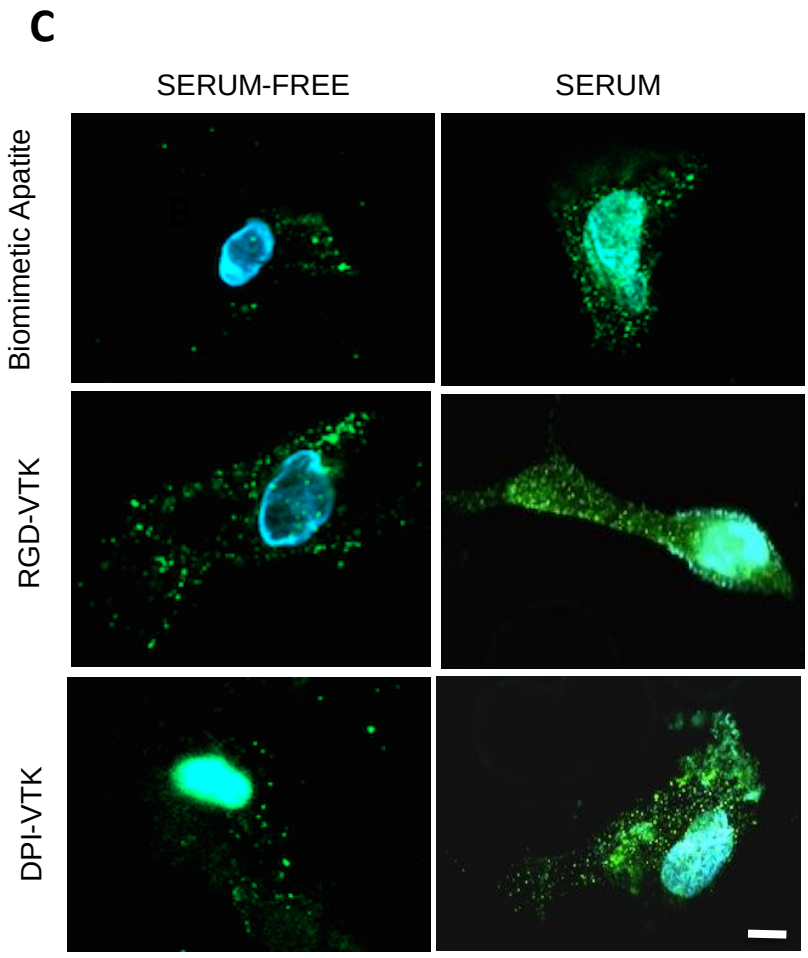
C
SERUM-FREE
SERUM
Biomimetic Apatite
RGD-VTK
DPI-VTK

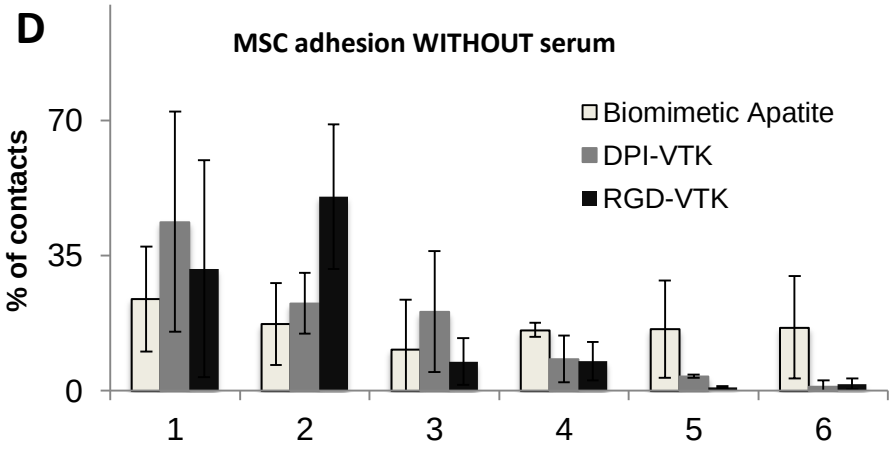
D
MSC adhesion WITHOUT serum
% of contacts
70
35
0
1
2
3
4
5
6
Biomimetic Apatite
DPI-VTK
RGD-VTK

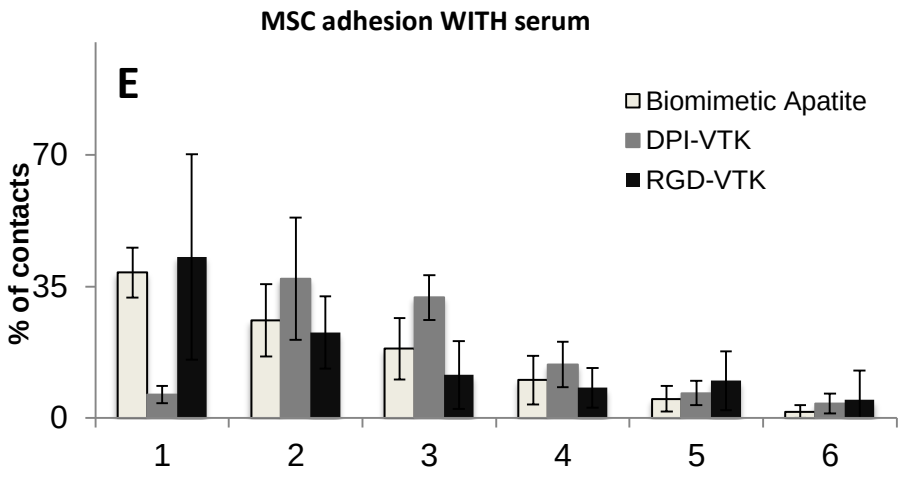


**Figure 3.1.** Cell spreading and contact distribution on peptide coated apatite surfaces. **A)** HBMSC diameter in serum and serum free conditions on peptide coated and uncoated mineralized substrates. Bars indicate significance within peptide groups. * indicates significantly different than BLM ($p < 0.01$). ** indicates significantly greater than RGD-VTK ($p < 0.02$). **B)** Total number of HBMSC focal contacts in the presence and absence of serum on peptide coated apatite films and un coated controls. *, **, *** indicate significant difference from biomimetic apatite ($p<0.001$), ($p<0.014$), ($p <0.004$) respectively. Bars indicate significant difference between serum and non-serum conditions ($p<0.001$) **C)** HBMSCs labeled with DAPI and anti-vinculin tagged with Alexa 488 demonstrating a greater number of adhesion contacts in serum vs. no serum conditions. RGD-VTK formed the most contacts in serum free media. However these differences in focal contacts are mitigated by the addition of serum (scale bar 5 μm). **D)** Focal contact distribution in the absence of serum. Significant differences between sections 1 and 2, compared to 5 and 6 ($p < 0.01$) except on uncoated BLM. **E)** Focal contact distribution in the presence of serum. Significant differences between section 1 and 2, compared to 5 and 6 ($p < 0.01$).

**FIGURE 3.2(A-C). IPS-MSC COMPETITION WITH SOLUBLE INTEGRIN BINDING COMPETITORS.**

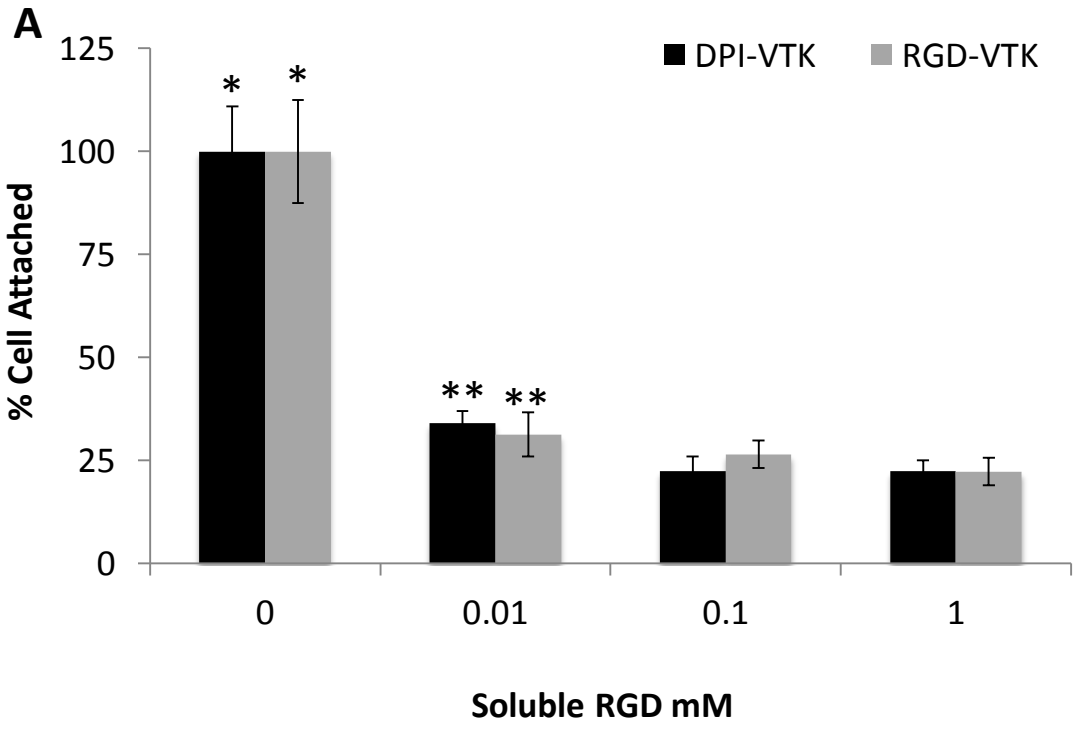


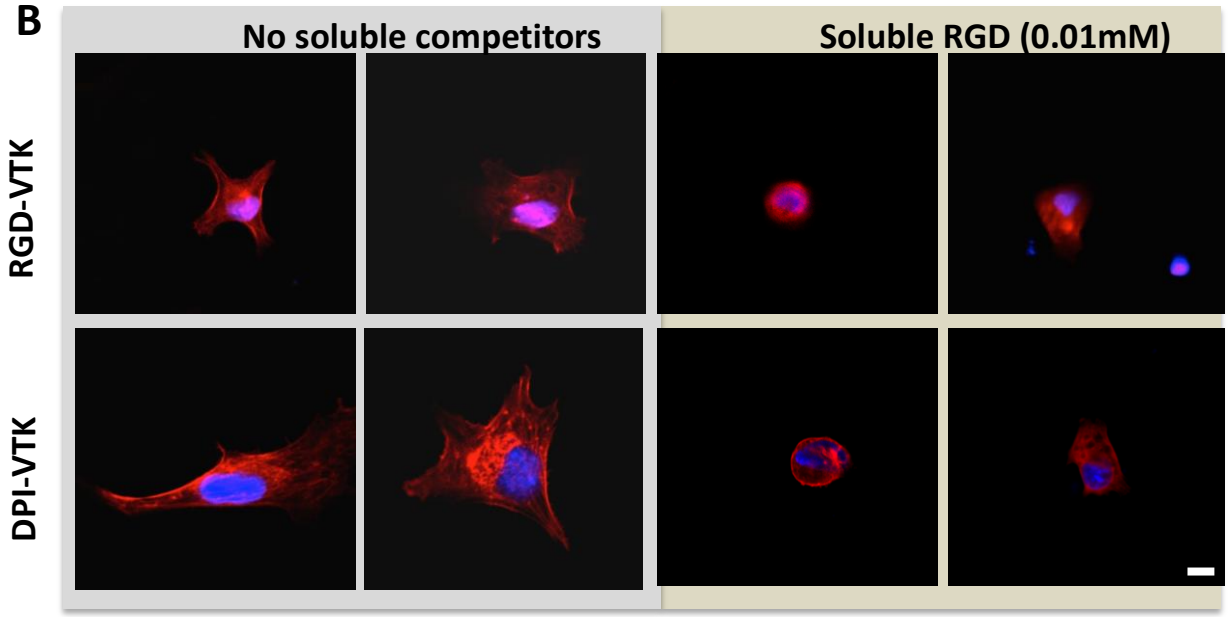

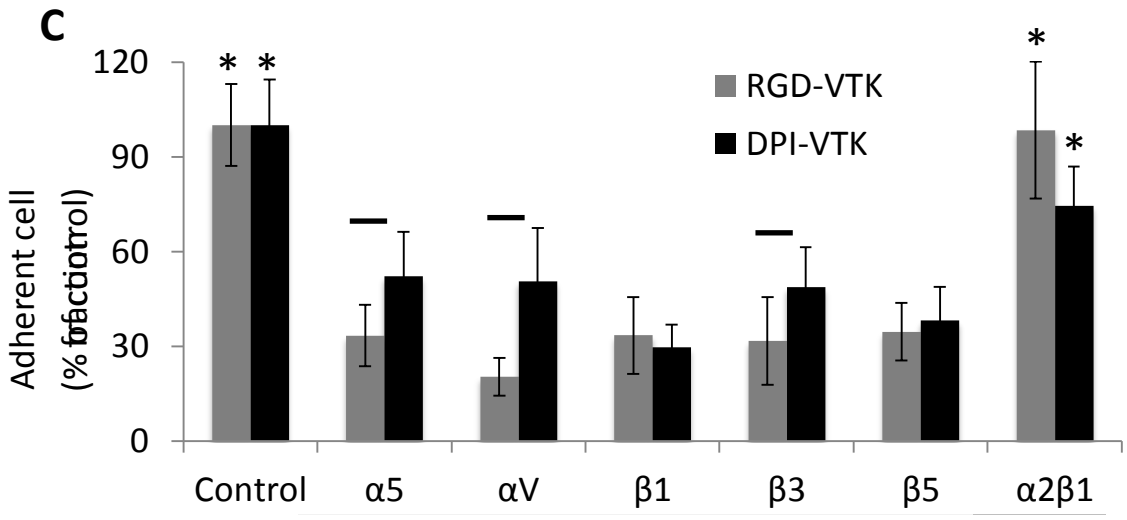


**Figure 3.2.** iPS-MSC competition with soluble integrin binding competitors. A) Fraction of adherent cells on peptide coated apatite in the presence of soluble RGD normalized to no soluble competitors. * denotes significant difference from remaining concentrations within peptide group ($p<0.01$). ** denotes significant difference from the 0.1 and 1mM concentrations ($p<0.02$) within each peptide group. B) Representative images at 40x of MSCs on DPI-VTK and RGD-VTK coated substrates in the presence and absence of soluble RGD. Nuclei are stained with DAPI and F-actin is stained with Rhodhamine-Pholloidin (scale bars 5 μm). C) Fraction of adherent cells on peptide coated apatite in the presence of RGD integrin binding antibodies and Col1binding antibodies normalized to cell bound in the absence of soluble competitors. * denotes difference from RGD binding integrins ($p <0.001$). Bars denote difference from RGD-VTK within same soluble treatment group ($p <0.05$).

**FIGURE 3.3. MSC PROLIFERATION ON PEPTIDE COATED APATITE SUBSTRATES.**

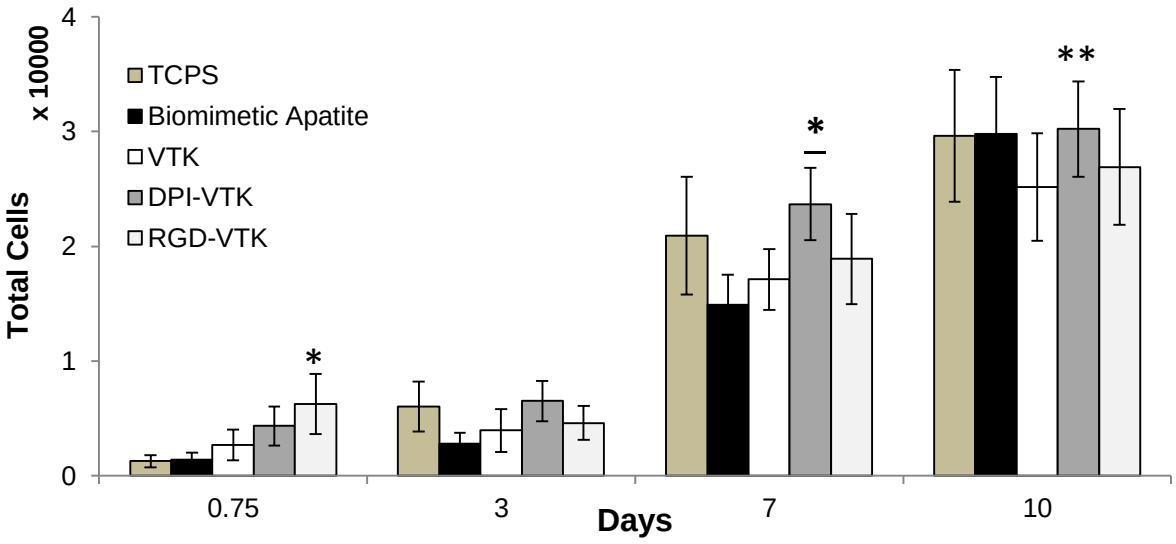


Figure 3.3. MSC proliferation on peptide coated apatite substrates. Histomorphometric analysis of 4 samples per group covering 10 fields of view per sample was analyzed to quantify the number of cells. * different from TCPS and apatite controls ($p < 0.001$). * Different from apatite control ($p < 0.001$). ** Different from VTK ($p < 0.05$).

**FIGURE 3.4(A-G). IPS-MSC DIFFERENTIATION ON TCPS IN OSTEOGENIC MEDIA.**

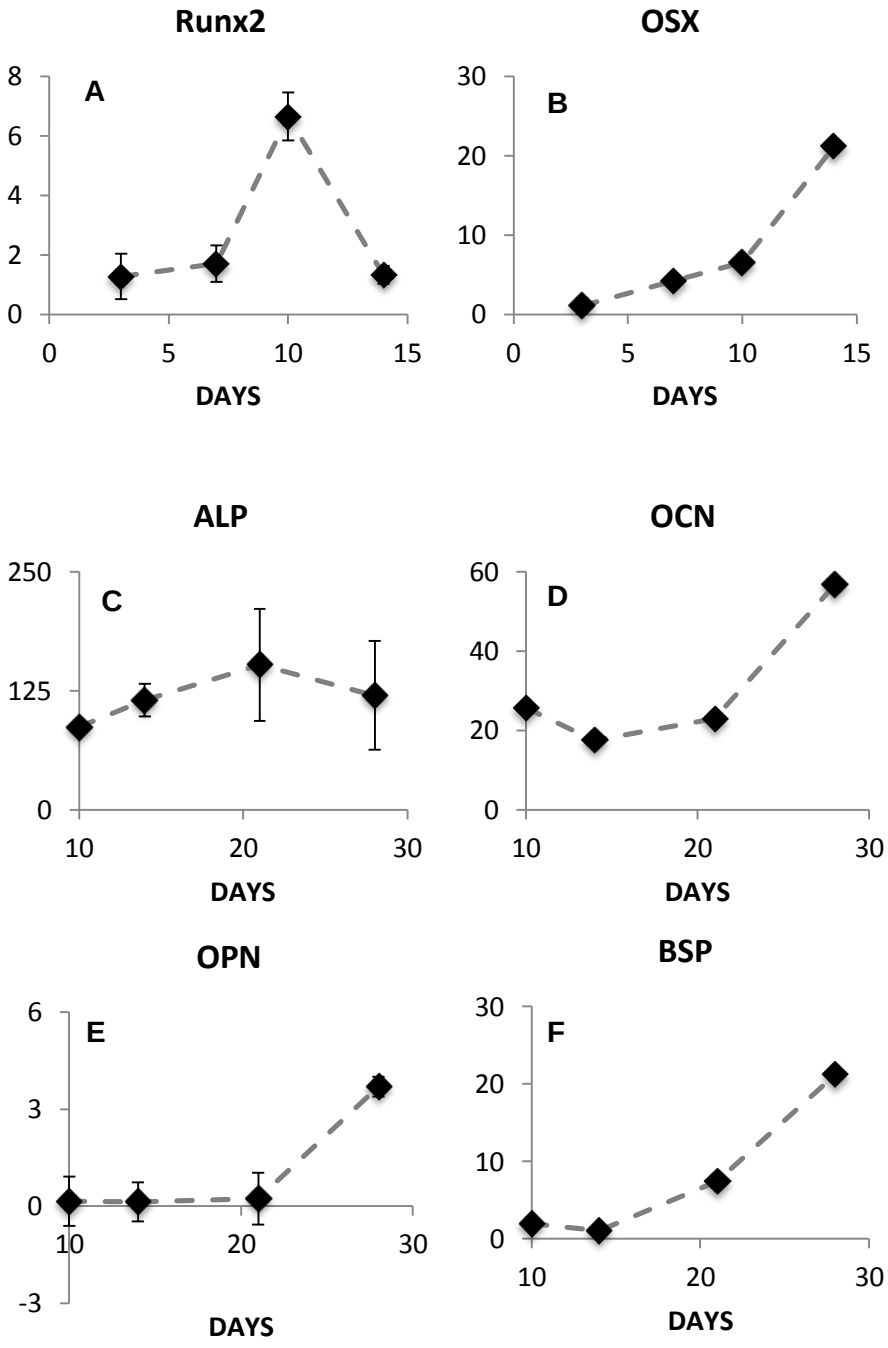

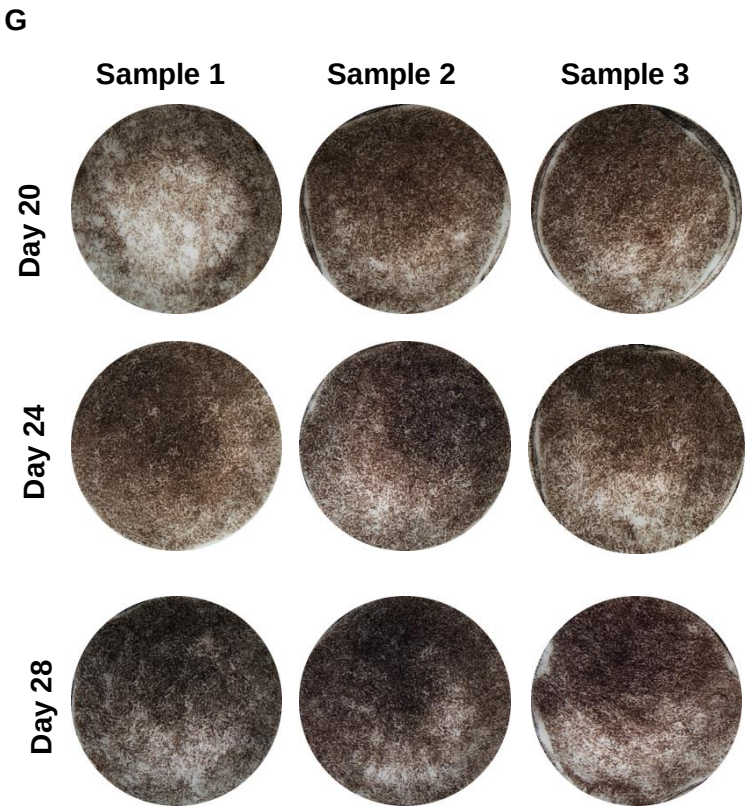


**Figure 3.4.** iPS-MSC differentiation on TCPS in osteogenic media. A,B). Relative gene expression of osteogenic transcription factors Runx2 and Osterix normalized to day zero and GAPDH values (n=3). C-F) relative gene expression of genes regulating osteogenic markers ALP, OCN, OPN, and BSP normalized to day zero and GAPDH values (n=3). G) von Kossa staining of mineral.

**FIGURE 3.5(A-F). DIFFERENTIATION OF IPS-MSCS ON BIOMIMETIC APATITE AND PEPTIDE COATED APATITE**

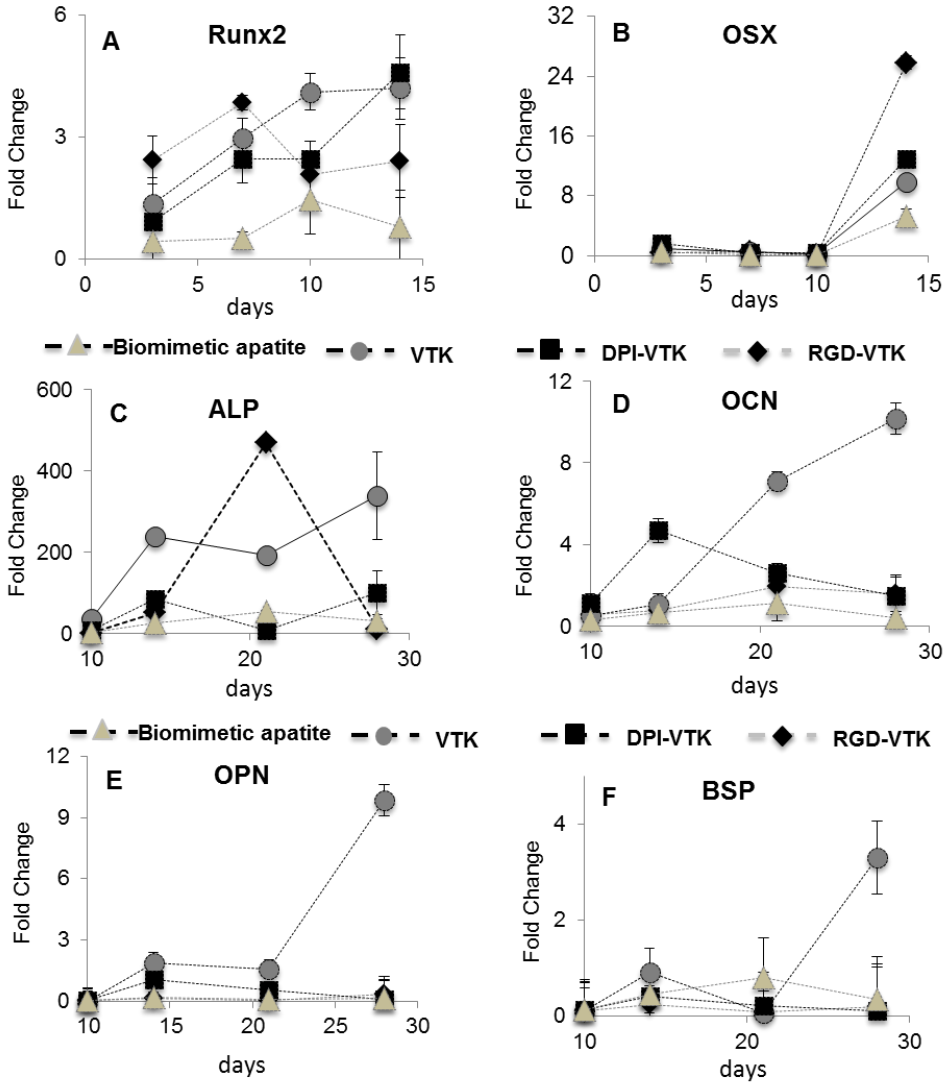


**Figure 3.5.** Differentiation of iPS-MSCs on biomimetic apatite and peptide coated apatite. A,B). Relative gene expression of osteogenic transcription factors Runx2 and OSX normalized to day zero and GAPDH values (n=3/group, 6 biological replicates pooled pairwise). C-F) relative gene expression of genes regulating osteogenic markers ALP, OCN, OPN, and BSP normalized to day zero and GAPDH values (n=3/group, 6 biological replicates pooled pairwise)

**FIGURE 3.6. CELL ASSOCIATION OF FLUORESCENTLY TAGGED VTK PEPTIDE AFTER 1 HR OF INCUBATION.**

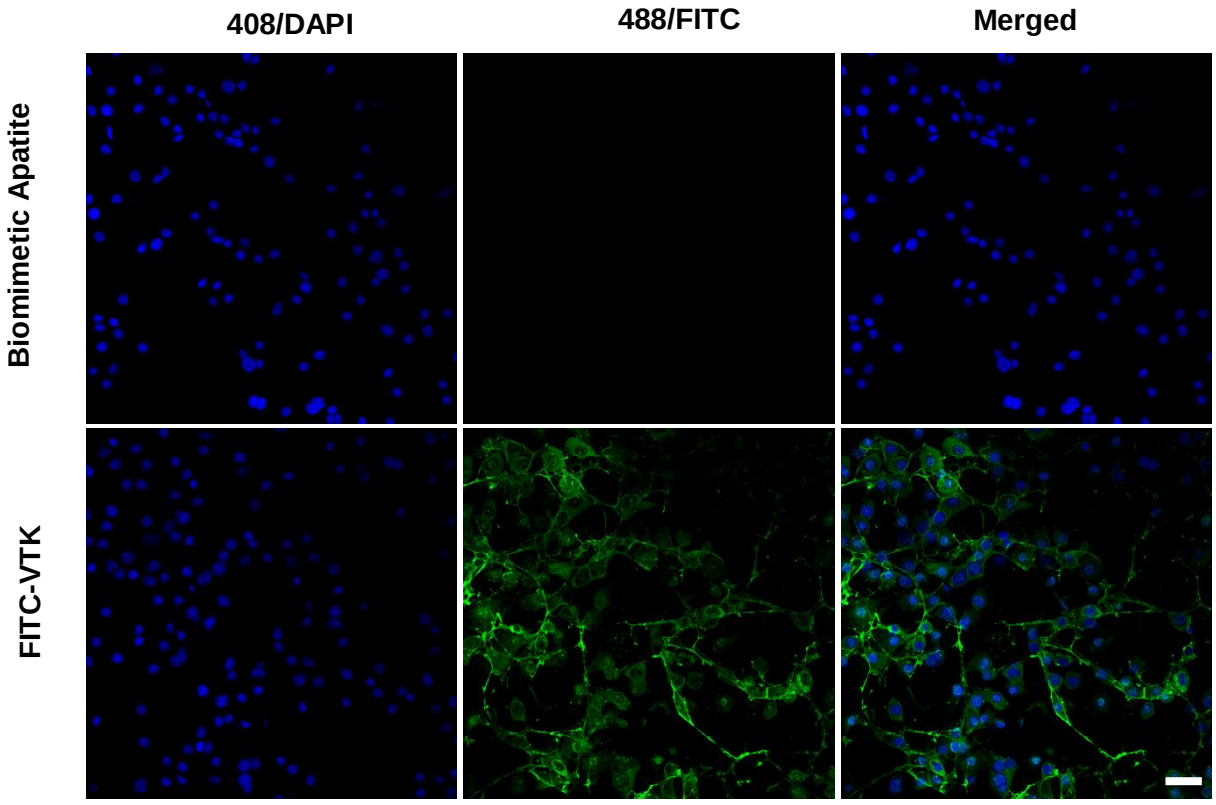


**Figure 3.6.** Cell association of fluorescently tagged VTK peptide after 1 hr of incubation. The pattern of internalization is indicative of cytoskeletal association. Association in punctate vesicular structures indicates intracellular processing.

**FIGURE 3.7. MULTIPOTENT MURINE-MSC RECRUITMENT ONTO PEPTIDE COATED APATITE**

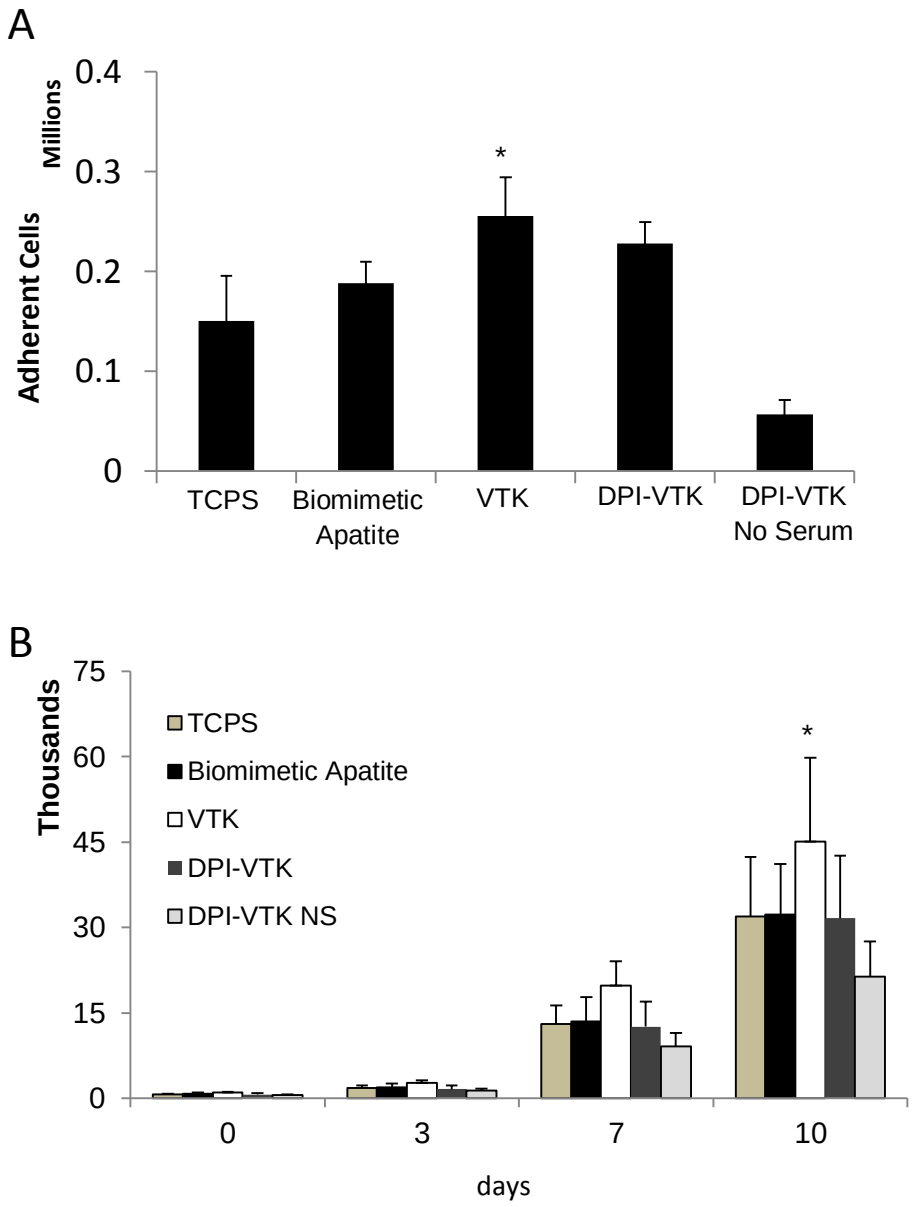


Multipotent MSC recruitment on peptide coated apatite. A) Initial adherent cell numbers on peptide coated apatite and controls. * significant from DPI-VTK no serum ($p<0.001$). B) Proliferation of adherent cell fractions plates at 3000cells/cm$^2$ on TCPS for 10 days. * significant from DPI-VTK no serum ($p<0.001$).

# REFERENCES


[1] A. G. Mikos, S. W. Herring, P. Ochareon, J. Elisseeff, H. H. Lu, R. Kandel, F. J. Schoen, M. Toner, D. Mooney, A. Atala, M. E. Van Dyke, D. Kaplan, and G. Vunjak-Novakovic, "Engineering complex tissues.," *Tissue Eng.*, vol. 12, no. 12, pp. 3307–39, Dec. 2006.

[2] E. Alsberg, E. E. Hill, and D. J. Mooney, "Craniofacial tissue engineering.," *Crit. Rev. Oral Biol. Med.*, vol. 12, no. 1, pp. 64–75, Jan. 2001.

[3] A. I. Caplan, "Review: mesenchymal stem cells: cell-based reconstructive therapy in orthopedics ," *Tissue Eng.*, vol. 11, no. 7–8, pp. 1198–1211, 2005.

[4] P. Bianco and P. G. Robey, "Skeletal stem cells," *Development*, vol. 142, no. 6, pp. 1023–1027, 2015.

[5] R. Hass, C. Kasper, S. Böhm, and R. Jacobs, "Different populations and sources of human mesenchymal stem cells (MSC): A comparison of adult and neonatal tissue-derived MSC.," *Cell Commun. Signal.*, vol. 9, p. 12, Jan. 2011.

[6] S. E. Brown, W. Tong, and P. H. Krebsbach, "The derivation of mesenchymal stem cells from human embryonic stem cells.," *Cells. Tissues. Organs*, vol. 189, no. 1–4, pp. 256–60, Jan. 2009.

[7] L. G. Villa-Diaz, S. E. Brown, Y. Liu, A. M. Ross, J. Lahann, J. M. Parent, and P. H. Krebsbach, "Derivation of mesenchymal stem cells from human induced pluripotent stem cells cultured on synthetic substrates.," *Stem Cells*, vol. 30, no. 6, pp. 1174–81, Jun. 2012.

[8] V. Russo, C. Yu, P. Belliveau, A. Hamilton, and L. E. Flynn, "Directed Differentiation of Human Induced Pluripotet Stem Cells Toard Bone and Cartilage In vitro Versus In Vivo Assays," *Stem Cells Transl. Med.*, vol. 3, pp. 206–217, 2014.

[9] P. Bianco, X. Cao, P. S. Frenette, J. J. Mao, P. G. Robey, P. J. Simmons, and C.-Y. Wang, "The meaning, the sense and the significance: translating the science of mesenchymal stem cells into medicine.," *Nat. Med.*, vol. 19, no. 1, pp. 35–42, Jan. 2013.

[10] P. Bianco, P. G. Robey, and P. J. Simmons, "Mesenchymal stem cells: revisiting history, concepts, and assays.," *Cell Stem Cell*, vol. 2, no. 4, pp. 313–9, Apr. 2008.

[11] B. J. Sworder, S. Yoshizawa, P. J. Mishra, N. Cherman, S. A. Kuznetsov, G. Merlino, A. Balakumaran, and P. G. Robey, "Molecular profile of clonal strains of human skeletal stem/progenitor cells with different potencies.," *Stem Cell Res.*, vol. 14, no. 3, pp. 297–306, May 2015.

[12] Ramaswamy, J., Ramaraju, H., and Kohn D. H., "Bone-Like Mineral and Organically Modified Bone-Like Mineral Coatings," in *Biological and Biomedical Coatings Handbook, Processing and Characterization*, S. Zhang, Ed. Boca Raton, FL: CRC Press, 2011, pp. 1–36.

[13] W. L. Murphy, D. H. Kohn, and D. J. Mooney, “Growth of continuous bonelike mineral within porous poly(lactide-co- glycolide) scaffolds in vitro,” *J. Biomed. Mater. Res.*, vol. 50, pp. 50–58, 2000.

[14] A. Shekaran and A. J. García, “Extracellular matrix-mimetic adhesive biomaterials for bone repair.,” *J. Biomed. Mater. Res. A*, vol. 96, no. 1, pp. 261–72, Jan. 2011.

[15] R. G. LeBaron and K. A. Athanasiou, “Extracellular matrix cell adhesion peptides: functional applications in orthopedic materials ,” *Tissue Eng.*, vol. 6, no. 2, pp. 85–103, Apr. 2000.

[16] a. a. Sawyer, D. M. Weeks, S. S. Kelpke, M. S. McCracken, and S. L. Bellis, “The effect of the addition of a polyglutamate motif to RGD on peptide tethering to hydroxyapatite and the promotion of mesenchymal stem cell adhesion,” *Biomaterials*, vol. 26, no. 34, pp. 7046–7056, 2005.

[17] R. Fujisawa, M. Mizuno, Y. Nodasaka, and Y. Kuboki, “Attachment of osteoblastic cells to hydroxyapatite crystals by a synthetic peptide (Glu7-Pro-Arg-Gly-Asp-Thr) containing two functional sequences of bone sialoprotein.,” *Matrix Biol.*, vol. 16, no. 1, pp. 21–8, Apr. 1997.

[18] C. Popov, T. Radic, F. Haasters, W. C. Prall, a Aszodi, D. Gullberg, M. Schieker, and D. Docheva, “Integrins α2β1 and α11β1 regulate the survival of mesenchymal stem cells on collagen I.,” *Cell Death Dis.*, vol. 2, no. 7, p. e186, 2011.

[19] K. M. Hennessy, B. E. Pollot, W. C. Clem, M. C. Phipps, A. A. Sawyer, B. K. Culpepper, and S. L. Bellis, “The effect of collagen I mimetic peptides on mesenchymal stem cell adhesion and differentiation, and on bone formation at hydroxyapatite surfaces.,” *Biomaterials*, vol. 30, no. 10, pp. 1898–909, Apr. 2009.

[20] C. D. Reyes, T. A. Petrie, K. L. Burns, Z. Schwartz, and A. J. Garcia, “Biomolecular surface coating to enhance orthopaedic tissue healing and integration ,” *Biomaterials*, vol. 28, no. 21, pp. 3228–3235, Jul. 2007.

[21] F. Gomar, R. Orozco, J. L. Villar, and F. Arrizabalaga, “P-15 small peptide bone graft substitute in the treatment of non-unions and delayed union. A pilot clinical trial.,” *Int. Orthop.*, vol. 31, no. 1, pp. 93–9, Feb. 2007.

[22] H. Ramaraju, S. J. Miller, and D. H. Kohn, “Dual-functioning phage-derived peptides encourage human bone marrow cell-specific attachment to mineralized biomaterials.,” *Connect. Tissue Res.*, vol. 55 Suppl 1, pp. 160–3, Aug. 2014.

[23] S. J. Segvich, “Design of Peptides with Targeted Apatite and Human Bone Marrow Stromal Cell Adhesion for Bone Tissue Engineering.,” University of Michigan, 2008.

[24] S. A. Kuznetsov, M. H. Mankani, and P. G. Robey, “In vivo formation of bone and haematopoietic territories by transplanted human bone marrow stromal cells generated in medium with and without osteogenic supplements.,” *J. Tissue Eng. Regen. Med.*, vol. 7, no. 3, pp. 226–35, Mar. 2013.

[25] S. a Kuznetsov, P. H. Krebsbach, K. Satomura, J. Kerr, M. Riminucci, D. Benayahu, and P. G. Robey, “Single-colony derived strains of human marrow stromal fibroblasts form bone after transplantation in vivo.,” *J. Bone Miner. Res.*, vol. 12, no. 9, pp. 1335–47, Sep. 1997.

[26] J. a. Rowley, G. Madlambayan, and D. J. Mooney, “Alginate hydrogels as synthetic extracellular matrix materials,” *Biomaterials*, vol. 20, no. 1, pp. 45–53, 1999.

[27] T. a. Petrie, J. R. Capadona, C. D. Reyes, and A. J. García, “Integrin specificity and enhanced cellular activities associated with surfaces presenting a recombinant fibronectin fragment compared to RGD supports,” *Biomaterials*, vol. 27, no. 31, pp. 5459–5470, 2006.

[28] Y. Feng and M. Mrksich, “The synergy peptide PHSRN and the adhesion peptide RGD mediate cell adhesion through a common mechanism,” *Biochemistry*, vol. 43, no. 50, pp. 15811–15821, 2004.

[29] E. V Leonova, K. E. Pennington, P. H. Krebsbach, and D. H. Kohn, “Substrate mineralization stimulates focal adhesion contact redistribution and cell motility of bone marrow stromal cells.,” *J. Biomed. Mater. Res. A*, vol. 79, no. 2, pp. 263–70, Nov. 2006.

[30] K. M. Hennessy, W. C. Clem, M. C. Phipps, A. A. Sawyer, F. M. Shaikh, and S. L. Bellis, “The effect of RGD peptides on osseointegration of hydroxyapatite biomaterials.,” *Biomaterials*, vol. 29, no. 21, pp. 3075–83, Jul. 2008.

[31] J. Eyckmans, T. Boudou, X. Yu, and C. S. Chen, “A hitchhiker’s guide to mechanobiology.,” *Dev. Cell*, vol. 21, no. 1, pp. 35–47, Jul. 2011.

[32] A. L. Berrier and K. M. Yamada, “Cell – Matrix Adhesion,” *J. Cell. Physiol.*, no. June, pp. 565–573, 2007.

[33] N. D. Gallant, “Stick and Grip,” *Cell Biochem. Biophys.*, vol. 39, no. 9, 2003.

[34] D. E. Ingber, “Cellular mechanotransduction: putting all the pieces together again ,” *FASEB J.*, vol. 20, no. 7, pp. 811–827, May 2006.

[35] K. K. Elineni and N. D. Gallant, “Regulation of cell adhesion strength by peripheral focal adhesion distribution.,” *Biophys. J.*, vol. 101, no. 12, pp. 2903–11, Dec. 2011.

[36] A. J. Engler, S. Sen, H. L. Sweeney, and D. E. Discher, “Matrix Elasticity Directs Stem Cell Lineage Specification,” *Cell*, vol. 126, no. 4, pp. 677–689, 2006.

[37] A. K. Kundu, C. B. Khatiwala, and A. J. Putnam, “Extracellular matrix remodeling, integrin expression, and downstream signaling pathways influence the osteogenic differentiation of mesenchymal stem cells on poly(lactide-co-glycolide) substrates.,” *Tissue Eng. Part A*, vol. 15, no. 2, pp. 273–283, 2009.

[38] D. Docheva, C. Popov, W. Mutschler, and M. Schieker, “Human mesenchymal stem cells in contact with their environment: surface characteristics and the integrin system.,” *J. Cell. Mol. Med.*, vol. 11, no. 1, pp. 21–38, Jan. .

# CHAPTER FOUR

# IMPROVING MSC BASED BONE TISSUE REGENERATION *IN VIVO* USING CELL-SPECIFIC PEPTIDE COATED MINERALIZED BIOMATERIALS

## INTRODUCTION

There are over 2 million bone grafting procedures worldwide with 500, 000 bone grafting procedures/year in the US alone required for the treatment of critical sized defects e[1], [2]. Autograft therapies utilizing resected host bone are the gold standard for bone augmentation and bone grafting, but are limited in availability and often result in donor site morbidity[3]. Allogenic bone or demineralized bone matrix from cadaveric sources are often used as an alternative, but exhibit a reduction in cellularity and vascularization with increased reabsorption rates [4]. Synthetic bone grafts using calcium phosphates, calcium sulfates, collagen, and collagen mineral composites promote osteoconduction at the defect site, but exhibit limited osteoinductivity[5]. As a result these materials are co-delivered with adsorbed growth factors which can result in further complications. The limitations of current therapies, coupled with an increasing aging population and increasing global access to healthcare, drive the need for new regenerative strategies that can alleviate the economic burden of non-union defects[6].

Cell based therapies are a promising alternative for conventional auto and allograft therapies[7]–[9]. Bioresorbable natural and synthetic polymers, calcium phosphates and sulfates and polymer mineral composites materials are often considered for delivering cell based therapies[10], [11]. Amongst these materials, biodegradable synthetic polymers of the α-hydroxyester family, specifically the co-polymer poly(D,L-lactide-co-glycolide), are also considered for their improved control over mechanical properties, chemical functionalization, degradation rates, and ease of manufacture compared to naturally derived polymers[12]–[14]. The mineral component provides mechanical support and recapitulates the chemical microenvironment conducive for osteogenecity[15], [16]. Amongst the various methods of incorporating a mineral component onto a soft material, growth of a heterogeneous mineral layer by immersion in simulated body fluid (SBF) containing the ionic concentrations of blood plasma under physiological pH is a promising strategy. [16]–[18].

A continuous mineral coating throughout a porous polymer scaffold can protect the polymer from hydrophilic attack consequently attenuating polymer degradation rates[15], [19]. The concentration of SBF can also control the physical and chemical properties of the mineral coating and which subsequently affects mineral dissolution rates. For instance, mineral precipitated from 2x SBF concentrations are more amorphous than 1x SBF and results in faster dissolution rates. Therefore characteristics of precipitated mineral coating can also be used to further control polymer degradation timeframes[17].

Coating polymer substrates with bone-like-mineral (BLM) improves osteoconductivity *in vitro* and *in vivo*[14], [15], [20]. Although dissolution byproducts of the mineral coating have been implicated in biological activity, the chemical and physical properties of the

mineral alone are insufficient to promote osteoinductivity. Nanoscale morphology, crystallinity, and compositional characteristics of the mineral surface drive the adsorption of serum proteins which subsequently affect osteoconduction[21]–[23]. However, the adhesion of cells to mineral-adsorbed serum proteins is non-specific and indiscriminative of bone forming cell populations. To improve bone forming cell specific attachment and osteoinductivity of mineral substrates, tissue engineers utilize extracellular matrix proteins, peptides, and motifs specific to integrin binding domains. For instance, integrins $\alpha_2\beta_1$ and $\alpha_5\beta_1$ promote osteoinductivy by mechanotransductively activating osteogenic differentiation pathways. Derivatives of extracellular protein cell binding motifs that bind $\alpha_2\beta_1$ and $\alpha_5\beta_1$, such as RGD and Col(a1) derived peptides like GFOGER and N-GTPGPQGIAGQRGVV-C (P15), are used to further enhance osteoconductivity and osteoinductivity [24]–[26].

Due to the limitations of immobilizing peptide to mineral substrates, ECM proteins associated with binding mineral are used for appropriate delivery and presentation of cell adhesive peptides[27], [28]. For instance the glutamic acid repeat motif($E_7$) in bone sialoprotien was combined with RGD to improve adsorption and promote osteoconductivity and osteoinductivity of mineral substrates[29]. Although RGD-$E_7$ peptide improves osteoconductivity and osteoinductivity on mineral substrates *in vitro,* it surprisingly inhibits osseointegration *in vivo*[26]. The varied successes with RGD and various integrin binding peptides prompted the identification of cell specific peptides that can selectively bind bone forming cell populations form a heterogeneous stem or progenitor source. A mineral binding peptide is also required to improve adsorption to the

apatite surface and control presentation of the cell specific peptide to the cell surface receptor.

To meet these objectives, we used a commercially available phage display coupled with bioinformatic approaches and *in vitro* screening techniques to identify MSC specific [DPIYALSWSGMA, DPI] and apatite specific [VTKHLNQISQSY, VTK] sequences which were combined into a dual peptide [GGDPIYALSWSGMAGGGSVTKHLNQISQSY, DPI-VTK] for cell specific recruitment to mineral substrates. DPI-VTK efficiently targets apatite substrates and improves adhesion strength and specificity to murine bone marrow, human bone marrow, and induced pluripotent stem cell(iPS) derived mesenchymal stem cells(MSCs)[30]. Moreover, DPI-VTK improves spreading and proliferation while supporting differentiation on dual peptide coated constructs compared to uncoated controls (Chapter 3). These findings suggest a role for *in vivo* biological potential

In addition to improving the quantity of tissue through improved conductivity and inductivity, improving the uniformity of newly reconstructed tissue throughout the defect site is an important regeneration outcomes. In this study we hypothesize that uniformity of mineral coverage, uniformity of DPI-VTK adsorption and consequent uniformity of ips-MSC distribution *in vitro* contribute to increase quantity and uniform distribution of bone regenerated *in vivo* compared to non-peptide coated controls. The ubiquitous cell binding domain RGD was combined with the mineral binding domain VTK to be used as a dual-peptide positive control (RGD-VTK) for *in vitro* characterization (Table 4.1). P15 peptide, a component of Pep-Gen P15-BGS (Dentsply Implants, CA) currently available

as a bone graft substitute for void filling and augmentation in the oral cavity[31], was used as an *in vivo* control.

## MATERIALS AND METHODS

### SCAFFOLD FABRICATION

Polylactic-co-glycolic acid(PLGA 85:15 , Lakeshore Biomaterials) was solubilized in chloroform at 5%w/v. NaCl was sieved to 250-425µm and packed into 5mm diameter well in a Delrin® mold. PLGA-chloroform solution was added to each well of the Delrin mold which was subsequently covered and dried for 36hrs. The mold was transferred to a vacuum chamber for 5 days and subsequently leached in double-distilled water ($ddH_2O$) for 36hrs with intermittent fluid changes. Leached scaffolds were etched in 0.5M sodium hydroxide under slight agitation and rinsed twice in $ddH_2O$.

### SCAFFOLD MINERALIZATION

Scaffolds were mineralized by filtration of simulated body fluid(SBF) through the interconnected pores as previously described[19]. SBF (1x) contains 141 mM NaCl, 4.0 mM KCl, 0.5 mM $MgSO_4$, 1.0 mM $MgCl_2$, 4.2 mM $NaHCO_3$, 5.0 mM $CaCl_2 \cdot 2H_2O$,and 2.0 mM $KH_2PO_4$[32]. SBF was sterile filtered using a 0.22µm filter and 0.005% sodium azide was added to prevent bacterial contamination. 2x SBF and 4x SBF solutions titrated to pH 6.4 with 1M NaOH were used with the filtration method. A Delrin® mold containing leached and etched scaffolds was attached to the actuator of an Instron 8521 servo-hydraulic system. The mold was lowered into a base containing sufficient pre-warmed 4x SBF ($37^oC$) to fully submerge all scaffolds during the course of mineralization. The fully submerged mold was cycled in the base at an amplitude of 25.4mm at 0.011Hz. The 4x SBF was changed every 6 hours the first day and was

replaced with 2x SBF which was changed every 12 hours on days 2-5. Solution temperature in the base was maintained at 37$^{o}$C using a heating sleeve connected to a thermocouple and temperature controller (Extech Instruments, Model 48VTR). Mineralized scaffolds (5mm diameter x 2 mm thickness) were carefully detached from the mold, rinsed in dd$H_2O$ for 12 hrs, air-dried in a biosafety cabinet for 12 hrs and stored in a desiccator. Scaffolds were distributed evenly across control and treatment groups to improve mean MV% and variance (Fig. 4.1i).

**SCAFFOLD CHARACTERIZATION**

Morphology of mineralized PLGA scaffolds was assessed using scanning electron microscopy (Philips XL30 FEG SEM). Scaffolds were gold coated and assessed at 20kV (n=9 total). Scanco μCT 100 was used to examine mineralization of scaffolds at 10 μm voxel size at 10 μm slice increments. MicroCT scans were attained at 70kV, 114 A using a 0.5 Al filter. Reconstructed images of all mineralized scaffolds were analyzed using the Scanco μCT_evaluation tool to calculate mineral volume fractions (MV%). Reconstructed images were rendered in (MicroView, Parallax Innovations Inc) using the isosurface tool at a threshold of 1000 with the smoothing filter and a surface quality factor of 0.51 (n=10/group). A custom volumetric shrinkage application was used to generate five concentric volumetric shells each 20% smaller than the previous volume. Mineral volume fractions were calculated for each shell and compared across the five volumetric shells to examine mineral distribution from the exterior toward the interior of the scaffold.

**PEPTIDE SYNTHESIS AND CHARACTERIZATION**

Peptides (Table 4.1) were synthesized at the University of Michigan peptide core. All peptides were chemically synthesized using solid phase synthesis and protective chemistry. HPLC was used to verify > 95% purity. Peptides were stored at -20$^{o}$C until use.

**PEPTIDE LOADING AND CHARACTERIZATION**

Scaffolds pre-wet overnight in dd$H_2O$ were sterilized, transferred to a new micro-plate, and incubated in Trizma buffer for 4hrs at 37$^{o}$C. Peptides were weighed, dissolved in sterile dd$H_2O$, and diluted in Trizma buffer pH 7.4. Trizma pre-incubated scaffolds were immersed in peptide solution (100ug/mL) and set on a shaker under gentle agitation for 3hrs at 37$^{o}$C. Pierce BCA assay (Thermo-Fisher Scientific Inc.) was used to determine total peptide amount on scaffolds (n=6/group) and compared to a standard curve (1-200µg/mL). Peptide distribution on scaffolds was assessed using fluorescein isothiocyanote (FITC) tagged peptides (n=6/group). FITC-VTK has equivalent binding affinity to apatite as unlabeled peptide. Fluorescently tagged peptide coated scaffolds were paper-embedded in cryosection molds in freezing media (OCT, Tissue Tek) on a bed of dry ice and acetone[33]. A Leica cryostat was used to make five 200µm thick sections along the thickness of each scaffold. Sections were mounted in Vectashield (Vector Laboratories) and imaged using a Nikon Ti-Eclipse confocal microscope. Sections were imaged at constant intensity and gain settings across all samples using a 4x objective that incorporated the entire section in the field of view[34]. Edges were clipped to limit artifact and 40 images were acquired along the thickness of each section at 5µm intervals. Image J software (NIH) was used to stack 40 images projected in the Z

direction based on average intensity. A modified concentric circle algorithm was used to measure fluorescence intensity or cell counts within each concentric circle (outmost circle(a) for section 1 to innermost circle(e) for section 5) (Fig. 4.1b,c-g). Intensity measurements were correlated with corresponding sections to assess distribution from the outside to the interior of the scaffold.

**CELL CULTURE**

Mesenchymal stem cells derived from induced pluripotent stem cells (iPS-MSCs) were a generous gift from Dr. Paul Krebsbach. These cells were verified for osteogenic differentiation and bone forming potential *in vivo*[35]. iPS-MSCs were cultured in (**α**-MEM), 10% FBS, antibiotics, 200mM L-glutamine, and 10mM non-essential amino acids. iPS-MSCs (passage 5) were expanded twice (passage 7) when they reached 80-90% confluence before transplantation. Growth media was replaced every 2-3 days and switched to osteogenic media supplemented with osteogenic factors ($10^{-8}$M Dexamethasone, 2-5mM β-glycerophosphate, $10^{-4}$ M ascorbic acid) for 7 days prior to transplantation.

**CELL SEEDING ON PEPTIDE COATED SCAFFOLDS**

Peptide-coated scaffolds were placed into 100uL PCR tubes. Confluent IPS-MSCs (passage 7) were trypsinized and suspended in either serum-free or complete media in a 20µL volume containing 50,000 cells. Cell suspension was added to each scaffold within each PCR tube for 3hrs at 5% $CO_2$ and 37$^{o}$C. Cells seeded on peptide-laden scaffolds (n=6/group) were fixed in 10% phosphate buffered formalin. Fixed cell-seeded scaffolds were paper embedded in cryosection molds in freezing media (OCT, Tissue Tek) on a bed of dry ice and acetone[33]. A Leica cryostat was used to make five 200µm thick

sections along the thickness of each scaffold. Cell-seeded scaffold sections were dried, permeablized in Triton X, and stained with DAPI. All sections were mounted in Vectashield (Vector Laboratories) and imaged using a Nikon Ti-Eclipse confocal microscope. Sections were imaged at constant intensity and gain settings across all samples using a 4x objective that incorporated the entire section in the field of view[34]. Edges were clipped to limit artifact and 40 images were acquired along the thickness of each section at 5μm intervals. Image J software (NIH) was used to stack 40 images projected in the Z direction based on average intensity. A modified concentric circle algorithm used for peptide distribution analysis was used to measure cell counts from the outside to the interior of the scaffold.

**SUBCUTANEOUS TRANSPLANTATION OF CELL-SEEDED CONSTRUCTS**

Peptide coated scaffolds and uncoated mineralized control scaffolds were placed in PCR tubes and statically seeded in a 20μL volume of complete media at $3 \times 10^6$ cells/construct for 3 hours. This micromass seeding method was used to improve seeding efficiency on peptide coated constructs. Moreover, a significantly higher cell number than in vitro studies was used to ensure bone formation in an ectopic model[36]. The cell seeded mineralized scaffolds and mineralized-peptide-laden scaffolds (n=10/group) were then stored on ice prior to transplantation and cell counts in the remaining volume of media in tube were used to calculate seeding efficiency. Acellular mineralized scaffolds and acellular mineralized scaffolds coated with DPI-VTK were included as controls (n=4/group). NIH guidelines for the care and use of laboratory animals (NIH Publication #85-23 Rev. 1985) were adhered to. All surgical procedures were performed in accordance with University of Michigan's Committee on Use and Care of Animals. Male

nude mice (NIH-Lyst$^{bg\text{-}J}$Foxn1$^{nu}$Btk$^{xid}$, Charles Rivers) between 25-30g were anesthetized with isoflurane in $O_2$ (5% induction and 2% maintenance at 1mL/min). A midline longitudinal incision was made on the back of each mouse and 4 pockets (2 on each side) were made in the subcutaneous tissue beneath the dorsal skin. Cell seeded constructs were placed into each pocket and the incision was closed with surgical staples. Animals were sacrificed 8 weeks postoperatively and transplants were harvested.

**OSSICLE MICROCOMPUTED TOMOGRAPHY**

Ossicles of regenerated bone were fixed in 4% phosphate buffered formalin, embedded in agarose and imaged in a Scanco μCT 100 at 12 μm voxel size at 12 μm slice increments at 70kV, 114 A using a 0.5 Al filter. Reconstructed images were rendered in MicroView ( Parallax Innovations Inc) using the iso-surface tool with the smoothing filter and a surface quality factor of 0.51 (n=10/group). Advanced ROI tool, combined with histogram values were used to calculate bone volume fraction (BVF). A custom volumetric shrinkage application in MATLAB was used to generate five concentric volumetric shells each 20% smaller than the previous volume. Bone volume fractions were calculated for each shell and compared across the five volumetric shells to examine mineral distribution from the exterior toward the interior of the scaffold.

**OSSICLE HISTOLOGY AND HISTOMORPHOMETRY**

Osscicles were retrieved from agarose and decalcified in 10% EDTA. Transplants (n=5/group) were sectioned through the midline, paraffin embedded, and 5μm thick triplicate sections were made of 3 ossicle regions progressing from the interior to the periphery. Sections were subsequently deparaffinized, hydrated, and stained with hematoxylin and eosin. Sections were scored using parameters outlined in Table 4.2[37],

[38]. A 20x field of view was used to scan sections and assess bone coverage. Totals for each ossicle region were averaged.

### STATISTICAL METHODS

Statistical analysis was conducted using Sigmaplot 13.0. One-way ANOVA on ranks using Tukey test for pairwise comparison was used to compare peptide adsorption, cell seeding efficiency, and bone quality across treatment groups. One-Way ANOVA on ranks with Dunn test for pairwise comparisons was used to assess bone volume fractions. Two-Way ANOVA on ranks using Tukey test for pairwise comparisons was used to assess peptide, cell, mineral and bone volume distribution. Multiple and single linear regression were conducted across peptide groups, cell distribution, peptide distribution, mineral distribution, bone volume distribution and histological bone scores.

## RESULTS

### CHARACTERIZATION OF MINERALIZED SCAFFOLDS

Continuous mineral coverage on porous PLGA scaffolds was visually verified across all batches using SEM (Fig 4.1 a,b). Average mineral volume fractions (MV%) for all treatment groups were 16.5±3.8% (Fig 4.1i). Filtration of SBF resulted in mineralization throughout each scaffold (Fig 4.1, d-i). There was a greater fraction of mineral in the interior region compared to shells 1 and 2 ($p < 0.001$, n=10/group). Greater mineralization in the interior region may arise from increased turbulent flow conditions, and early nucleation within the interior of the scaffold pores. Regardless, there was no observable pore occlusion which limits transport and vascularization.

**PEPTIDE LOADING ON MINERALIZED SCAFFOLDS**

Peptide adsorption on mineralized scaffolds was consistent no significantly different between VTK, DPI-VTK and RGD-VTK groups (Fig 4.2a, n=6/group). The amount of P15 adsorbed to the scaffold surface (0.75 ±0.053 nmols, n=6/group) was less than DPI-VTK ($p < 0.001$) , RGD-VTK ($p < 0.01$) and VTK ($p < 0.001$). Adsorbed VTK, DPI-VTK and RGD-VTK were distributed uniformly across scaffold sections spanning from the periphery to the innermost shell (Fig 4.2 c-h). Fraction of adsorbed peptide was not significantly different within peptide groups (Fig 4.2h). There was a higher adsorbed fraction of VTK than RGD-VTK in the outermost section ($p < 0.02$).

**CELL ATTACHMENT AND DISTRIBUTION ON PEPTIDE-LADEN SCAFFOLDS**

Cells adhered readily to DPI-VTK coated mineral scaffolds (Fig. 4.3 a). Seeding 50,000 cells on a DPI-VTK coated scaffold (Fig. 4.3a) did not result in the surface saturation with cells evident on scaffolds seeded with $3 \times 10^6$ cells for in-vivo implantation (Fig. 4.3b-d). There was more efficient IPS-MSC seeding on VTK ($p<0.04$), DPI-VTK ($p<0.002$), RGD-VTK ($p<0.001$), and serum coated BLM ($p<0.001$) compared to serum-free BLM control groups (Fig 4.3e). RGD-VTK exhibited higher seeding efficiency than BLM ($p < 0.001$), VTK ($p<0.001$), and DPI-VTK ($p<0.01$). Seeding efficiency was greater on DPI-VTK and serum-coated BLM compared to VTK ($p < 0.05$). The fraction of cells adherent to VTK in the outermost section of the mineralized scaffold was greater than BLM with serum (Fig. 4.3f; $p < 0.02$). Moreover, the fraction of cells adherent to the outermost section on VTK coated scaffolds was greater than the middle and inner-most sections (Fig. 4.3g; $p<0.001$). Seeding efficiency on scaffolds prior to *in vivo* implantation was 98.3% ±5.35% across all peptide and control groups (n=6/group).

**OSSICLE BONE VOLUME FRACTION AND DISTRIBUTION**

MicroCT images reveal, qualitatively greater bone formation on scaffolds with DPI-VTK (Fig 4e) and P15 (Fig 4.4f) compared to scaffolds with cells, but no peptide (Fig, 4.4c), scaffolds with just the mineral-binding peptide (Fig. 4.4d) and acellular controls (Fig 4.4a,b) controls. However, scaffolds coated with both DPI-VTK and P15 exhibited shell formation characteristic of ectopically reconstructed ossicles. MicroCT analysis (Fig 4.4g) quantify the greater BVF in constructs coated with DPI-VTK compared to VTK ($p < 0.002$), BLM ($p < 0.037$), acellular DPI-VTK ($p < 0.003$) and acellular BLM controls ($p < 0.00$). P15 coated constructs had greater BVF than BLM($p < 0.05$) and acellular BLM ($p < 0.005$). There were noticeable differences between VTK coated constructs and uncoated and acellular controls, however the large and unequal variance resulted in failed significance. Total volumes were also greater for DPI-VTK and P15 groups compared to BLM, VTK and acellular controls (Fig 4.4h, $p < 0.001$).

Rendered MicroCT images of concentric shells of regenerated bone (Fig 4.5b-f) revealed greater bone formation towards the peripheral sections compared to interior sections. There were no significant differences in bone volume within sections across peptide groups (Fig 4.5g). VTK coated constructs had a significantly greater fraction of bone in section 2 compared to sections 4 ($p<0.004$) and 5 ($p < 0.026$). DPI-VTK coated constructs had a greater fraction of bone in section 1 compared to section 5 ($p<0.002$) and section 4 ($p<0.003$), as well as a greater fraction of bone in section 2 compared to section 5 ($p<0.005$) and section 4 ($p<0.008$). Similarly, P15 coated constructs had a greater fraction of bone in section 1 compared to section 5 ($p<0.004$) and section 4 ($p<0.005$), as

well as a greater fraction of bone in section 2 compared to section 5 ($p<0.015$) and section 4 ($p<0.019$).

**HISTOLOGY OF RECONSTRUCTED OSSICLES**

There was greater bone formation on DPI-VTK and P15 coated constructs compared to VTK and BLM constructs (Fig 4.6 a-h). Ossicles from BLM and VTK demonstrated some bone formation surrounding scaffold pores (p), however the DPI-VTK and P15 constructs were relatively devoid of pores(p) and struts(t). Ossicles from BLM and VTK coated scaffolds look compressed and elongated compared to pre-transplanted scaffolds, whereas DPI-VTK and P15 constructs appear larger than the originally transplanted constructs which is consistent with total volumes. Regenerated bone from DPI-VTK and P15 also demonstrated greater vascularization (h) and cellularity (c) compared to VTK coated and BLM constructs. Bone score indicate greater bone formation on DPI-VTK and P-15 compared to VTK and BLM (Fig. 4.6i; $p <0.001$). There were no significant differences in bone score within different sections of scaffolds for each peptide group (Fig 6j). Across sections (Fig 6k), DPI-VTK and P15 exhibited greater bone scores compared to VTK and BLM ($p <0.001$).

**REGRESSION ANALYSIS**

Multivariate linear regression revealed no correlation between *in vitro* cell distribution, peptide distribution, and mineral distribution on bone distribution *in vivo*. Similarly regressing bone distribution against *in vitro* cell distribution, peptide distribution, and mineral distribution by individual treatment group revealed no correlation with a desired $p<0.05$. Regressing cell distribution against mineral distribution and peptide distribution

revealed no correlation with P <0.05. Similarly regressing cell distribution by individual treatment group revealed no correlation with a desired p<0.05.

## DISCUSSION

DPI-VTK coated on mineralized PLGA constructs improved overall bone formation in a ectopic model compared to non-peptide coated, VTK and acellular controls. Moreover, bone formed by DPI-VTK coated constructs exhibited increased cellularity and vascularization compared to uncoated, VTK and acellular controls. However, uniform peptide distribution, cell distribution, and mineral distribution did not correlate to improved bone distribution *in vivo*.

Peptides containing the VTK, DPI-VTK, and RGD-VTK mineral specific sequence improved overall adsorption to mineral and delivery of cell binding sequences to apatite compared to collagen derived P15 sequence (Fig 4.2a). The increase in mineral binding between VTK vs. RGD-VTK in the outermost region of mineralized scaffolds can result from different packing efficiencies arising from conformational differences in solution and bound states. Furthermore VTK and RGD-VTK both have a net charge of 1 however; the distribution of charged residues within the peptide can result in varying steric repulsions when saturating the mineral surface.

Although less RGD-VTK was bound in the outermost region of the construct(Fig 4.2h), there were no observable differences in the fraction of bound cells between VTK and RGD-VTK in the outermost region(Fig 4.3f). Cell attachment to DPI-VTK is improved compared to BLM without serum and VTK without serum. Although cell seeding efficiency on DPI-VTK is equivalent to RGD-VTK and BLM in serum, the DPI peptide

promotes cell specific attachment to MSC whereas RGD and serum proteins are non-specific. Moreover, RGD coated substrates exhibit poorer osteogenic activity *in vivo* hypothesized to result from unfavorable serum protein interactions[26], [39]. However, DPI-VTK cooperatively interacts with serum proteins towards improving MSC attachment (Chapter 2). The cell-specific interaction combined with cooperative serum interaction could also play a role in observed improvements in the quantity and quality of bone formation *in vivo*. Serum-free or xeno-free media are increasingly used to meet current good manufacturing practices for clinical grade MSCs in order to limit risk of disease transmission and immunogenicity while maintaining consistency of appropriately tested and qualified starting materials[40]–[42]. The ability of DPI-VTK to attach equivalent numbers of cells in serum free media as serum coated BLM also implies a potential *ex vivo* application for serum-free expansion on mineral substrates[43], [44].

Cell-seeded mineralized scaffolds containing DPI-VTK significantly improved the total volume, the volume fraction and bone scores compared to VTK coated and uncoated BLM, and acellular BLM and DPI-VTK scaffolds (Fig 4.4). Acellular mineral and acellular DPI-VTK was unable to form bone in the ectopic mouse model. Although the adipose tissue surrounding the ectopic implantation pocket contain a resident population of mesenchymal stem cells, the low percentage of mesenchymal cells within the tissue and their location with respect to the DPI-VTK transplant may preclude infiltration and recruitment. Furthermore, the rate of degradation of the mineral and construct can impact conduction. Regardless, both acellular BLM and acellular DPI-VTK coated constructs provide a baseline for comparing transplanted IPS-MSC driven tissue reconstruction on control and peptide coated substrates.

Initial mineral volumes are commonly subtracted from the final bone volumes in order to calculate total regenerated bone volume. However, these calculations assume inert mineral substrates that do not dissolve over the course of the transplantation. The mineralized PLGA substrate coated with 2x SBF results in a rapidly dissolving mineral substrate that is nearly resorbed as evidenced in the acellular controls. Even within cellularized constructs, the 2x precipitated SBF results in poor bone formation compared to previous studies utilizing 1x SBF precipitated mineral[45]. Moreover, a thrombin-fibrin clot is typically used to provide further retention of cells within the construct. The inability to use the fibrin clot in order to directly test peptide-cell effects resulted in poor bone formation on BLM constructs compared to previously observed studies. Although there were no significant differences in total volume, bone volume fraction or bone scores of regenerated bone between P15 and DPI-VTK coated cellular constructs, further engineering the dual-peptide sequence to improve cell specificity can drive greater bone formation.

Cell-seeded constructs, especially those containing MSCs, can drive vascularization through secretion of pro-angiogenic factors contributing to hematopoiesis which concomitantly drives greater bone formation[46], [47]. Hematopoietic regions were evident across all cell-transplanted treatment groups. Greater cell numbers were observed within constructs coated with DPI-VTK and P-15(Fig 4.6). VTK cell-seeded constructs exhibited observably greater bone formation compared to BLM controls and acellular controls however the variance was too large for significance.

Bone regenerated from murine bone marrow stromal cells on a mineralized PLGA scaffold construct in an ectopic mouse model exhibited 90% of cells with donor origin

up to 12 weeks post transplantation[45], [48], [49]. MSC driven bone formation on β-TCP constructs also reveals retention of donor cells for up to 45 weeks post transplantation[50]. It can be inferred that the majority of cells present within DPI-VTK and P15 are from a donor origin. Moreover, the limited cellularity within acellular DPI-VTK and acellular BLM constructs further indicates the lack of host cell contribution to regenerating ectopic ossicles. Taken together, the ability of DPI-VTK to sequester donor cells and/or recruit host cells within transplanted constructs is one of the leading drivers of improved quantity and quality of bone formation.

However, regression analysis indicates no correlation between in vitro mineralization, peptide distribution, cell distribution and in vivo bone formation. Furthermore, a characteristic shell of bone indicating non-uniformity was evident in both P15 and DPI-VTK coated constructs (Fig 4.5). A shell is commonly formed in an ectopic model[48], [51], [52]. The subcutaneous environment is physically and temporally limited by the ability to form deeply penetrating vascular networks before cell mediated mineral formation causes pore occlusion and isolation of the interior regions[53].Furthermore, attenuated clearance of biomaterial substrate degradation byproducts can increase toxicity of the interior microenvironment adding to the shell [54]. Another artifact arising from the shell formation could cause attenuated degradation of the scaffold interior resulting in higher measured bone volume fractions. There was limited to no evidence of this artifact from histological assessment of bone (Fig 4.6). Bony spicules within the center regions of both DPI-VTK coated and P15 coated constructs exhibited thick cellularized sections which are inconsistent with latent mineral from pre-implanted sources. Despite the shell

formation, DPI-VTK promoted moderate bone formation penetrating 60% of the scaffold interior.

Osteoinductive potential of DPI-VTK could also be a contributing factor towards improved bone formation. DPI-VTK competes with many of the same integrin domains involved in osteogenic differentiation namely $\alpha_5\beta_1$ and $\beta_5$ domain(Chapter 2). These domains are implicated in osteoblastic differentiation and could drive the differentiation of initially adherent cell fractions. P15 is also suggested to promote osteogenic differentiation through the $\alpha_2\beta_1$ cell binding domain which is implicated in activation of osteoblastic differentiation pathways [25].

The marked improvement in *in vivo* osteogenic potential of DPI-VTK compared to non-peptide coated constructs warrants further investigation towards the mechanism of action. Future studies to elucidate specific cell binding targets in addition to conformational regulation DPI sequence when present with the VTK sequence can further improve the osteogenic potential of these phage derived peptides. As tissue engineering shifts from developing technologies to meet general clinical challenges to addressing more focused clinical applications, there will be an increased need for delivering cell specific cues to material surfaces with defined surface chemistries [7], [55]. Combinatorial phage display is a powerful technology platform to enable focused cell based tissue regeneration through the discovery of cell specific and material specific peptide sequences.

**ACKNOWLEDGEMENTS**

I would like to thank Dr. Paul Krebsbach and Luis Villa for iPS-MSCs used in these studies, Michelle Lynch for her assistance with MicroCT and Chris Strayhorn for the histology. This work is supported by NIH R01 DE 013380, DE 015411 (DHK).

## CHAPTER FOUR TABLES

### TABLE 4.1 PEPTIDE PROPERTIES

| Peptide | Sequence | Description | MW (g/mol) | Net Charge | Acidic residues |
|---|---|---|---|---|---|
| VTK | VTKHLNQISQSY | Phage derived mineral binding sequence | 1417.59 | 1 | 2 |
| DPI-VTK | GGDPIYALSWSGMAGGGSVTKHLNQISQSY | **Dual functioning peptide containing phage derived cell and mineral binding sequences** | 3025.35 | 0 | 5 |
| RGD-VTK | GGRGDGGGSVTKHLNQISQSY | Dual functioning peptide containing cell binding control sequence and phage derived mineral binding sequence | 2061.20 | 1 | 3 |
| P15 | GTPGPQGIAGQRGVV [23] | Col1a1 derived cell and mineral binding peptide for in vivo control | 1393.57 | 1 | 0 |

**TABLE 4.2 HISTOLOGY SCORING PARAMETERS**

| Score | Bone Coverage |
|---|---|
| 0 | No Bone |
| 1 | 1%-5% in a particular region |
| 2 | 5%-10% in a particular region |
| 3 | 10%-25% throughout section |
| 4 | >25% throughout section |

## CHAPTER FOUR FIGURES

### FIGURE 4.1(A-J) MORPHOLOGY AND DISTRIBUTION OF BONE-LIKE MINERAL PRECIPITATED ON PLGA SCAFFOLDS

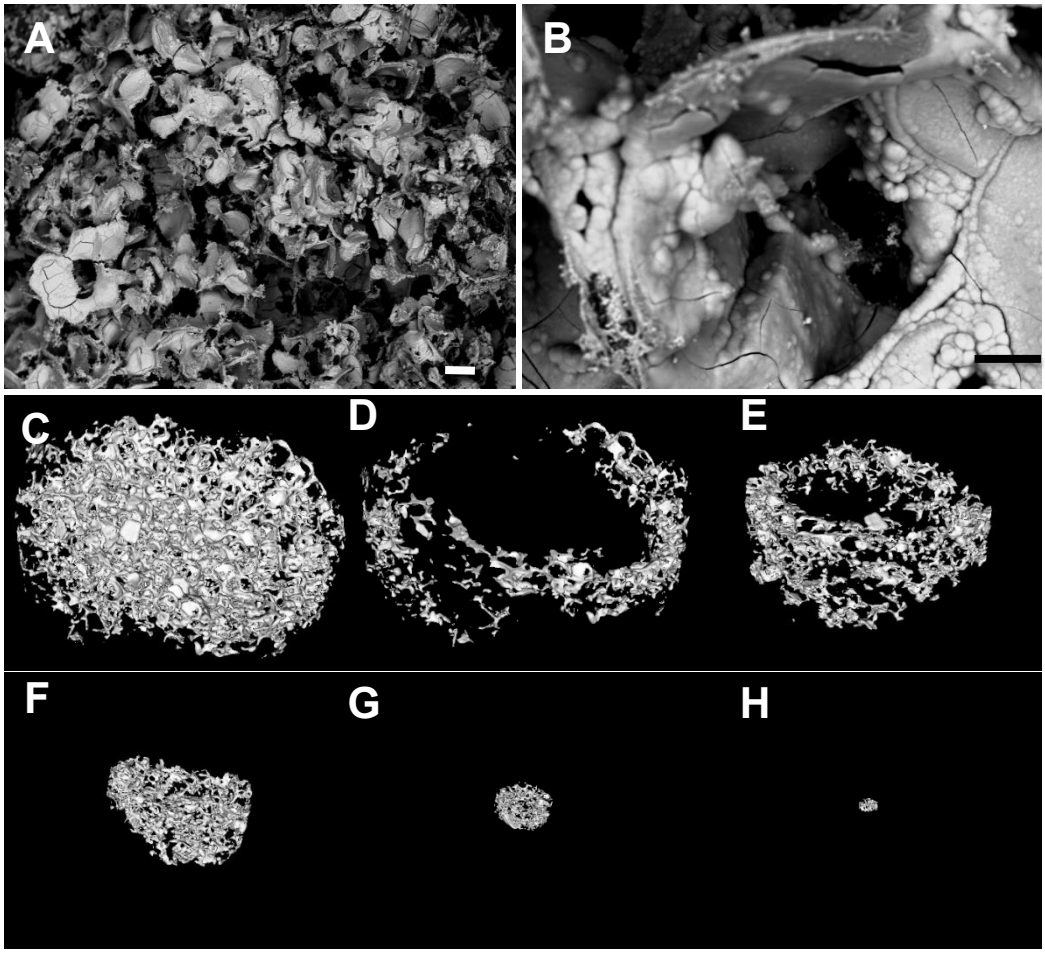

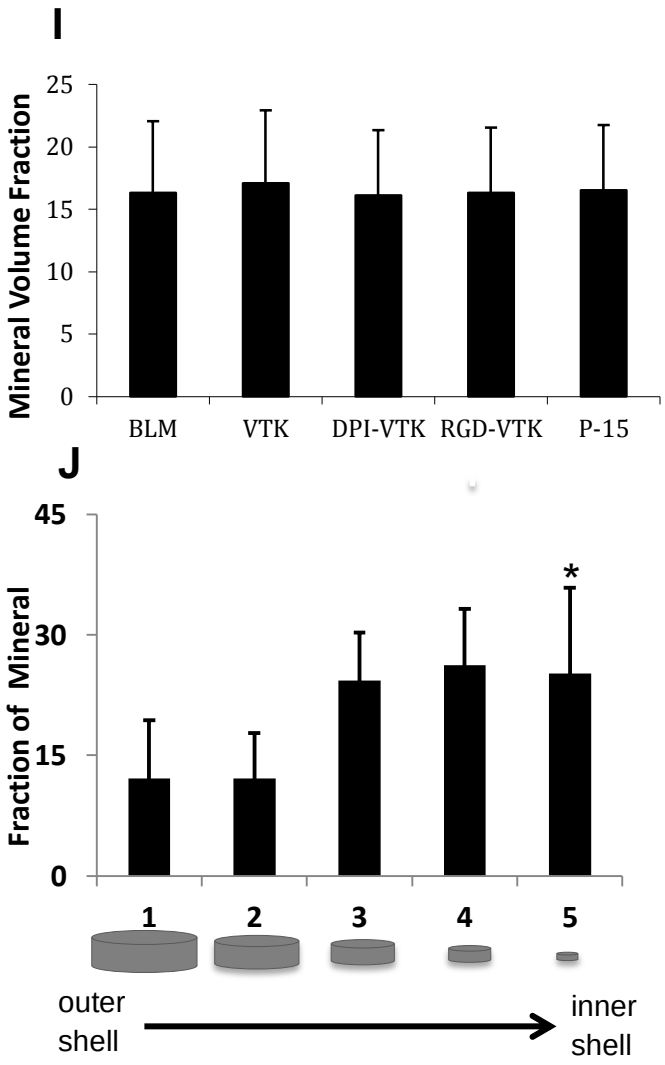


**Figure 4.1:** Morphology and distribution of bone-like mineral precipitated on PLGA scaffolds. Representative SEM images of mineralized scaffolds at A)low and B)high magnification. scale bars 200µm and 50µm respectively. C)Representative MicroCT image of mineralized scaffold rendered in MicroView® D-H)Representative images of mineral distribution volumetric shells progressing from the outermost to innermost regions of the scaffold. I) Mineral volume fraction across peptide groups. Fraction of mineral volume progressing from the outermost to the innermost volumetric shell of the scaffold (J). * indicates significant difference from section 1 and 2 ($p<0.001$).

**FIGURE 4.2(A-H). PEPTIDE ADSORPTION AND DISTRIBUTION ON MINERALIZED PLGA SCAFFOLDS.**

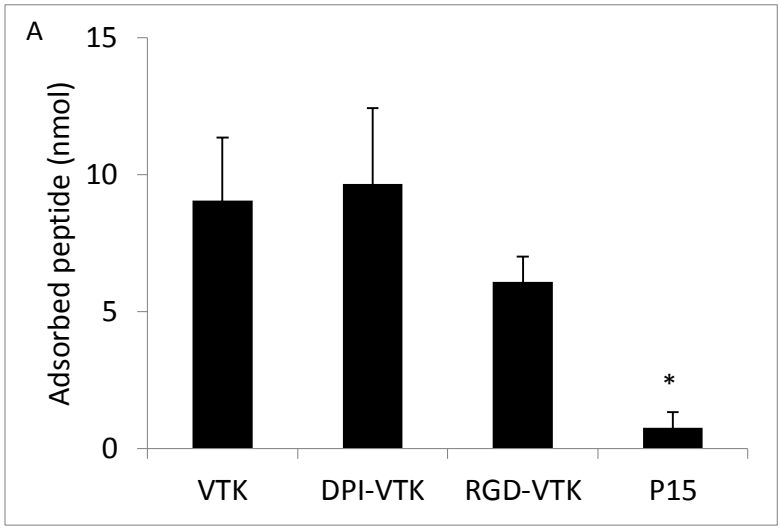


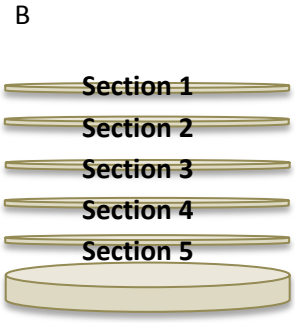


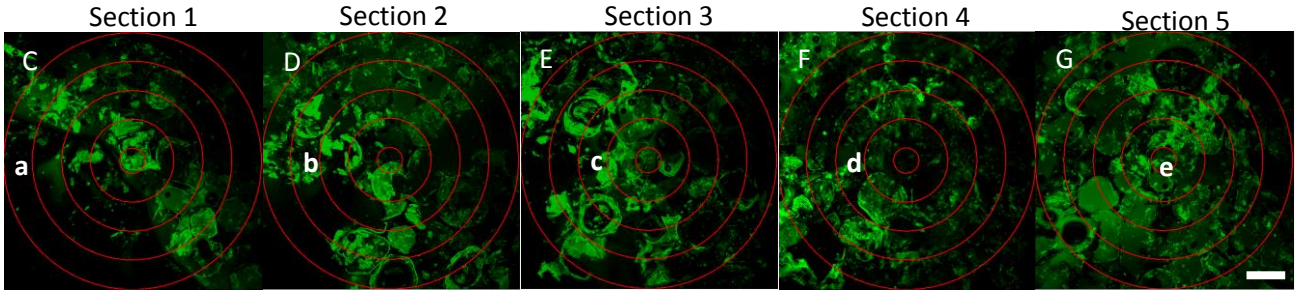

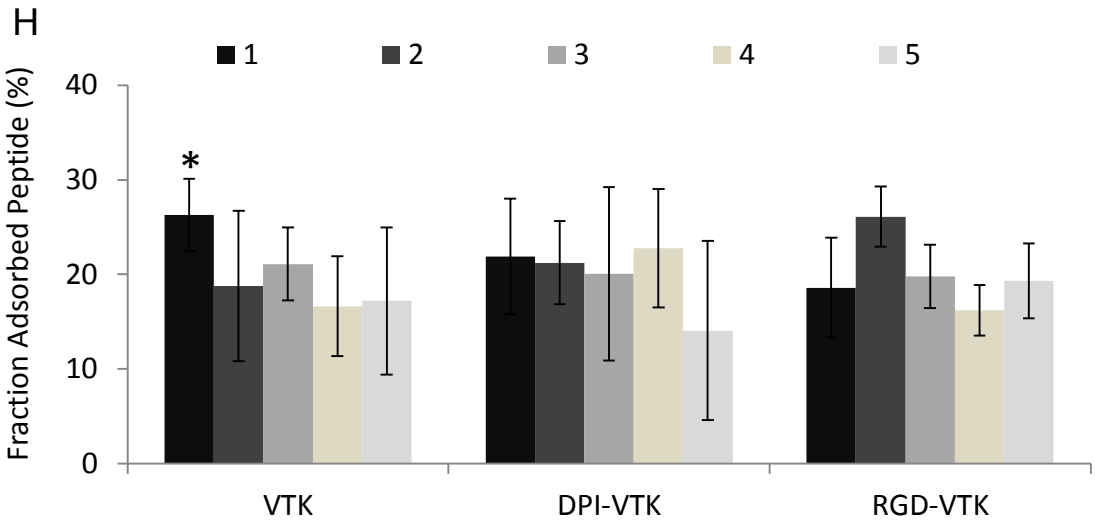


**Figure 4.2.** Peptide adsorption and distribution on mineralized PLGA Scaffolds. (A) Peptide adsorption evaluated by BCA assay demonstrates no significant differences across peptide groups. (B) Schematic depicting relative position of each cryosection within the scaffold. (C-F) Representative images of DPI-VTK distribution on PLGA mineralized scaffolds with (a-e) regions indicating sampled area within corresponding sections. Each image is a composite stack of 40 images projected in the Z direction based on average intensity (scale bar 0.5mm). (H) Uniform distribution of adsorbed peptide (n=6) across all groups was analyzed using Image J(NIH) software with a customized concentric circle algorithm. * indicates significantly different from Section 1 of RGD-VTK ($p < 0.02$).

**FIGURE 4.3(A-G) - CELL SEEDING EFFICIENCY AND CELL DISTRIBUTION ON PEPTIDE COATED SCAFFOLDS.**

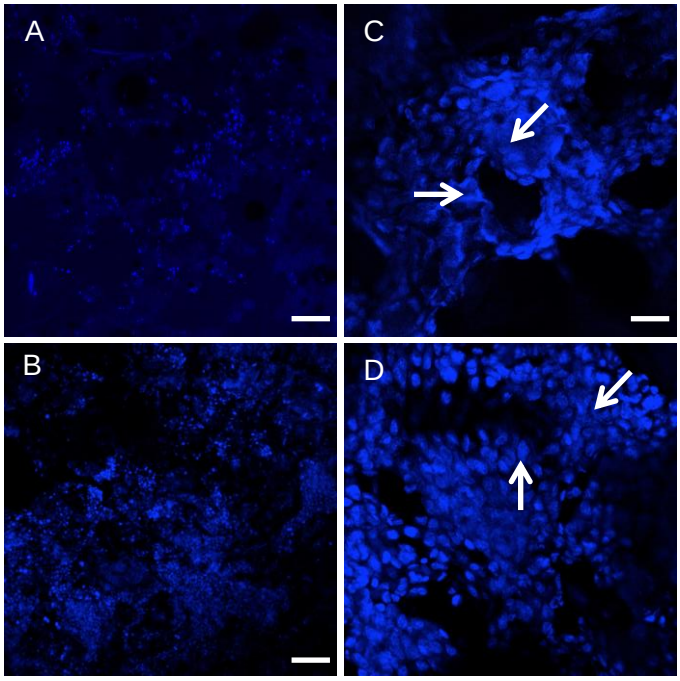


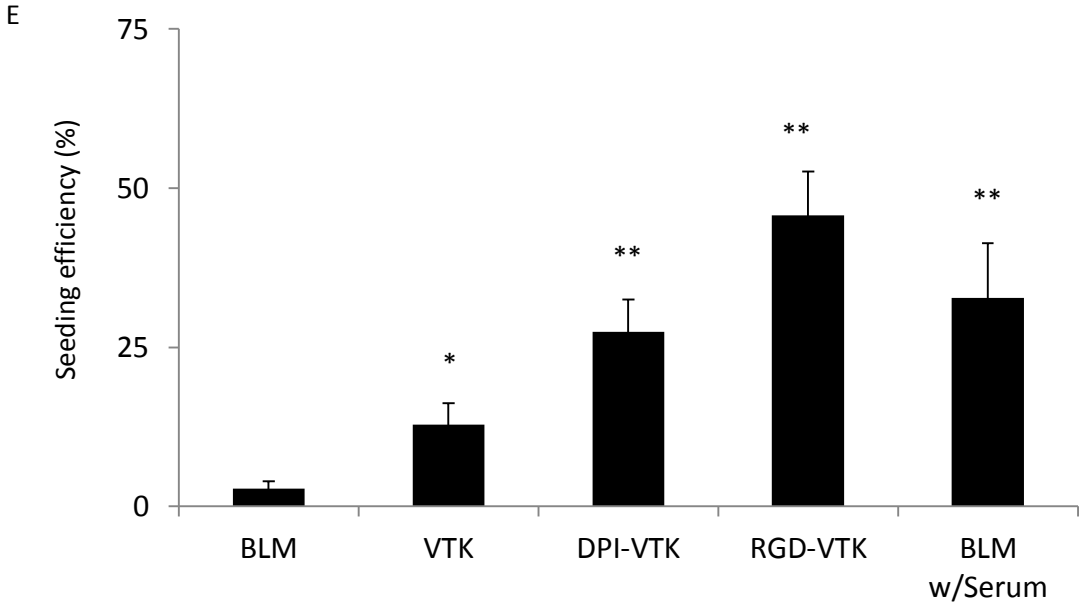

F

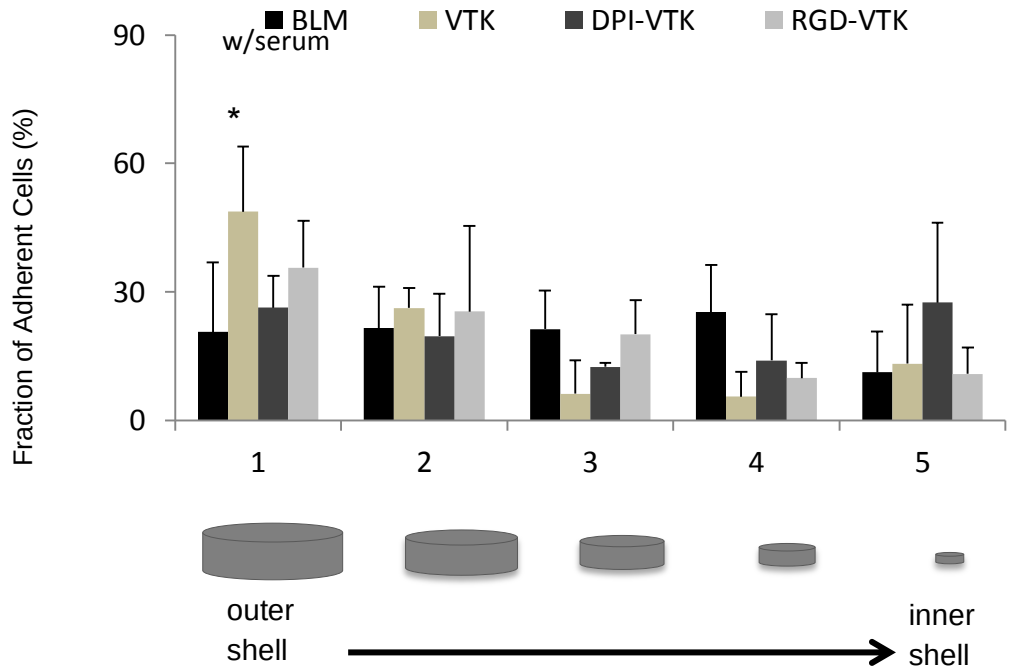
BLM w/serum
VTK
DPI-VTK
RGD-VTK
Fraction of Adherent Cells (%)
90
60
30
0
*
1
2
3
4
5
outer shell
inner shell

G

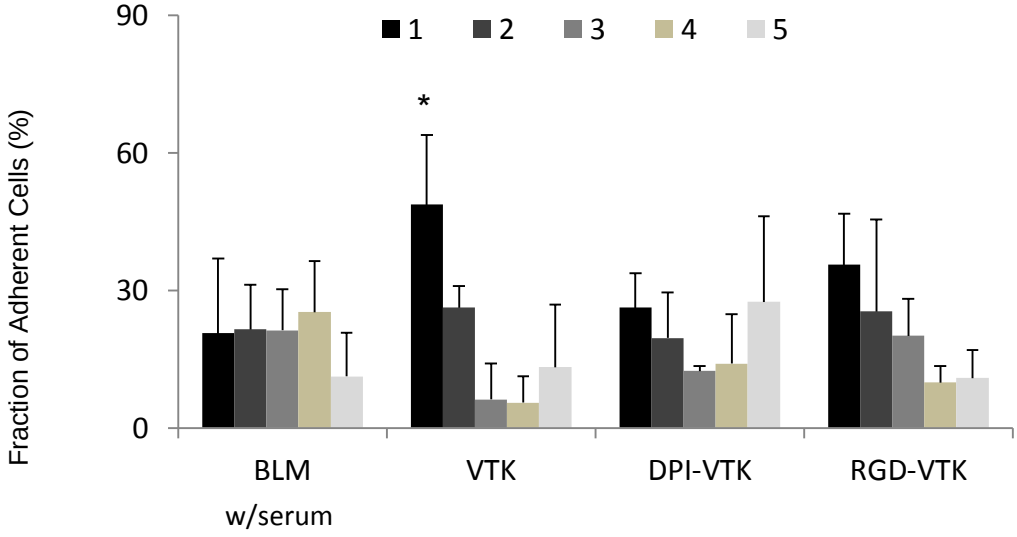
1
2
3
4
5
Fraction of Adherent Cells (%)
90
60
30
0
*
BLM w/serum
VTK
DPI-VTK
RGD-VTK

**Figure 4.3 -** Cell Seeding efficiency and distribution on peptide coated scaffolds. A) DAPI stained cells on DPI-VTK coated scaffolds at 50,000 cells/scaffold (scale bar 500 µm). B) DAPI stained cells on scaffolds to be used for in vivo implantation at 3x106 cells/scaffold (scale bar 200µm). C) Top and D) bottom view of scaffolds before implantation indicating complete surface saturation and clustering around scaffold pores indicated by arrows(scale bar 100µm). E) Seeding efficiency on peptide coated scaffolds based on histomorphometric analysis. *** indicates significant difference from DPI-VTK ($p<0.01$), VTK ($p<0.001$), and BLM ($p<0.001$). ** indicates significant difference from VTK ($p <0.05$) and BLM ($p <0.002$) groups. * indicates significant difference from BLM ($p<0.04$) group. F) Fraction of adherent cells as a function of spatial location indicating higher cell fraction bound to VTK in section 1 compared to BLM (*, $p<0.02$). G) Fraction of adherent cells by peptide groups indicating higher cell fractions bound to section 1 compared to sections 3, 4, and 5 (*, $p<0.001$).

**FIGURE 4.4(A-H). BONE VOLUME FRACTIONS OF ECTOPICALLY REGENERATED OSSICLES 8 WEEKS POST TRANSPLANTATION.**

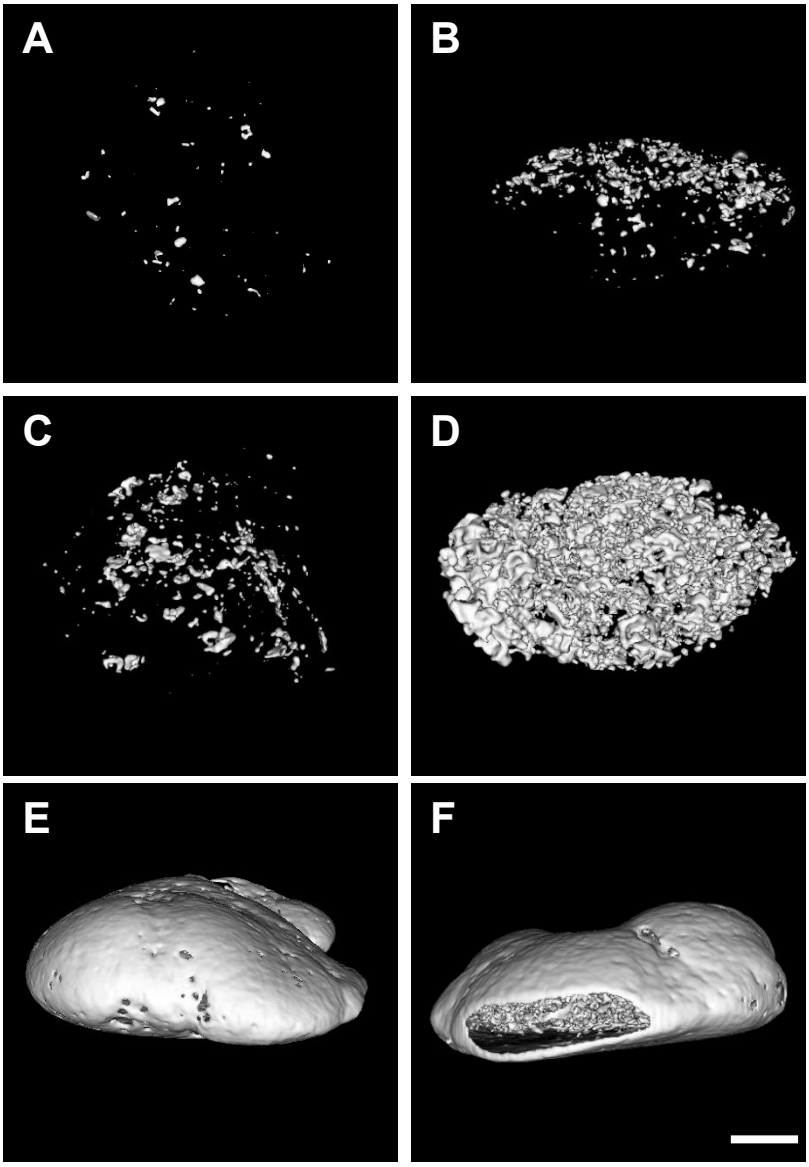

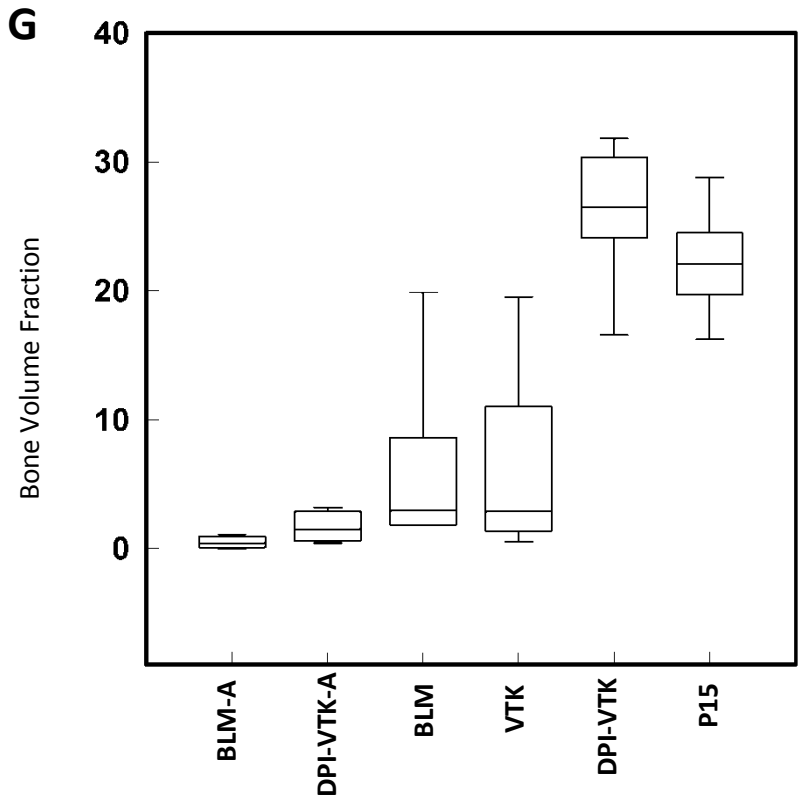
G
40
30
20
10
0
Bone Volume Fraction
BLM-A
DPI-VTK-A
BLM
VTK
DPI-VTK
P15

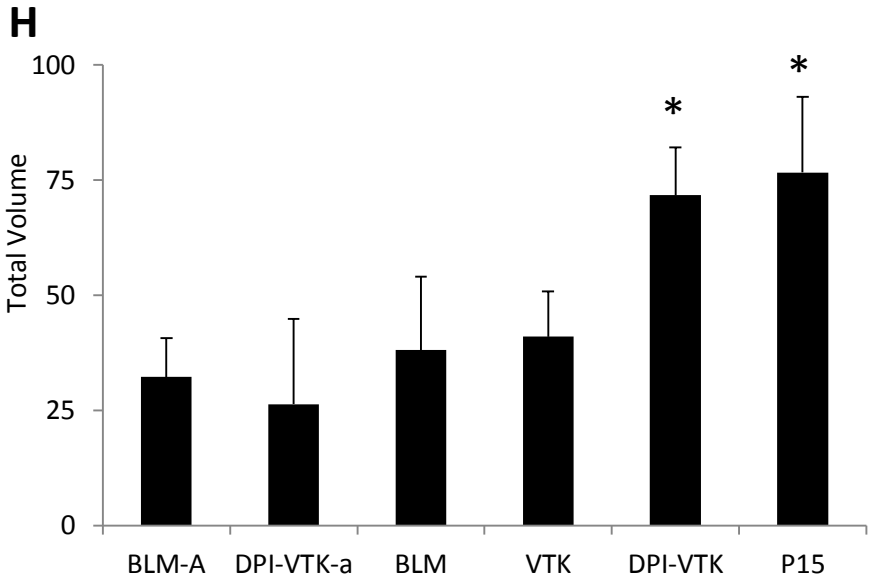
H
100
75
50
25
0
Total Volume
*
*
BLM-A
DPI-VTK-a
BLM
VTK
DPI-VTK
P15

**Figure 4.4.** Bone volume fractions of ectopically regenerated ossicles 8 weeks post transplantation. Representative rendered MicroView® images of A) acellular BLM, B) acellular BLM containing DPI-VTK, C) BLM with iPS-MSCs, D) BLM containing VTK with iPS-MSCs, E) BLM containing DPI- VTK with iPS-MSCs, F) P15 coated BLM constructs (scale bar=1mm). G) Bone volume fractions from MicroCT analysis indicate greater bone formation in scaffolds with DPI-VTK and P15 compared to VTK, BLM, DPI-VTK acellular and BLM acellular controls. * indicates a significant difference from BLM and acellular BLM ($p < 0.003$). ** indicates a significant difference from VTK ($p < 0.017$),BLM ($p < 0.001$), acellular DPI-VTK ($p < 0.002$) and acellular BLM controls ($p < 0.01$). H) Total volume is greater on DPI-VTK and P15 compared to

**FIGURE 4.5(A-H). BONE DISTRIBUTION IN ECTOPICALLY REGENERATED OSSICLES 8 WEEKS POST TRANSPLANTATION.**

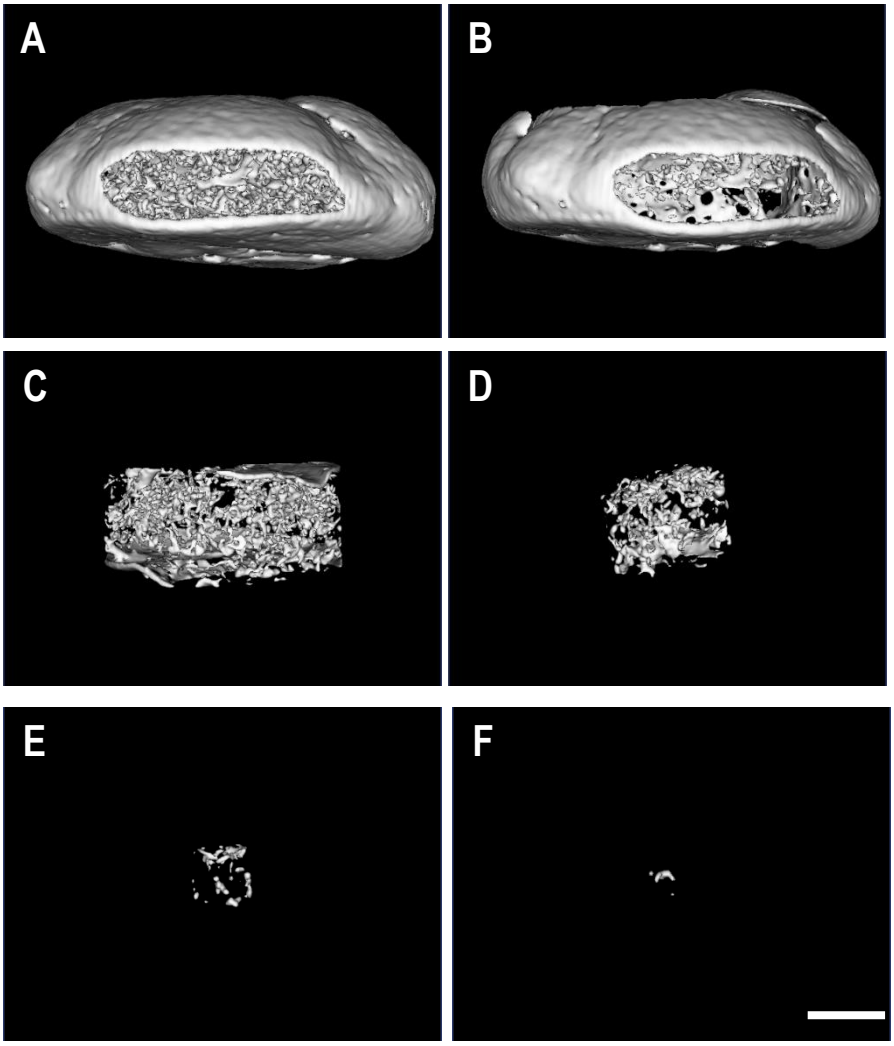

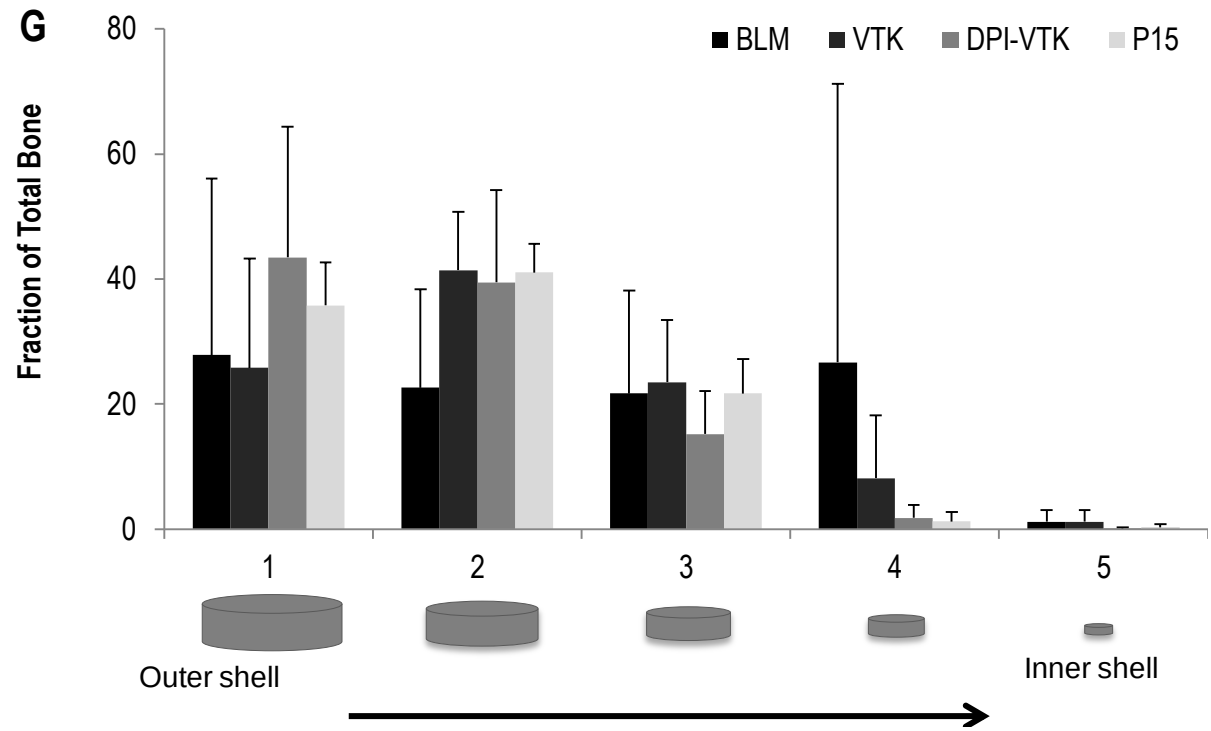


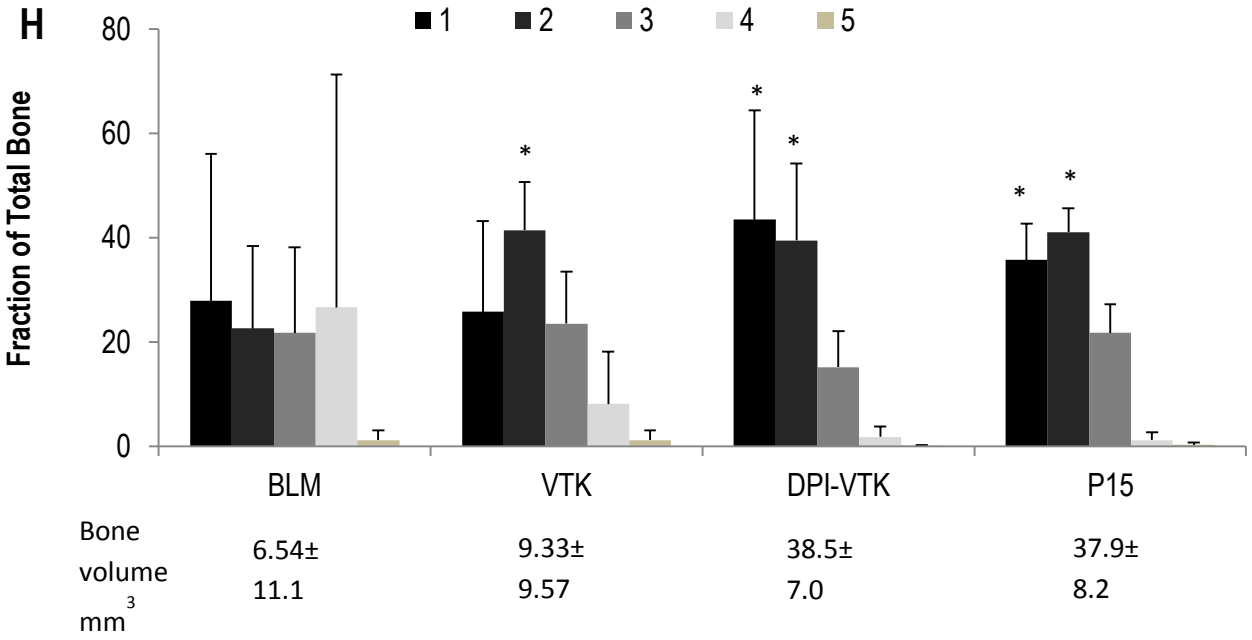


| Bone volume $mm^3$ | BLM | VTK | DPI-VTK | P15 |
|---|---|---|---|---|
| | 6.54± 11.1 | 9.33± 9.57 | 38.5± 7.0 | 37.9± 8.2 |

**Figure 4.5.** Bone distribution in ectopically regenerated ossicles 8 weeks post transplantation. A) Representative rendered MicroCT image of ossicle regenerated from cell seeded DPI-VTK coated mineralized scaffold (1mm scale bar). B-F) Concentric volumetric shells progressing from the outermost to innermost region of regenerated ossicle. G) Fraction of total bone by section indicating no significant differences in % of total bone in each section amongst peptides. H) Fraction of total bone by peptide revealing greater fraction of bone towards the periphery compared to the interior regions in peptide groups. * indicates significant difference from sections 4 and 5.

**FIGURE 4.6(A-K). HISTOLOGICAL STAINING AND BONE QUALITY SCORING OF ECTOPICALLY REGENERATED OSSICLES 8 WEEKS POST TRANSPLANTATION.**

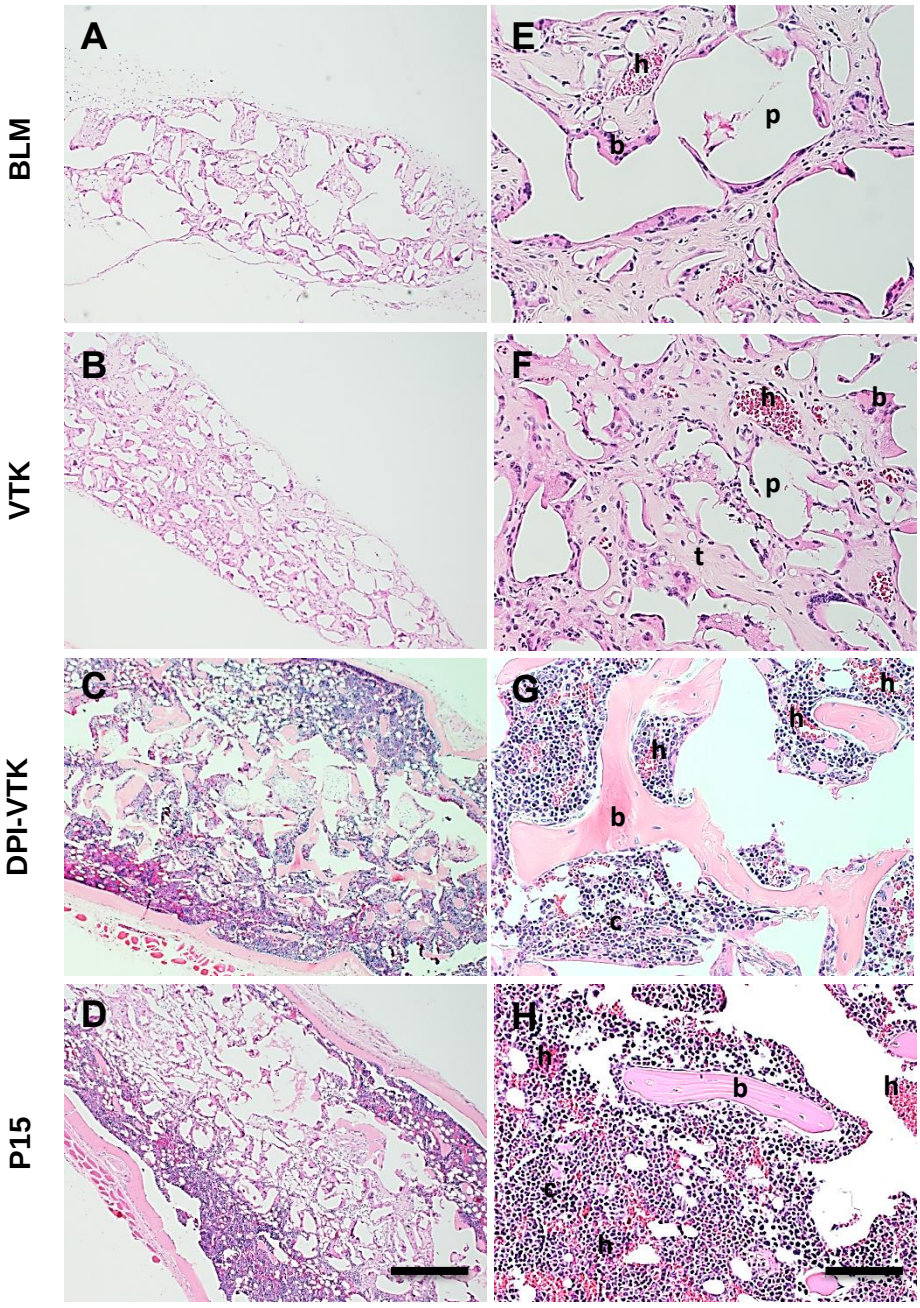

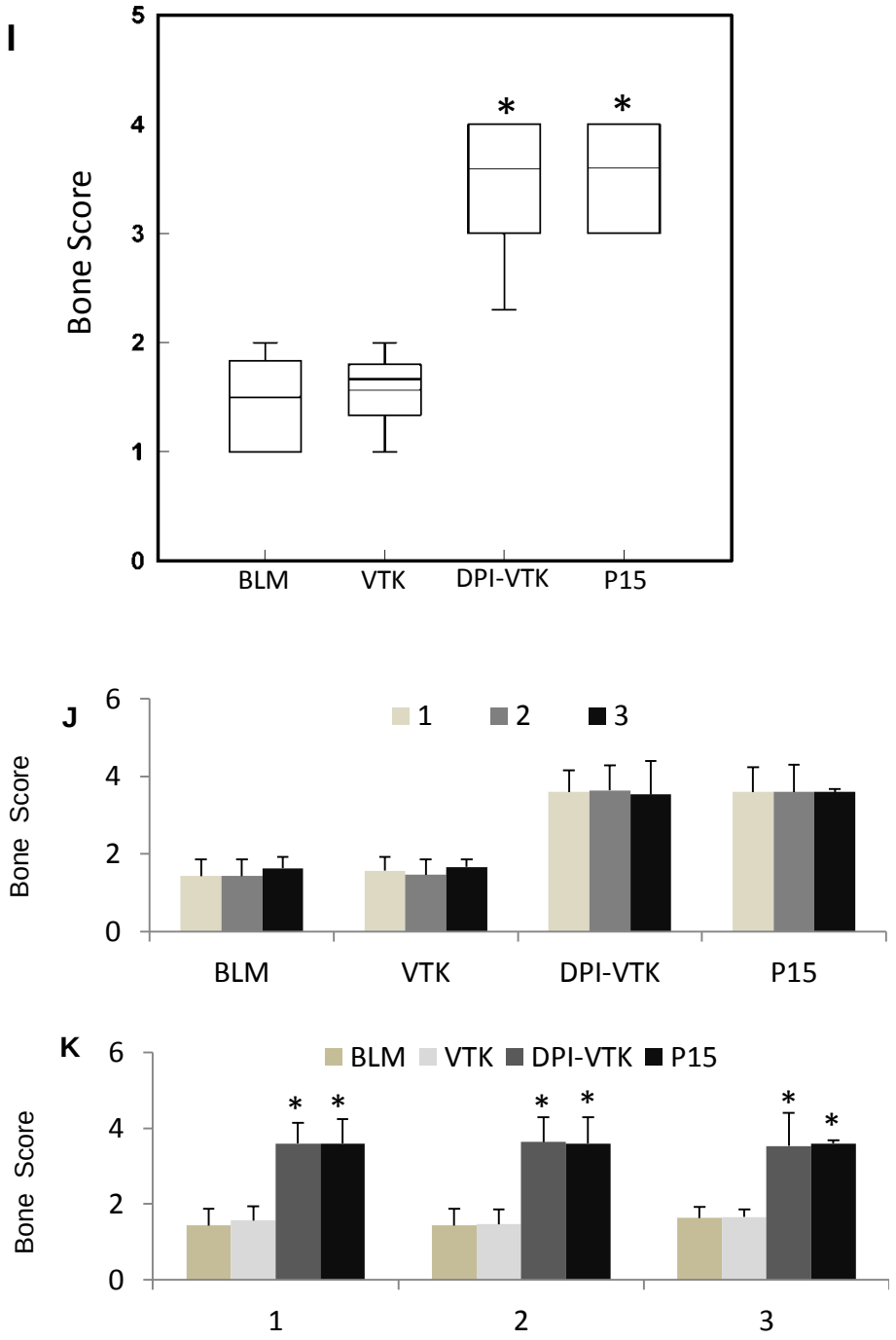
I
Bone Score
5
4
3
2
1
0
*
*
BLM
VTK
DPI-VTK
P15
J
Bone Score
6
4
2
0
1
2
3
BLM
VTK
DPI-VTK
P15
K
Bone Score
6
4
2
0
BLM
VTK
DPI-VTK
P15
1
2
3

**Figure 4.6.** Histological staining and bone quality scoring of ectopically regenerated ossicles 8 weeks post transplantation. A-D) Representative low magnification images of cross sections through the center of ossicles indicating overall degree of bone formation in the interior of the construct (scale bar 500μm). E-H) High Magnification images of cross sections through the center of ossicles indicating increased bone formation, vascularization, and cellularity on DPI-VTK and P15 compared to VTK and BLM. (b) indicates bone, (h) indicates hematopoesis, (c) indicates greater density of cells, (p) indicates pores, (t) indicate scaffold struts replaced by tissue (scale bars 100μm). I) Bone score based on bone coverage. * indicates significant differences from BLM and VTK ($p < 0.001$). J) Bone Score by peptide group across innermost section 1 to outermost section 3. K) Bone score by section across peptide groups. * indicates significant difference from BLM and VTK ($p<0.001$).

# REFERENCES


[1] V. Campana, G. Milano, E. Pagano, M. Barba, C. Cicione, G. Salonna, W. Lattanzi, and G. Logroscino, “Bone substitutes in orthopaedic surgery: from basic science to clinical practice.,” *J. Mater. Sci. Mater. Med.*, vol. 25, no. 10, pp. 2445–61, Oct. 2014.

[2] O. Faour, R. Dimitriou, C. A. Cousins, and P. V Giannoudis, “The use of bone graft substitutes in large cancellous voids: any specific needs?,” *Injury*, vol. 42 Suppl 2, pp. S87–90, Sep. 2011.

[3] W. L. Grayson, M. Fröhlich, K. Yeager, S. Bhumiratana, M. E. Chan, C. Cannizzaro, L. Q. Wan, X. S. Liu, X. E. Guo, and G. Vunjak-Novakovic, “Engineering anatomically shaped human bone grafts.,” *Proc. Natl. Acad. Sci. U. S. A.*, vol. 107, no. 8, pp. 3299–304, Feb. 2010.

[4] G. J. Meijer, J. D. de Bruijn, R. Koole, and C. A. van Blitterswijk, “Cell-Based Bone Tissue Engineering ,” *PLoS Med.*, vol. 4, no. 2, p. e9, Feb. 2007.

[5] T. T. Roberts and A. J. Rosenbaum, “Bone grafts, bone substitutes and orthobiologics: the bridge between basic science and clinical advancements in fracture healing.,” *Organogenesis*, vol. 8, no. 4, pp. 114–24, Jan. .

[6] P. G. W, U. S. Bone, and J. Decade, “Burden of Musculoskeletal Disease Overview,” *Popul. (English Ed.*, no. March 2002, pp. 1–19, 2011.

[7] A. Atala, F. K. Kasper, and A. G. Mikos, “Engineering complex tissues.,” *Sci. Transl. Med.*, vol. 4, no. 160, p. 160rv12, 2012.

[8] H. Shin, S. Jo, and A. G. Mikos, “Biomimetic materials for tissue engineering ,” *Biomaterials*, vol. 24, no. 24, pp. 4353–4364, Nov. 2003.

[9] A. G. Mikos, S. W. Herring, P. Ochareon, J. Elisseeff, H. H. Lu, R. Kandel, F. J. Schoen, M. Toner, D. Mooney, A. Atala, M. E. Van Dyke, D. Kaplan, and G. Vunjak-Novakovic, “Engineering complex tissues.,” *Tissue Eng.*, vol. 12, no. 12, pp. 3307–39, Dec. 2006.

[10] J. D. Kretlow and A. G. Mikos, “Founder’s award to Antonios G. Mikos, Ph.D., 2011 Society for Biomaterials annual meeting and exposition, Orlando, Florida, April 13-16, 2011: Bones to biomaterials and back again--20 years of taking cues from nature to engineer synthetic polymer scaffold,” *J. Biomed. Mater. Res. A*, vol. 98, no. 3, pp. 323–31, Sep. 2011.

[11] E. J. Lee, F. K. Kasper, and A. G. Mikos, “Biomaterials for tissue engineering.,” *Ann. Biomed. Eng.*, vol. 42, no. 2, pp. 323–37, Feb. 2014.

[12] L. Lu, S. J. Peter, M. D. Lyman, H. L. Lai, S. M. Leite, J. A. Tamada, J. P. Vacanti, R. Langer, and A. G. Mikos, “In vitro degradation of porous poly(L-lactic acid) foams,” *Biomaterials*, vol. 21, no. 15, pp. 1595–1605, 2000.

[13] L. Wu and J. Ding, “In vitro degradation of three-dimensional porous poly(D,L-lactide-co-glycolide) scaffolds for tissue engineering.,” *Biomaterials*, vol. 25, no. 27, pp. 5821–5830, 2004.

[14] W. L. Murphy, S. Hsiong, T. P. Richardson, C. a Simmons, and D. J. Mooney, “Effects of a bone-like mineral film on phenotype of adult human mesenchymal stem cells in vitro.,” *Biomaterials*, vol. 26, no. 3, pp. 303–10, Jan. 2005.

[15] J. D. Kretlow and A. G. Mikos, “Review: mineralization of synthetic polymer scaffolds for bone tissue engineering.,” *Tissue Eng.*, vol. 13, no. 5, pp. 927–38, May 2007.

[16] W. L. Murphy, D. H. Kohn, and D. J. Mooney, “Growth of continuous bonelike mineral within porous poly(lactide-co- glycolide) scaffolds in vitro,” *J. Biomed. Mater. Res.*, vol. 50, pp. 50–58, 2000.

[17] L. N. Luong, S. I. Hong, R. J. Patel, M. E. Outslay, and D. H. Kohn, “Spatial control of protein within biomimetically nucleated mineral.,” *Biomaterials*, vol. 27, no. 7, pp. 1175–86, Mar. 2006.

[18] S. J. Segvich and D. H. Kohn, *Biological Interactions on Materials Surfaces*. New York, NY: Springer US, 2009.

[19] S. Segvich, H. C. Smith, L. N. Luong, and D. H. Kohn, “Uniform deposition of protein incorporated mineral layer on three-dimensional porous polymer scaffolds ,” *J. Biomed. Mater. Res. B, Appl. Biomater.*, vol. 84, no. 2, pp. 340–349, Feb. 2008.

[20] W. L. Murphy, C. a. Simmons, D. Kaigler, and D. J. Mooney, “Bone Regeneration via a Mineral Substrate and Induced Angiogenesis,” *J. Dent. Res.*, vol. 83, no. 3, pp. 204–210, Mar. 2004.

[21] E. V Leonova, K. E. Pennington, P. H. Krebsbach, and D. H. Kohn, “Substrate mineralization stimulates focal adhesion contact redistribution and cell motility of bone marrow stromal cells.,” *J. Biomed. Mater. Res. A*, vol. 79, no. 2, pp. 263–70, Nov. 2006.

[22] K. Shin, A. C. Jayasuriya, and D. H. Kohn, “Effect of ionic activity products on the structure and composition of mineral self assembled on three-dimensional poly ( lactide-co-glycolide ) scaffolds,” *J. Biomed. Mater. Res. Part A*, 2007.

[23] Y. Ramaswamy, C. Wu, and H. Zreiqat, “Orthopedic coating materials: considerations and applications ,” *Expert Rev. Med. Devices*, vol. 6, no. 4, pp. 423–430, Jul. 2009.

[24] A. Shekaran and A. J. García, “Extracellular matrix-mimetic adhesive biomaterials for bone repair.,” *J. Biomed. Mater. Res. A*, vol. 96, no. 1, pp. 261–72, Jan. 2011.

[25] K. M. Hennessy, B. E. Pollot, W. C. Clem, M. C. Phipps, A. A. Sawyer, B. K. Culpepper, and S. L. Bellis, “The effect of collagen I mimetic peptides on mesenchymal stem cell adhesion and differentiation, and on bone formation at hydroxyapatite surfaces.,” *Biomaterials*, vol. 30, no. 10, pp. 1898–909, Apr. 2009.

[26] K. M. Hennessy, W. C. Clem, M. C. Phipps, A. A. Sawyer, F. M. Shaikh, and S. L. Bellis, “The effect of RGD peptides on osseointegration of hydroxyapatite biomaterials.,” *Biomaterials*, vol. 29, no. 21, pp. 3075–83, Jul. 2008.

[27] M. Gilbert, W. J. Shaw, J. R. Long, K. Nelson, G. P. Drobny, C. M. Giachelli, and P. S. Stayton, “Chimeric peptides of statherin and osteopontin that bind hydroxyapatite and mediate cell adhesion.,” *J. Biol. Chem.*, vol. 275, no. 21, pp. 16213–8, May 2000.

[28] D. L. Masica and J. J. Gray, “Solution- and adsorbed-state structural ensembles predicted for the statherin-hydroxyapatite system.,” *Biophys. J.*, vol. 96, no. 8, pp. 3082–91, Apr. 2009.

[29] R. Fujisawa, M. Mizuno, Y. Nodasaka, and Y. Kuboki, “Attachment of osteoblastic cells to hydroxyapatite crystals by a synthetic peptide (Glu7-Pro-Arg-Gly-Asp-Thr) containing two functional sequences of bone sialoprotein.,” *Matrix Biol.*, vol. 16, no. 1, pp. 21–8, Apr. 1997.

[30] H. Ramaraju, S. J. Miller, and D. H. Kohn, “Dual-functioning phage-derived peptides encourage human bone marrow cell-specific attachment to mineralized biomaterials.,” *Connect. Tissue Res.*, vol. 55 Suppl 1, pp. 160–3, Aug. 2014.

[31] F. Gomar, R. Orozco, J. L. Villar, and F. Arrizabalaga, “P-15 small peptide bone graft substitute in the treatment of non-unions and delayed union. A pilot clinical trial.,” *Int. Orthop.*, vol. 31, no. 1, pp. 93–9, Feb. 2007.

[32] T. Kokubo, H. Kushitani, C. Ohtsuki, S. Sakka, and T. Yamamuro, “Chemical reaction of bioactive glass and glass-ceramics with a simulated body fluid,” *J. Mater. Sci. Mater. Med.*, vol. 3, no. 2, pp. 79–83, Mar. 1992.

[33] S. R. Peters, *A Practical Guide to Frozen Section Technique*. New York: Springer Science & Business Media, 2010.

[34] P. Thevenot, M. Sc, A. Nair, M. Sc, J. Dey, M. Sc, J. Yang, D. Ph, L. Tang, and D. Ph, “Method to Analyze Three-Dimensional Cell Distribution and Infiltration in Degradable Scaffolds,” vol. 14, no. 4, 2008.

[35] L. G. Villa-Diaz, S. E. Brown, Y. Liu, A. M. Ross, J. Lahann, J. M. Parent, and P. H. Krebsbach, “Derivation of mesenchymal stem cells from human induced pluripotent stem cells cultured on synthetic substrates.,” *Stem Cells*, vol. 30, no. 6, pp. 1174–81, Jun. 2012.

[36] K. Kim, D. Dean, A. G. Mikos, and J. P. Fisher, “Effect of initial cell seeding density on early osteogenic signal expression of rat bone marrow stromal cells cultured on cross-linked poly(propylene fumarate) disks.,” *Biomacromolecules*, vol. 10, no. 7, pp. 1810–7, Jul. 2009.

[37] B. D. Boyan, C. H. Lohmann, a. Somers, G. G. Niederauer, J. M. Wozney, D. D. Dean, D. L. Carnes, and Z. Schwartz, “Potential of porous poly-D,L-lactide-co-glycolide particles as a carrier for recombinant human bone morphogenetic protein-2 during osteoinduction in vivo,” *J. Biomed. Mater. Res.*, vol. 46, no. 1, pp. 51–59, 1999.

[38] M. H. Mankani, S. A. Kuznetsov, R. M. Wolfe, G. W. Marshall, and P. G. Robey, “In vivo bone formation by human bone marrow stromal cells: reconstruction of the mouse calvarium and mandible.,” *Stem Cells*, vol. 24, no. 9, pp. 2140–9, Sep. 2006.

[39] C. D. Reyes, T. A. Petrie, K. L. Burns, Z. Schwartz, and A. J. Garcia, “Biomolecular surface coating to enhance orthopaedic tissue healing and integration ,” *Biomaterials*, vol. 28, no. 21, pp. 3228–3235, Jul. 2007.

[40] P. Swamynathan, P. Venugopal, S. Kannan, C. Thej, U. Kolkundar, S. Bhagwat, M. Ta, A. Sen Majumdar, and S. Balasubramanian, “Are serum-free and xeno-free culture conditions ideal for large scale clinical grade expansion of Wharton’s jelly derived mesenchymal stem cells? A comparative study.,” *Stem Cell Res. Ther.*, vol. 5, no. 4, p. 88, Jan. 2014.

[41] F. dos Santos, P. Z. Andrade, M. M. Abecasis, J. M. Gimble, L. G. Chase, A. M. Campbell, S. Boucher, M. C. Vemuri, C. L. da Silva, and J. M. S. Cabral, “Toward a clinical-grade expansion of mesenchymal stem cells from human sources: a microcarrier-based culture system under xeno-free conditions.,” *Tissue Eng. Part C. Methods*, vol. 17, no. 12, pp. 1201–10, Dec. 2011.

[42] R. Giancola, T. Bonfini, and A. Iacone, “Cell therapy: cGMP facilities and manufacturing.,” *Muscles. Ligaments Tendons J.*, vol. 2, no. 3, pp. 243–7, Jul. 2012.

[43] S. Alimperti, P. Lei, Y. Wen, J. Tian, A. M. Campbell, and S. T. Andreadis, “Serum-free spheroid suspension culture maintains mesenchymal stem cell proliferation and differentiation potential.,” *Biotechnol. Prog.*, vol. 30, no. 4, pp. 974–83, Jan. .

[44] K. Y. Tan, K. L. Teo, J. F. Y. Lim, A. K. L. Chen, S. Reuveny, and S. K. Oh, “Serum-free media formulations are cell line-specific and require optimization for microcarrier culture.,” *Cytotherapy*, vol. 17, no. 8, pp. 1152–65, Aug. 2015.

[45] R. A. Rossello and D. H, “Cell communication and tissue engineering.,” *Commun. Integr. Biol.*, vol. 3, no. 1, pp. 53–6, Jan. 2010.

[46] A. I. Caplan, “Review: mesenchymal stem cells: cell-based reconstructive therapy in orthopedics ,” *Tissue Eng.*, vol. 11, no. 7–8, pp. 1198–1211, 2005.

[47] P. G. Robey, S. A. Kuznetsov, M. Riminucci, and P. Bianco, “Skeletal (‘mesenchymal’) stem cells for tissue engineering.,” *Methods Mol. Med.*, vol. 140, pp. 83–99, Jan. 2007.

[48] R. A. Rossello and D. H. Kohn, “Gap junction intercellular communication: a review of a potential platform to modulate craniofacial tissue engineering ,” *J. Biomed. Mater. Res. B, Appl. Biomater.*, vol. 88, no. 2, pp. 509–518, Feb. 2009.

[49] R. A. Rosselló, Z. Wang, E. Kizana, P. H. Krebsbach, and D. H. Kohn, “Connexin 43 as a signaling platform for increasing the volume and spatial distribution of regenerated tissue.,” *Proc. Natl. Acad. Sci. U. S. A.*, vol. 106, no. 32, pp. 13219–24, Aug. 2009.

[50] S. A. Kuznetsov, P. H. Krebsbach, K. Satomura, J. Kerr, M. Riminucci, D. Benayahu, and P. G. Robey, “Single-colony derived strains of human marrow stromal fibroblasts form bone after transplantation in vivo.,” *J. Bone Miner. Res.*, vol. 12, no. 9, pp. 1335–47, Sep. 1997.

[51] B. A. Byers, R. E. Guldberg, and A. J. García, “Synergy between genetic and tissue engineering: Runx2 overexpression and in vitro construct development enhance in vivo mineralization.,” *Tissue Eng.*, vol. 10, no. 11–12, pp. 1757–66, Jan. .

[52] D. Wendt, A. Marsano, M. Jakob, M. Heberer, and I. Martin, “Oscillating perfusion of cell suspensions through three-dimensional scaffolds enhances cell seeding efficiency and uniformity.,” *Biotechnol. Bioeng.*, vol. 84, no. 2, pp. 205–14, Oct. 2003.

[53] S. N. Stephansson, B. A. Byers, and A. J. García, “Enhanced expression of the osteoblastic phenotype on substrates that modulate fibronectin conformation and integrin receptor binding,” *Biomaterials*, vol. 23, no. 12, pp. 2527–2534, 2002.

[54] K. Fu, D. W. Pack, A. M. Klibanov, and R. Langer, “Visual evidence of acidic environment within degrading poly(lactic-co-glycolic acid) (PLGA) microspheres.,” *Pharm. Res.*, vol. 17, no. 1, pp. 100–6, Jan. 2000.

[55] S. J. Segvich, H. C. Smith, and D. H. Kohn, “The adsorption of preferential binding peptides to apatite-based materials.,” *Biomaterials*, vol. 30, pp. 1287–1298, 2009.

# CHAPTER FIVE

# SUMMARY AND FUTURE WORK

The work in this dissertation addressed the discovery and design of novel peptides for tissue engineering. Bony non-unions arising from pathological conditions or trauma are often surrounded by poorly cellularized tissue with interrupted vasculature, further attenuating regenerative bridging processes. Cell-based therapies to heal critical sized defects through *de novo* tissue regeneration are a promising alternative to conventional auto-, allo- and xenograft therapies. The primary objectives for tissue engineering require the mechanical, structural and compositional properties of regenerated tissue to seamlessly match those of native tissues surrounding non-unions and critical sized defects[1].

Biomaterial carriers used to deliver cells to a defect site provide physical support, as well as instructive cues. A multitude of stem and progenitor cell sources from various lineages and anatomic locations show promise in regenerating defects for a multitude of clinical applications[2]–[5]. For instance, mesenchymal stem cells from both adult and neonatal sources, as well as pluripotent stem cells from both embryonic and induced systems, are commonly considered for tissue regeneration applications[6]–[8]. Similarly, a variety of biomaterial carriers are used to deliver cells to defects. For instance, natural and synthetic

polymers, polymer-mineral composites, and biomineral composites are used to heal critical sized bone defects. Biomaterial design strategies that control the attachment and delivery of specific regenerative cell populations to a critical size defect can promote functional tissue regeneration *in vivo*[9], [10]. Moreover, strategies to specifically recruit host cells towards biomaterial implants can further improve the quantity and quality of regenerated tissue. In addition to tissue regeneration strategies, grafting to bridge non-unions can also be improved though specific host cell recruitment to implanted metal, ceramic and polymer biomaterials.

Use of display technologies to identify cell specific targets is prevalent in the areas of oncology and immunology. Many of the monoclonal antibody based therapeutics are generated from humanizing antibodies from animal sources using phage display. Through a combinatorial phage display, we identified bone marrow MSC binding (DPIYALSWSGMA-DPI) and mineral binding sequences (VTKHLNQISQSY-VTK), and combined them with glycine linkers to form a dual-functioning cell and mineral binding peptide (GGDPIYALSWSGMAGGGSVTKHLNQISQSY, DPI-VTK)[11], [12]. The work presented in this thesis demonstrated that DPI-VTK improves adhesion strength towards MSCs compared to fibroblasts and pre-osteoblasts (Chapter 2), promotes spreading and proliferation on mineral substrates compared to apatite controls through an RGD integrin binding receptor, and supports differentiation of adherent MSCs (Chapter 3). Delivering MSCs on a mineralized porous polymer scaffold coated with DPI-VTK improves the quantity and quality of bone compared to uncoated and acellular controls (Chapter 4).

## PHAGE DISPLAY DERIVED PEPTIDE DESIGN

The DPI sequence, when added to VTK, directly or indirectly regulates attachment to apatite (Chapter 2, Table 2). DPI-$VTK_{phos}$, containing phosphorylated serine residues in the VTK domain, resulted in less adsorption to apatite, a result which is contrary to the greater binding affinity of $VTK_{phos}$ compared to VTK. Apatite binding affinity differences between DPI-VTK and DPI-$VTK_{phos}$ can be driven by differences in solution state conformation, as well as degree of freedom in bound state peptide conformation. For instance, the binding DPI to the apatite surface using the VTK peptide can improve the conformational flexibility of DPI compared to delivery with DPI-$VTK_{phos}$. The bound state conformation of DPI-$VTK_{phos}$ also limited hBMSC adhesion strength towards apatite surfaces. Cell attachment to VTK indicates potential cell association with the mineral binding sequence however the lack of spreading and adhesion strength on these surfaces indicates that the DPI sequence exhibits greater cell binding affinity.

The greater specificity of MSCs toward DPI-VTK indicates affinity towards a cell specific target. Phage display on clonally derived human bone marrow stromal cells identified peptide sequences that bound specifically to cell surface receptors. MSC surfaces contain a variety of receptors involved in signal transduction, ion transport, and cell adhesion. There is an equal likelihood of phage display identifying peptide sequences that bind specifically to the most highly expressed cell surface receptor or the most highly expressed profile of cell surface receptors. The relative promiscuity of DPI-VTK towards the RGD binding integrin receptor subunits suggests either a non-integrin mediated cell attachment, specificity to a profile of integrins expressed on MSCs, or a combination of these mechanisms.

Integrins can direct osteoinduction by transducing mechanical stimuli from the extracellular matrix into biological responses. For instance, $\alpha_2\beta_1$ and $\alpha_5\beta_1$ are involved in osteogenic differentiation of MSCs and osteoblasts through the MAPK/PI3K/ERK pathways [13]–[16]. DPI-VTK demonstrates competition with both $\alpha_5$ and $\beta_1$ antibody in solution and partial competition with $\alpha_2\beta_1$ in solution. Furthermore, the ability to specifically adhere MSCs may arise from the conformational flexibility of DPI when binding various integrin receptors. Designing peptide sequences that target a profile of integrin receptors can be a promising design strategy to deliver greater numbers of specific regenerative cell populations on a biomaterial to a critical sized defect.

## DUAL-PEPTIDE TISSUE ENGINEERING APPLICATIONS

DPI-VTK improved cell proliferation on apatite coated substrates compared to biomimetic apatite without peptide and with just the mineral binding peptide VTK (Chapter 3 Figure 3). The role of integrin mediated attachment to DPI-VTK can explain the greater proliferation of cells on DPI-VTK. DPI-VTK also supports osteogenic differentiation *in vitro*. ALP and OCN expression was increased in MSCs cultured on DPI-VTK compared to apatite surfaces with serum or the dual peptide RGD-VTK. Surprisingly, there was an increase in osteogenic markers on VTK compared to DPI-VTK, apatite controls and RGD-VTK. The inductive role of VTK may be affiliated with the ability to associate with the cell surface and internalize. Further investigations regarding the translocation of VTK can elucidate osteoinductive mechanisms of action. Furthermore, understanding the stability, degradation rate, and potential translocation of cleaved VTK fragments from DPI-VTK coated apatite in the presence of cells, can provide further insight towards inductive mechanisms of DPI-VTK.

The *in vivo* biological activity of MSCs transplanted on DPI-VTK coated mineral-PLGA composite scaffolds was examined in an ectopic model (Chapter 4). Constructs containing DPI-VTK formed more bone, contained more cells, and exhibited greater vascularization compared to acellular controls, non-peptide coated apatite and VTK coated apatite. Increased bone formation with DPI-VTK can be attributed to improved cell attachment and potentially improved osteoinduction.

However, uniformity of bone-like mineral coverage, peptide distribution and cell distribution did not result in uniform bone formation. The dynamics of bone formation within the subcutaneous environment may ultimately drive this characteristic shell formation. The subcutaneous environment is limited by the ability to form deeply penetrating vascular networks before cell mediated mineral formation causes peripheral pore occlusion causing isolation of the interior [17]. Evaluating bone regeneration in a critical-sized calvarial defect model may reveal the relative contributions of uniform mineral, peptide and cell distribution to *in vivo* bone formation.

## FUTURE DIRECTIONS

Computational modeling identified basic Lys-3 and the polar residues Gln-10 and Tyr-12 in the VTK sequence as key residues responsible for binding to apatite [18]. Computational modeling of DPI, DPI-VTK, and scrambled sequences coupled with solid-state NMR or Raman spectroscopy could reveal sequence and conformational aspects that regulate cell and apatite specificity. This information regarding specific peptide sequence characteristics associated with cell binding and conformation will further improve peptide design and functionality[19], [20]. In addition to the cell and mineral binding domains, the linker sequence can be used to improve mineral binding and

mineral association. Identifying sequences and lengths of linkers that control solution and bound state conformation towards improving apatite affinity and cell attachment.

In addition to promoting MSC specific attachment to apatite, DPI-VTK improves spreading in the presence of serum proteins, indicating a cooperative interaction (Chapter 3). Peripheral focal contact distribution relates to adhesion strength and spreading area until a particular threshold of spread area[21]. The peripheral focal adhesion contact distribution on DPI-VTK clustered towards the peripheral sections compared to BLM in a no serum condition (Chapter 3. Figure 1c. $p < 0.001$), which implies greater adhesion strength. A more rigorous detachment force assay using DPI-micropatterned surfaces and higher fluid shear forces could quantify the aggregate strength of focal contacts formed on DPI in relation to spread area during later stages of adhesion.

Rigorous quantification of adhesion strength using the DPI sequence immobilized to a polymer substrate could be used to more specifically identify cell binding targets. Competitive inhibition assays can be coupled with adhesion strength assays to quantify binding affinity of DPI to a specific integrin or integrin subunit [22]–[24]. Fragmentation of the DPI sequence and sequence scrambling can also be used to identify amino acid residues in DPI that interact with cell surface receptors. Finally, examining the role of DPI-MSC receptor mediated osteoinductivity through cytoskeletal, signal transduction, and mineralization inhibitors could provide further information regarding mechanism of action with relation to peptide design.

Longitudinal *in vivo* studies using fluorescent peptide labeling, MSC-labeling, and *in vivo* imaging techniques can reveal the interplay between transplanted versus host cell

contributions towards increasing bone volume, cellularity, and vascularization. Although an ectopic model demonstrates proof-of-concept for *in vivo* biological activity, an orthotopic model provides a more clinically relevant environment to assess tissue regeneration. A critical sized calvarial defect model can be used to assess the ability of DPI-VTK not only improve the ostoinductivity of transplanted cells but also recruit host cell populations, promote anastomosis and form penetrating vascular networks, and generate functional bone matching the structural and tissue level properties native bone.

In addition to improving cell based therapies, DPI-VTK can also be applied towards functionalizing grafting materials. A variety of natural and synthetic materials are used for grafting, including synthetic hydroxyapatite, mineral substituted calcium phosphates and sulfates, collagen, mineral collagen composites, and synthetic biodegradable polymers. Although these materials are commonly used for bridging non critical-sized defects, they exhibit limited osteoinductivity, thereby requiring cells, growth factors or osteoinductive peptides to improve reconstruction of non-union defects. For instance, the osteoinductive peptide P15 adsorbed to bone graft substitutes is approved for clinical use in the oral cavity. Furthermore, the application of BMP2 antibodies, BMP2 mimicking peptides, and BMP2 sequestering receptors on bone grafting materials have shown promise in laboratory and clinical settings [25]–[27]. Verifying the osteoinductive potential of DPI-VTK in promoting host cell infiltration and osteoinduction in a critical-sized calvarial defect model can provide further insight towards a clinical opportunity for bone grafting applications.

The cell specific DPI sequence could be applied to separate or extract specific cell populations from primary tissues prior to *ex vivo* expansion. For instance, p-selectin

coated tubing was used to extract CD34+ at 94% purity and CD45+ at 93% purity compared to 74% purity with flow cytometer and ficoll extraction systems [28], [29]. Furthermore, sorting cells based on fluorescent-antibodies can interfere with cell proliferation and differentiation, while the adhesive nature of mononuclear cells results in loss during density gradient purification[30], [31]. Similarly, DPI-coated or immobilized substrates coupled with detachment flow technologies could be used to improve extraction purity of MSCs from primary tissue populations. Moreover, fluorescently labeled DPI peptide could be used to sort specific MSC subpopulations. Specifically extracting MSCs could significantly reduce *ex vivo* expansion time and subsequent time to therapy. Therefore, extracting cells using adhesion strength or fluorescent cell sorting can improve purity in a non-invasive manner. For instance, adhering populations of fibroblasts undergoing induced pluripotent reprogramming within a microfluidic substrate and subjecting them to fluidic flow to detach non-adherent cells can improve the extraction efficiency of specific iPSCs with up to 95% efficiency significantly reducing culture and characterization times.

## ADVANCEMENTS IN DISPLAY TECHNOLOGY

At the time of discovery, there were relatively few studies utilizing phage display in tissue regeneration. However, over recent years phage display has been used to identify sequences specific towards various biomaterials and cells[32]–[38]. Furthermore, display technologies are becoming increasingly sophisticated by customizing the presentation and structure of the displayed proteins or peptides through organism selection, engineering coat proteins, or engineering fusion protein expression. For instance, retroviral, bacterial, yeast, mammalian and even ribosomal display systems are being

used to customize display technologies towards specific target identification[39]. Furthermore, the conformation of presented sequences are being engineered to provide more physiologically relevant secondary structures. For instance cyclized and bicyclized peptide libraries have been created to improve the specificity and binding affinity of identified sequences towards receptor targets[40], [41]. Advancements in computational processing power coupled with development of computational modeling algorithms for identifying structure function relationships have further expanded the potential for new molecule discovery[20], [42]. Coupling these advancements in display technologies with new methodologies for identifying specific binding targets can further improve display technology based biomolecular discovery towards tissue engineering applications.

## REFERENCES


[1] F. Guilak, D. L. Butler, S. A. Goldstein, and F. P. T. Baaijens, "Biomechanics and mechanobiology in functional tissue engineering.," *J. Biomech.*, vol. 47, no. 9, pp. 1933–40, Jun. 2014.

[2] R. Hass, C. Kasper, S. Böhm, and R. Jacobs, "Different populations and sources of human mesenchymal stem cells (MSC): A comparison of adult and neonatal tissue-derived MSC.," *Cell Commun. Signal.*, vol. 9, p. 12, Jan. 2011.

[3] L. G. Villa-Diaz, S. E. Brown, Y. Liu, A. M. Ross, J. Lahann, J. M. Parent, and P. H. Krebsbach, "Derivation of mesenchymal stem cells from human induced pluripotent stem cells cultured on synthetic substrates.," *Stem Cells*, vol. 30, no. 6, pp. 1174–81, Jun. 2012.

[4] S. E. Brown, W. Tong, and P. H. Krebsbach, "The derivation of mesenchymal stem cells from human embryonic stem cells.," *Cells. Tissues. Organs*, vol. 189, no. 1–4, pp. 256–60, Jan. 2009.

[5] P. G. Robey, S. A. Kuznetsov, M. Riminucci, and P. Bianco, "Skeletal ('mesenchymal') stem cells for tissue engineering.," *Methods Mol. Med.*, vol. 140, pp. 83–99, Jan. 2007.

[6] A. I. Caplan, "Review: mesenchymal stem cells: cell-based reconstructive therapy in orthopedics ," *Tissue Eng.*, vol. 11, no. 7–8, pp. 1198–1211, 2005.

[7] A. G. Mikos, S. W. Herring, P. Ochareon, J. Elisseeff, H. H. Lu, R. Kandel, F. J. Schoen, M. Toner, D. Mooney, A. Atala, M. E. Van Dyke, D. Kaplan, and G. Vunjak-Novakovic, "Engineering complex tissues.," *Tissue Eng.*, vol. 12, no. 12, pp. 3307–39, Dec. 2006.

[8] P. G. Robey, S. A. Kuznetsov, M. Riminucci, and P. Bianco, "Skeletal Development and Repair," vol. 1130, pp. 279–293, 2014.

[9] R. G. LeBaron and K. A. Athanasiou, "Extracellular matrix cell adhesion peptides: functional applications in orthopedic materials ," *Tissue Eng.*, vol. 6, no. 2, pp. 85–103, Apr. 2000.

[10] A. Shekaran and A. J. García, "Extracellular matrix-mimetic adhesive biomaterials for bone repair.," *J. Biomed. Mater. Res. A*, vol. 96, no. 1, pp. 261–72, Jan. 2011.

[11] H. Ramaraju, S. J. Miller, and D. H. Kohn, "Dual-functioning phage-derived peptides encourage human bone marrow cell-specific attachment to mineralized biomaterials.," *Connect. Tissue Res.*, vol. 55 Suppl 1, pp. 160–3, Aug. 2014.

[12] S. Segvich, S. Biswas, U. Becker, and D. H. Kohn, "Identification of peptides with targeted adhesion to bone-like mineral via phage display and computational modeling.," *Cells. Tissues. Organs*, vol. 189, no. 1–4, pp. 245–51, Jan. 2009.

[13] J. Eyckmans, T. Boudou, X. Yu, and C. S. Chen, "A hitchhiker's guide to mechanobiology.," *Dev. Cell*, vol. 21, no. 1, pp. 35–47, Jul. 2011.

[14] A. K. Kundu, C. B. Khatiwala, and A. J. Putnam, "Extracellular matrix remodeling, integrin expression, and downstream signaling pathways influence the osteogenic differentiation of mesenchymal stem cells on poly(lactide-co-glycolide) substrates.," *Tissue Eng. Part A*, vol. 15, no. 2, pp. 273–283, 2009.

[15] G. Xiao, D. Wang, M. D. Benson, G. Karsenty, and R. T. Franceschi, "Role of the alpha2-integrin in osteoblast-specific gene expression and activation of the Osf2 transcription factor.," *J. Biol. Chem.*, vol. 273, no. 49, pp. 32988–32994, 1998.

[16] A. J. García, J. E. Schwarzbauer, and D. Boettiger, "Distinct activation states of α5β1 integrin show differential binding to RGD and synergy domains of fibronectin," *Biochemistry*, vol. 41, no. 29, pp. 9063–9069, 2002.

[17] S. N. Stephansson, B. A. Byers, and A. J. García, "Enhanced expression of the osteoblastic phenotype on substrates that modulate fibronectin conformation and integrin receptor binding," *Biomaterials*, vol. 23, no. 12, pp. 2527–2534, 2002.

[18] W. N. Addison, D. L. Masica, J. J. Gray, and M. D. McKee, "Phosphorylation-dependent inhibition of mineralization by osteopontin ASARM peptides is regulated by PHEX cleavage.," *J. Bone Miner. Res.*, vol. 25, no. 4, pp. 695–705, Apr. 2010.

[19] D. L. Masica, J. J. Gray, and W. J. Shaw, “Partial High-resolution structure of phosphorylated and non-phosphorylated leucine-rich amelogenin protein adsorbed to hydroxyapatite,” *J. Phys. Chem. C*, vol. 115, pp. 13775–13785, 2011.

[20] D. L. Masica and J. J. Gray, “Solution- and adsorbed-state structural ensembles predicted for the statherin-hydroxyapatite system.,” *Biophys. J.*, vol. 96, no. 8, pp. 3082–91, Apr. 2009.

[21] K. K. Elineni and N. D. Gallant, “Regulation of cell adhesion strength by peripheral focal adhesion distribution.,” *Biophys. J.*, vol. 101, no. 12, pp. 2903–11, Dec. 2011.

[22] T. a. Petrie, J. R. Capadona, C. D. Reyes, and A. J. García, “Integrin specificity and enhanced cellular activities associated with surfaces presenting a recombinant fibronectin fragment compared to RGD supports,” *Biomaterials*, vol. 27, no. 31, pp. 5459–5470, 2006.

[23] T. A. Petrie, J. E. Raynor, C. D. Reyes, K. L. Burns, D. M. Collard, and A. J. García, “The effect of integrin-specific bioactive coatings on tissue healing and implant osseointegration,” *Biomaterials*, vol. 29, no. 19, pp. 2849–2857, 2008.

[24] B. A. Byers, R. E. Guldberg, and A. J. García, “Synergy between genetic and tissue engineering: Runx2 overexpression and in vitro construct development enhance in vivo mineralization.,” *Tissue Eng.*, vol. 10, no. 11–12, pp. 1757–66, Jan. .

[25] M. Freire, J.-H. Choi, A. Nguyen, Y. D. Chee, J.-K. Kook, H.-K. You, and H. H. Zadeh, “Application of AMOR in craniofacial rabbit bone bioengineering.,” *Biomed Res. Int.*, vol. 2015, p. 628769, Jan. 2015.

[26] P. T. Hamilton, M. S. Jansen, S. Ganesan, R. E. Benson, R. Hyde-Deruyscher, W. F. Beyer, J. C. Gile, S. A. Nair, J. A. Hodges, and H. Grøn, “Improved bone morphogenetic protein-2 retention in an injectable collagen matrix using bifunctional peptides.,” *PLoS One*, vol. 8, no. 8, p. e70715, Jan. 2013.

[27] Z. Sardar, D. Alexander, W. Oxner, S. du Plessis, A. Yee, E. K. Wai, D. G. Anderson, and P. Jarzem, “Twelve-month results of a multicenter, blinded, pilot study of a novel peptide (B2A) in promoting lumbar spine fusion.,” *J. Neurosurg. Spine*, vol. 22, no. 4, pp. 358–66, Apr. 2015.

[28] S. D. Narasipura, J. C. Wojciechowski, N. Charles, J. L. Liesveld, and M. R. King, “P-Selectin coated microtube for enrichment of CD34+ hematopoietic stem and progenitor cells from human bone marrow.,” *Clin. Chem.*, vol. 54, no. 1, pp. 77–85, Jan. 2008.

[29] S. D. Narasipura, J. C. Wojciechowski, B. M. Duffy, J. L Liesveld, and M. R. King, “Purification of CD45+ hematopoietic cells directly from human bone marrow using a

flow-based P-selectin-coated microtube.," *Am. J. Hematol.*, vol. 83, no. 8, pp. 627–9, Aug. 2008.

[30] P. G. Robey, S. a Kuznetsov, J. Ren, H. G. Klein, M. Sabatino, and D. F. Stroncek, "Generation of clinical grade human bone marrow stromal cells for use in bone regeneration," *Bone*, vol. 70, pp. 87–92, 2014.

[31] J. Tong, R. Hoffman, S. Siena, E. F. Srour, M. Bregni, and A. M. Gianni, "Characterization and quantitation of primitive hematopoietic progenitor cells present in peripheral blood autografts.," *Exp. Hematol.*, vol. 22, no. 10, pp. 1016–24, Oct. 1994.

[32] M. Gungormus, E. E. Oren, J. A. Horst, H. Fong, M. Hnilova, M. J. Somerman, M. L. Snead, R. Samudrala, C. Tamerler, and M. Sarikaya, "Cementomimetics-constructing a cementum-like biomineralized microlayer via amelogenin-derived peptides.," *Int. J. Oral Sci.*, vol. 4, no. 2, pp. 69–77, Jun. 2012.

[33] U. O. S. Seker, B. Wilson, J. L. Kulp, J. S. Evans, C. Tamerler, and M. Sarikaya, "Thermodynamics of engineered gold binding peptides: establishing the structure-activity relationships.," *Biomacromolecules*, vol. 15, no. 7, pp. 2369–77, Jul. 2014.

[34] D. Khatayevich, M. Gungormus, H. Yazici, C. So, S. Cetinel, H. Ma, A. Jen, C. Tamerler, and M. Sarikaya, "Biofunctionalization of materials for implants using engineered peptides.," *Acta Biomater.*, vol. 6, no. 12, pp. 4634–41, Dec. 2010.

[35] S. Segvich and D. H. Kohn, "Phage Display as a Strategy for Designing Organic/Inorganic Biomaterials," in *Biological Interactions on Material Surfaces*, D. A. Puleo and R. Bizios, Eds. Springer US, 2009, pp. 115–132.

[36] L. M. Alvarez, J. J. Rivera, L. Stockdale, S. Saini, R. T. Lee, and L. G. Griffith, "Tethering of Epidermal Growth Factor (EGF) to Beta Tricalcium Phosphate (βTCP) via Fusion to a High Affinity, Multimeric βTCP-Binding Peptide: Effects on Human Multipotent Stromal Cells/Connective Tissue Progenitors."

[37] J. Wang, M. Yang, Y. Zhu, L. Wang, A. P. Tomsia, and C. Mao, "Phage nanofibers induce vascularized osteogenesis in 3D printed bone scaffolds.," *Adv. Mater.*, vol. 26, no. 29, pp. 4961–6, Aug. 2014.

[38] R. N. Shah, N. a Shah, M. M. Del Rosario Lim, C. Hsieh, G. Nuber, and S. I. Stupp, "Supramolecular design of self-assembling nanofibers for cartilage regeneration.," *Proc. Natl. Acad. Sci. U. S. A.*, vol. 107, no. 8, pp. 3293–8, Feb. 2010.

[39] J. McCafferty and D. Schofield, "Identification of optimal protein binders through the use of large genetically encoded display libraries.," *Curr. Opin. Chem. Biol.*, vol. 26C, pp. 16–24, Jan. 2015.

[40] C. Heinis, T. Rutherford, S. Freund, and G. Winter, “Phage-encoded combinatorial chemical libraries based on bicyclic peptides.,” *Nat. Chem. Biol.*, vol. 5, no. 7, pp. 502–7, Jul. 2009.

[41] S. W. Millward, S. Fiacco, R. J. Austin, and R. W. Roberts, “Design of Cyclic Peptides That Bind Protein Surfaces with Antibody-Like Affinity,” Sep. 2007.

[42] D. Masica, J. Gray, and W. Shaw, “partial high-resolution structure of phosphorylated and non-Phosphorylated leucine-rich amelogenin protein adsorbed to hydroxyapatite,” *J. Phys. Chem. …*, 2011.

# APPENDICIES

## APPENDIX A ADSORPTION ISOTHERM

***Materials***

| | Cat# | Lot |
|---|---|---|
| **Hydroxyapatite** | **289396** | **MKBK2210V** |

1. Trizma preset crystals T7818 pH 7.5 Batch 115k5423
2. 96-well plate - corning clear bottom - UV grade plate
3. 96-well plate black flat bottom
4. Millipore filter plate
5. FITC-BSA
6. BSA

***Methods***

***Trizma buffer preparation***

a. Make 50mM Trizma preset crystal pH 7.4 (MW = 151.6)
   i. 7.58g/L, 3.79g/500mL, 1.85g/250mL, 0.9475g/125mL

***HA Suspension preparation***

(slurry is 25% w/v),

b. Add 1 gram of HA/CaP + 24mL buffer --> pH 7.172 after 20hr incubation at 37$^{o}$C
c. Place on shaker plate to equilibrate overnight (~18 hrs)

d. Check pH

**Verify consistent HA suspension**

**a.** Pipette 40mg/mL @ 50uL(3x), 100uL (3x), 200uL (3x) to verify consistency of pipetting equal amounts

**b.** Pipette 20mg/mL @ 50uL(3x), 100uL (3x), 200uL (3x)…0mg/mL (see table) Add buffer for remaining volume so all wells have 200uL sln in them

**c.** Incubate for 1hr on titer plate @ setting 5 and RT

**d.** Choose lowest concentration of powder that is statistically significant from the concentration that is immediately greater

**e.** Verify absorbance at 200, 250, 300, 350, 400, 450, 500nm

***Make peptide stock solution***

a. 1mg/ml stock --> 3mg in 3mL buffer

b. Aliquot 1mL into eppendorf tubes

**Peptide Binding Assay**

1. Add 100 uL of dilution to 96 well plate in triplicate 0, 0.5, 1, 2.5, 5, 10, 25, 50, 75, 100, 250, 500 μg/mL
2. Repeat for standard curve
3. Take pre-reading 200 -300 nm after incubation at 37oC for 15 min
4. Transfer dilutions to 96 well Millipore filter plate
5. Add 50uL of 10mg/mL HA suspension to samples
6. Add 50uL of Trizma buffer to standard curve
7. Incubate on shaker at 37oC for 4hrs
8. Centrifuge plate @ 1000RPM for 20min
9. Incubate at 37oC for 15 min

10. Take post reading

**Micro BCA Assay**

1. Preparation of working reagents
2. Pipette 150uL into each well containing filtered solution
3. Place on plate shaker for 30seconds
4. Cover plate using sealing tape and incubate at 37oC for 2 hrs
5. Cool plate to RT
6. Measure absorbance at 562nm

# APPENDIX B CELL CENTRIFUGATION ASSAY

***PLGA film fabrication***

**Materials**

- 85:15 poly-(D,L)-lactide-co-(glycolide) ester capped (Lakeshore biomaterials, 8515DLG7E)
- Glass coverslips ( cat#64-703 Warner Instruments)
- Chloroform (Sigma Aldrich, cat# 366919, batch 47796DM)
- Sigmacote (Sigma Aldrich, SL2, Lot: 039K4364)
- Plastic 100mm petri dishes (Corning)
- Glass petri dishes
- Glass vials
- Kimwipes
- PLGA films on glass coverslips
- Plastic Petri dishes
- 1x mSBF
- NaOH (Sigma-Aldrich, S2567, Lot: 127K6105)

**Methods**

**Glassware prep**

1. Clean glass petri dish with chloroform removing all residual adherent polymer
2. Wash with $dH_20$ and soap
3. Rinse in chloroform and let it evaporate
4. Wash all glassware in sigmacote and evaporate overnight

*sigma cote allows for easier removal of polymer from glass surface

**Polymer solution prep**

1. Thaw out appropriate number of polymer pellet aliquots and bring to RT
2. Weight out appropriate amount to make 5 wt% solution of PLGA: Chloroform
3. Add PLGA to glass vial and add appropriate amount of chloroform to vial
    i. 1.186 g in 16mL = 5 wt% makes about 50-60 films
    ii. 0.5932 g in 8mLs = 5 wt% makes about 25-30 films
4. Place on titer (setting 3) for 3-4hrs or overnight wrapped in aluminum foil

**Film preparation**

1. Place 6-7 glass coverslips in each glass petri dish
2. Rinse glass syringe 2X with chloroform
3. Load PLGA:Chloroform solution into syringe
4. Gently and Smoothly inject 250-300uL of PLGA chloroform solution on to surface of each glass coverslip
5. Dry overnight in fume hood
6. Move glass petri dishes back to fume hood for 2-3 days
7. Move films from glass petri dishes to plastic petri dishes lined with Kimwipes
8. Cover with aluminum foil
9. Store in desiccator for 2-3 days or for later use

**Notes**

- *Sigmacote limits polymer adhesion to glass surface so glass prep does not need to be done for most of the dishes for up to 2weeks. It is recommended when batch processing films.*
- *Inject polymer solution onto each film in one swift, smooth and gentle motion. Dripping can perturb surface tension and cause spillover*
- *Do not bump into or knock against fume hood during or after film preparation to avoid spill over*

- *No other work should be done in fume hood until they have been moved to back of the fume hood the following day*

*Mineralization of films*

**Methods**

1. Add 50mL 0.5M NaOH to each 100mm$^2$ plastic petri dish
2. Remove films from desiccator
3. Submerge films per dish in NaOH for 7 min
4. Wash twice in 50mL dd$H_2O$ for 10 min each
5. Add 50mL 1x mSBF in cell culture hood to new petri dishes
6. Warm up the SBF to 37oC
7. Add films to SBF cover dish and seal with parafilm
8. Place at 37oC and replace SBF every day for 5-7 days
9. Remove and rinse in ddH20 1x for 10 min
10. Remove 1-3 samples to verify degree of mineralization and Ca/P ratio using SEM-EDX

## *Preparation of biomaterial surfaces*

Make dBSA solution > block the background to improve signal: noise

**specific time and temperature conditions of denaturation are very critical for proper blocking

- Solubilize BSA 1.5 g in 150 mL PBS(1%) in a glass Nalgene bottle on stir plate using magnetic stir bar for 1hr
- Pre-heat hybridization oven to 90oC
- Microwave 300mL tap water in 500mL beaker until it reaches 90oC
- Place 1% BSA solution bottle in hot water beaker and transfer to hybridization chamber.
- Measure solution temperature of sample using thermocouple.
- Start timer once solution temperature reaches 80$^o$C.
- Remove after 11-12 min.
- Cool in RT water bath and sterile filter in cell culture hood.

***Centrifugation Assay***

1. Wash cells in PBS
2. Trypsinize Cells, stop in complete media and spin down
3. Resuspend in serum free media and count
4. Remove dBSA and add **50k** cells/well
5. Incubate at 37$^{o}$C for 3 hrs
6. Add 3.5mL PBS and seal 24 well plate with adhesive sealing film (Nalgene).
7. Ensure no air-bubbles are present within wells.
8. Centrifuge upside down at designated centrifugation speed.
9. Wash and add 450uL serum free media to each well
10. Add 50uL of WST1 reagent to each well
11. Add water to the Von Kossa wells
12. Transfer WST-1 reagent in duplicate to 96 well plate
13. Take a reading of WST-1 @420nm on microplate reader after 4 hrs
14. Take Post reading of von Kossa wells after 1 hr

**Histology**

1. Aliquot 5mL of Formalin
2. Make 0.2% Triton X-100 (Sigma Aldrich, T8787 50mL) by diluting 10 μL of Triton X in 4990uL of PBS
    a. Vortex thoroughly
3. Wash cells twice with pre-warmed phosphate-buffered saline, pH 7.4 (PBS)
4. Fix the sample in 10% formalin for 10 minutes at room temperature (1mL of fixative in 24 well)

a. Tissue to fixative volume ratio should be 15-20% if specimen receives more, than recommended then it is ok, but undersaturation should be avoided.
b. Note: Methanol can disrupt actin during the fixation process. Therefore, it is best to avoid any methanol containing fixatives. The preferred fixative is methanol-free formaldehyde.

5. Wash two or more times with PBS.
6. Place each coverslip in a glass petri dish and extract it with a solution of acetone at ≤–20°C or 0.1% Triton X-100 in PBS for 3 to 5 minutes.
7. Wash two or more times with PBS.
8. When staining with any of the fluorescent phallotoxins, dilute 5 µL methanolic stock solutioninto 200 µL PBS for each coverslipto be stained.
    a. To reduce nonspecific background staining with these conjugates, add 1% bovine serum albumin (BSA) to the staining solution. It may also be useful to pre-incubate fixed cells with PBS containing 1% BSA or with the Image-iT™FX signal enhancer (I36933) for 20–30 minutes prior to adding the phallotoxin staining solution.
9. When staining more than one coverslip, adjust volumes accordingly. For a stronger signal, use 2 or 3 units per coverslip.
10. Place the staining solution on the coverslip for 20 minutes at room temperature (generally, any temperature between 4°C and 37°C is suitable). To avoid evaporation, keep the coverslips inside a covered container during the incubation.
11. Wash two or more times with PBS.
12. For long-term storage, the cells should be air dried and then mounted in a permanent mountant such as ProLong® Gold reagent or Cytoseal. Specimens prepared in this manner retain actin staining for at least six months when stored in the dark at 2–6°C.